3 Functional structure of the peritoneum as a dialysing membrane

L. GOTLOIB, A. SHOSTAK AND V. WAJSBROT

... conduire ... par ordre mes pensées, en commençant par les objects les plus simples et les plus aisés à connaître, pour monter peu a peu, comme par degrés, jusque à la connaissance des plus composés ...

(René Descartes, in: *Discours de la mèthode*, 1637)

Introduction

More than 90 years ago Robinson [1], after summarizing more than two centuries of research, defined the diverse natural functions of the peritoneum as follows: (a) to regulate fluid for nutrient and mechanical purposes; (b) to facilitate motion; (c) to minimize friction, and (d) to conduct vessels and nerves to the viscera.

Several medical and scientific developments which occurred during the twentieth century originated a new approach for the peritoneum being used as a dialysing membrane for long-term life support [2–6]. These same developments created the need for a deeper understanding of peritoneal structure and function.

The peritoneum is a serous membrane embryologically derived from mesenchyma and composed of thin layers of the connective tissue covered by a sheet of mesothelium [7]. When the membrane is folded, forming the omentum and the mesentery, both luminal surfaces are covered by mesothelium.

The peritoneal surface area for the human adult is considered to range between 2.08 [8] and 1.72 m^2 [9], with a ratio of area/body weight of 0.284. The intestinal mesothelium, together with that of mesentery, makes up to 49% of the total mesothelial area [10]. For infants having a body weight of 2700–2900 g, the total peritoneal surface was found to oscillate between 0.106 [10] and 0.151 m^2 [8], with an area to body weight ratio that fluctuates between 0.383 [10] and 0.522. In infants the contribution of intestine and mesentery to the total surface area is 67.5% [10].

Peritoneal thickness is not uniform and varies according to the area examined. Measurements are quite problematic in parietal and diaphragmatic peritoneum due to the considerable amount of connective tissue, and at times fat, intervening between the peritoneum itself and the underlying tissue (Fig. 1). The submesothelial connective tissue layer of visceral peritoneum is firmly bound to the fibrous tissue of the viscus. Therefore the mesentery, having mesothelial lining on both surfaces and including its trabecular connective framework, appears to be the most appropriate peritoneal portion for estimation of membrane thickness which, in the rabbit, ranges between 30 and 38 μm [11, 12] (Figs 2 and 3).

Normal mesothelium

Electron microscopic studies performed on mouse embryo disclosed that the mesothelium is derived from mesenchymal cells which become flattened, form their own basement membrane, and develop intercellular junctions, mostly desmosomes [13] (Fig. 4, inset). Both pinocytotic vesicles and rough endoplasmic reticulum were present. Yolk sac of human embryos at the 5th–7th week of gestation also exhibit flattened mesothelial cells lying on a hyaline, homogeneous basement membrane [14, 15].

The cell plasmalemma, when stained specifically, shows the typical trilaminar structure observed in all biological cell membranes [16]. The normal mesothelium occasionally shows macrophages implanted on the luminal peritoneal surface instead of mesothelial cells (Fig. 5).

The luminal aspect of the mesothelial cell plasmalemma has numerous cytoplasmic extensions: the microvilli (Figs 2, 3 and 4), whose existence was originally reported by Kolossov [17] and many

R. Gokal, R. Khanna, R.Th. Krediet and K.D. Nolph (eds.), Textbook of Peritoneal Dialysis, 2nd Edition, 37–106.

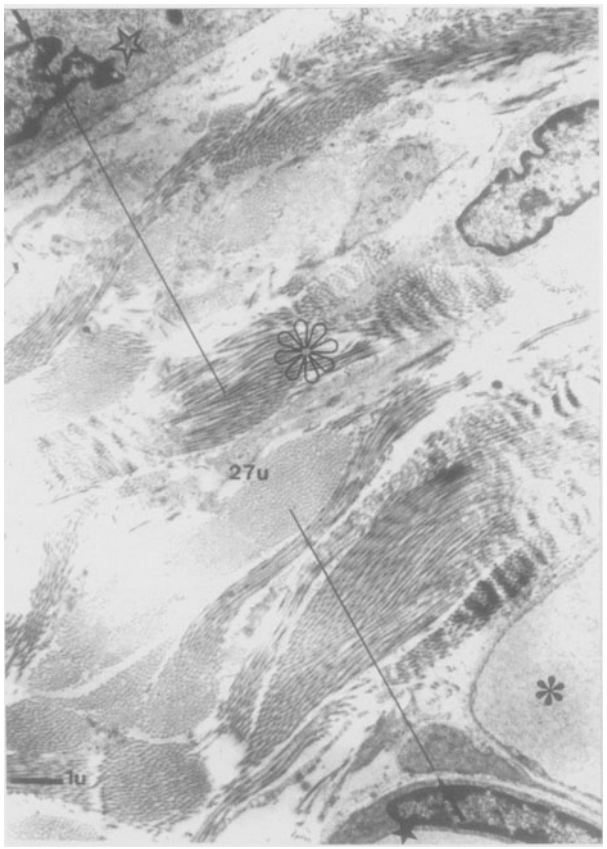

Figure 1. Sample of diaphragmatic rabbit peritoneum. The distance (straight line) between the peritoneal space (upper arrow) and the lumen of the blood capillary (black star) is around 27 μm. The actual pathway through the collagen fibres (open asterisk) is longer (open star: mesothelial cell; black asterisk: fenestrated capillary (× 14 250).

years later confirmed by electron microscopy on the serosa covering the rat oviduct [18, 19]. Even though microvilli are more frequently observed in visceral than in parietal peritoneum [20, 21], their distribution is variable and fluctuates from very numerous to completely absent [21, 22]. It should be taken into account, however, that microvilli are extremely sensitive to minor injury or even to dryness, and can therefore be lost from the cell surface if removal and handling of samples are not done with extremely careful techniques. On the other hand, loss of microvilli, as described in CAPD patients [23] (Fig. 6), represent an early sign of impending apoptosis [24–26] that can be easily identified in mesothelial cell imprints (Fig. 7).

Light microscopy applied to the observation of resting mesothelium imprints [27] shows a continuous monolayer made up mostly of polygonal mononuclear cells (Fig. 8), showing, in mice visceral peritoneum, a density of about 300 000 cells/cm^2 [28]. The number of mesothelial cells per unit area seems higher on the visceral than on the parietal peritoneal surface. Of those cells 1–2% are binucleated (Fig. 8, lower left inset), whereas cells showing three nuclei can be observed (Fig. 8).

Under normal circumstances the cell population of the monolayer is not stained by vital dyes such as Trypan Blue (Fig. 9). This is an indication of their viability. In perpendicular cuts observed under light microscopy, the resting normal mesothelium appears as a continuous layer formed by flattened cells, that are apparently elongated, as a result of the angle of section (Fig. 10). The mesothelial sheet lies on a layer of connective interstitial tissue (Fig. 10), the thickness of which varies in the different portions of the peritoneum (Figs 1 and 3). The relevance of this point on peritoneal permeability will be discussed later.

Thickness of mesothelial cells in the rabbit ranges between 0.6 and 2 μm [11, 12] (Fig. 11).

The human omentum has not yet been studied in great depth. However, some ultrastructural investigations performed in mice and rats [19, 29] seem to indicate that there is little variation between species [30] and that, in mice, omental mesothelial cells can transiently increase their population of microvilli up to seven-fold, suggesting that their concentration in any given area could reflect functional adaptation rather than static structural variation [31].

The presence of pinocytotic vesicles in microvilli has been both reported [18, 20, 32], and denied [31].

Experimental studies done in mice and rats [32–34] using cationic tracers such as ruthenium-red (MW 551 da) and cationized ferritin (MW 445 da) revealed the existence of anionic fixed charges on the luminal surface of the microvilli cytoplasmic membrane (Fig. 12, inset). This cell membrane coating, or glycocalyx, composed of fine fibres that are continuous with the membrane itself [35], furnishes the microvilli surface with electronegative charge which most probably plays a significant role in the transperitoneal transfer of anionic macromolecules such as plasma proteins [33, 36], as well as in that of charged small molecules, as suggested by Curry and Michel [37] in their fibre matrix model of capillary permeability. This surface charge is substantially reduced in cells undergoing apoptosis [38]. The relevance of these charges upon peritoneal permeability will be discussed later.

Length of microvilli in rodents ranges between 0.42 and 2.7 μm, and their average diameter is 0.1 μm

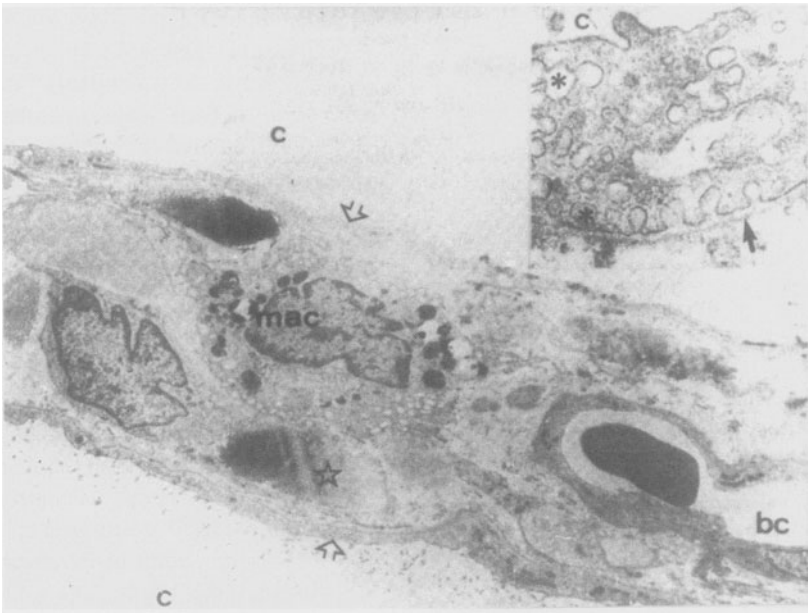

Figure 2. Section of normal rabbit mesentery showing the mesothelial layer (open arrows) covering both aspects of the mesenteric surface area facing the abdominal cavity (c). The interstitium contains a continuous blood capillaty (bc), bundles of collagen (open star), as well as a macrophage (mac). Numerous microvilli can be seen at the lower mesothelial surface (original magnification $\times 4750$).

Upper right inset. Parietal peritoneum of normal mice. Note the presence of numerous pinocytotic vesicles (*) which, on the left side of the electron micrograph, form a chain between the luminal aspect of the mesothelial cell facing the abdominal cavity (c) and the abluminal one, lying on the continuous basement membrane (arrow) ($\times 41\,500$).

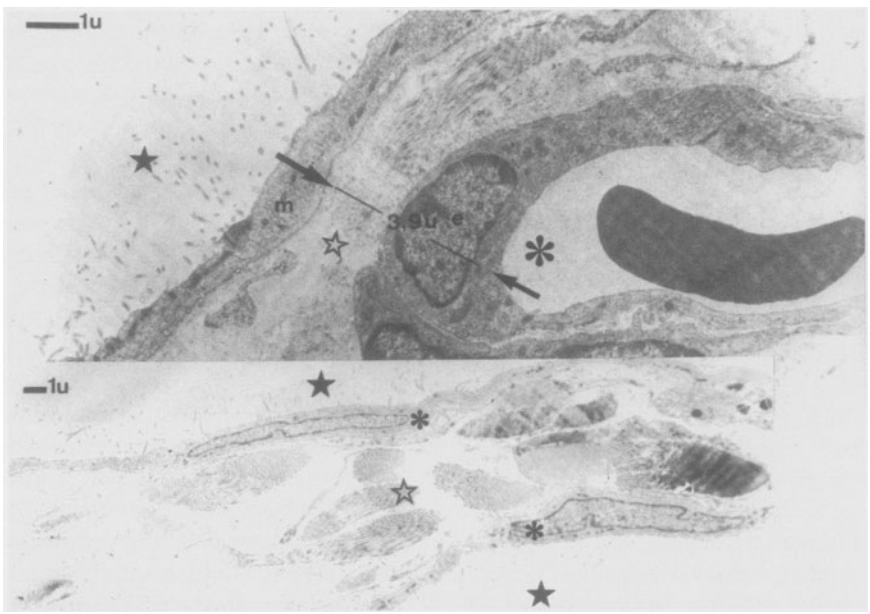

Figure 3. The main photograph shows a sample of rabbit mesenteric peritoneum where the distance (straight line) between the peritoneal space (upper black star) and the microvascular lumen (*) is 3.9 μm (open star: interstitial connective tissue) ($\times 14\,250$).

Lower inset. Section of a 42.1 μm length avascular rabbit mesenteric peritoneum sample (black star: peritoneal space; asterisk: mesothelial cell; open star: interstitial connective tissue) ($\times 4750$).

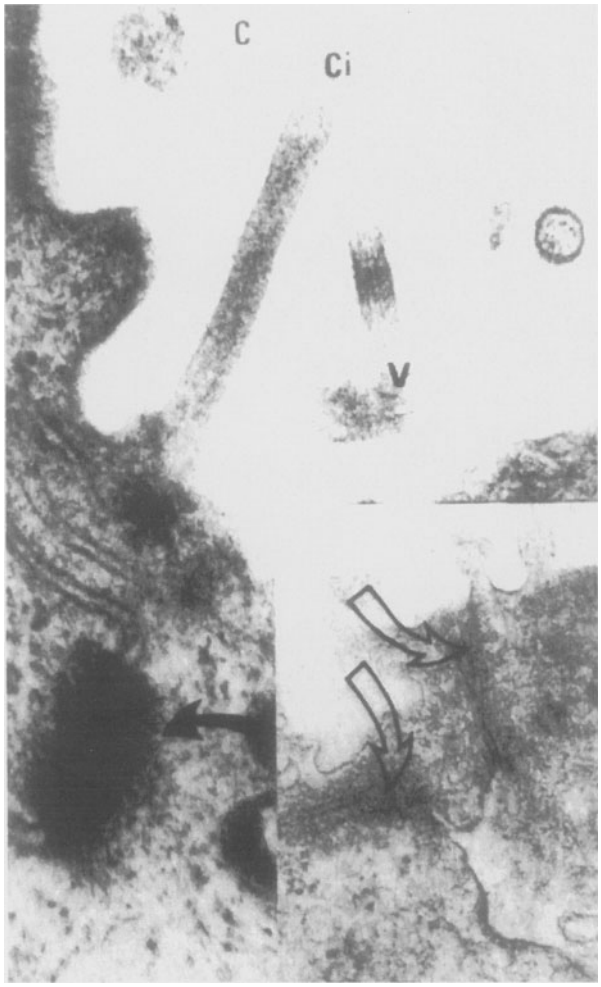

Figure 4. Biopsy of parietal peritoneum taken from a chronic uraemic patient on maintenance peritoneal dialysis. Note the presence of an oligocilium (Ci) showing the deviated axial microtubule (open arrow) and the attached basal body (black arrow). Their function is unknown (C: abdominal cavity; V: microvilli) (×42 900).

Inset. (Lower right). Rabbit mesentery: the open arrows show tight junctions between adjoining mesothelial cells (×62 500).

[11, 18, 20, 29). We have observed a similar range in adult humans. However, mesothelial cells of human embryos (5th–7th week of gestation) showed microvilli up to 3.5 μm long [14].

It has been estimated that microvilli present in the striated border of intestinal epithelium increase the surface area of the intestine by a factor of 20 [39]. Consequently, it has been speculated that mesothelial microvilli could increase the actual peritoneal surface up to 40 m^2 [40].

Plasmalemma of mesothelial cells, like that of microvilli, shows electronegatively charged glycocalyx (Fig. 12) [32–34, 41].

Plasmalemmal vesicles, or caveolae, originally described by Lewis [42] in macrophages of rat omentum, are conspicuously present in mesothelial cells at both the basal and luminal borders, as well as in the paranuclear cytoplasm [18–20, 29, 43–45] (Fig. 2, inset). Their average diameter is approximately 0.717 μm [11]. At times, pinocytotic vesicles appear clustered together and communicating with each other (Fig. 2, inset). Occasionally they appear forming transcellular channels similar to those described in endothelial cells of blood capillaries [46, 47] (Fig. 13, inset), apparently communicating both aspects, luminal and abluminal, of the mesothelial cell. These channels can be formed by a chain of several vesicles (Fig. 13, inset) or just by two adjoining vesicles (Fig. 14, inset). Often pinocytotic vesicles appear to open through the plasma membrane into the luminal or abluminal aspect of the cell (Fig. 2, inset; Fig. 12), as well as into the intercellular space (Fig. 12); exhibiting a neck and a mouth whose respective average diameters are 0.176 and 0.028 μm [11]. With respect to the density distribution of these caveolae, it has been suggested that the parietal mesothelium is less well endowed than the visceral [44].

Palade [48] first proposed that a large part of the macromolecular transport across capillary walls could be attributed to exchange of pinocytotic vesicles between the internal and external surfaces of endothelial cells. This concept was repeatedly applied to the mesothelium. Several electron-dense tracers such as native ferritin [45], iron dextran [11, 29] and melanin [19] were found randomly distributed within pinocytotic vesicles of mesothelial cells after being injected intraperitoneally. Casley-Smith and Chin [44] calculated that the median transit time of vesicles through mesothelial cells ranges between 3 and 5 s, and that approximately 40% of the released vesicles reach the cytoplasmic membrane on the opposite side of the cell. It was even observed that metabolic inhibitors such as dinitrophenol, poisons (cyanide) or slow cooling to 0°C did not completely preclude the uptake of electron-dense macromolecules by pinocytosis [45, 49]. This information, supporting Palade's prediction [48] that vesicles could be the structural equivalent of the large pore theory [50], was challenged by stereological analysis of plasmalemmal vesicles. This study apparently showed that vesicles represent merely invaginations of the plasmalemma from both sides of the capillary wall in frog mesentery [51]. It was suggested that this organization of the vesicular system is incompatible with the concept that macro-

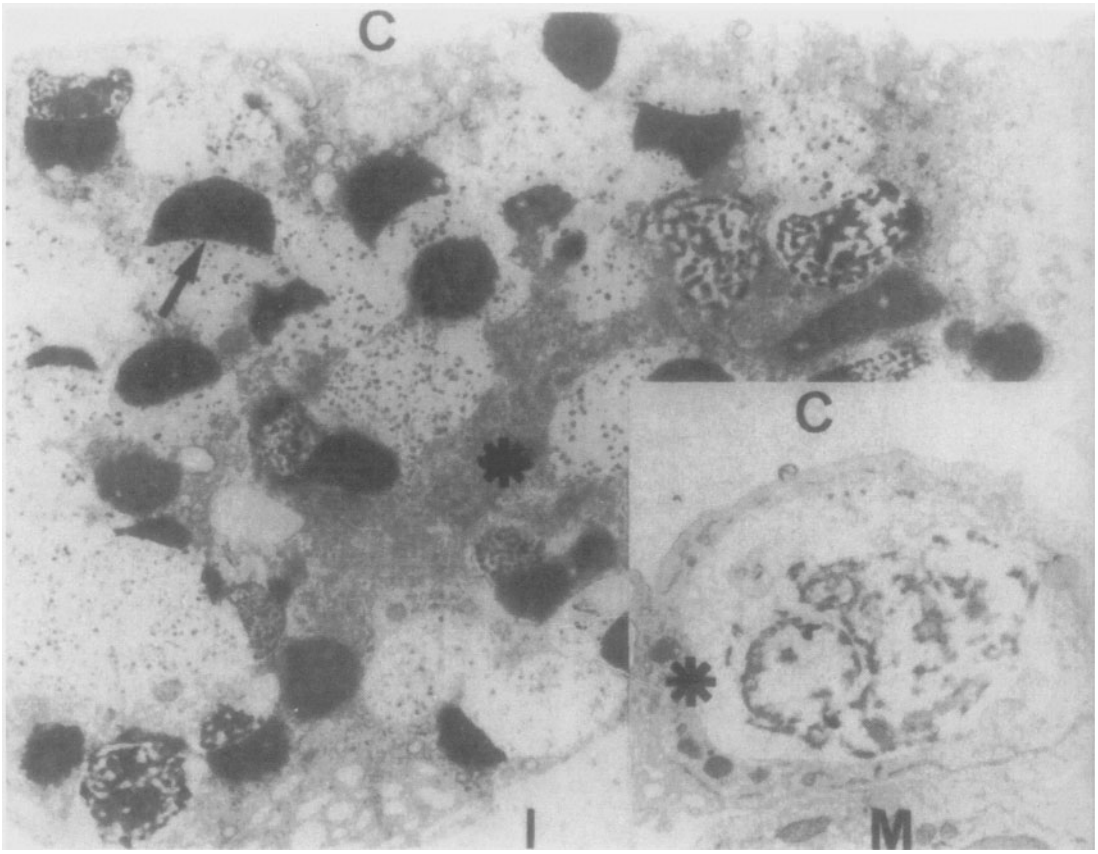

Figure 5. Mesentery of normal rabbit. A macrophage (*) is covering a denuded area of peritoneum (C: abdominal cavity; black arrow: lysosome; I: interstitium). Original magnification ×27 500.
Inset. (Lower right). Mouse mesenteric mesothelium: a signet-ring macrophage (*) is covering a recently implanted mesothelial cell (M) (original magnification ×15 400).

molecules could be transferred across cells by vesicular transport. The methodology followed in this study has been reviewed and criticized, and its conclusions have been refuted [52].

Furthermore, a huge body of scientifically based evidence indicates that endocytosis, transcytosis, as well as potocytosis (an endocytic pathway that utilizes phosphatylinositol anchored membrane proteins and plasmalemmal vesicles or caveolae to concentrate and internalize small molecules) are basic mechanisms used by cells to carry in, out and through the cytoplasm a variety of substances [53]. The following part of our description applies to both mesothelium and endothelium.

Work done basically during the past decade shed new light on the intimal structure of pinocytotic vesicles. Even though their morphometric parameters are more or less homogeneous, differences in nature, function and biochemical structure identified at least two kinds of vesicles showing distinctive characteristics.

Caveolae or plasmalemmal vesicles are membrane domains that represent a subcompartment of the plasma membrane [54], characteristic of all vascular endothelium [55]. In capillary endothelial cells, morphological studies indicate that caveolae are effectors of transcytosis of certain macromolecules across the microvascular endothelium: native as well as modified albumins [56–64) LDL [65–68], protein hormones [69, 70], AGE [71], as well as orosomucoid [72], a 41 kDa glycoprotein that qualifies as a probe for the postulated small pore [73–75]. Furthermore, endocytosis and transcytosis of albumin–gold complexes have been observed in mice peritoneal mesothelium [76] (Fig. 15, inset; Fig. 16, inset).

Schnitzer has demonstrated that transendothelial transport of native albumin through caveolae in both experimental situations (*in vivo* as well as in the *in vitro* set-up) is dependent on the interactions of the probe with the endothelial cell surface protein albondin, a 60 kDa albumin binding protein for-

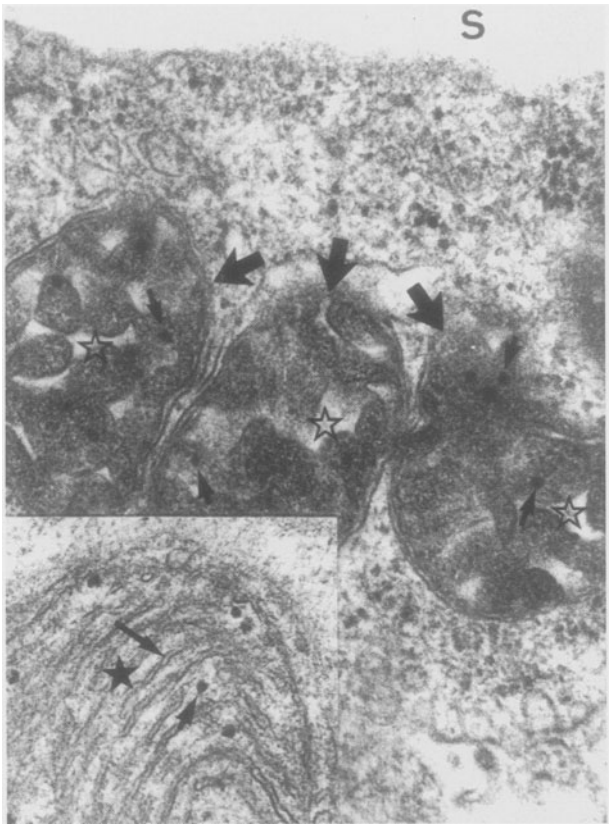

Figure 6. Section of a mesothelial cell seen in a biopsy of parietal peritoneum taken from a patient on CAPD. Mitochondria (open stars) assumed a condensed configuration with increased density of the matrix, blurring of cristae as well as fusions and adhesions of the inner membrane (thick arrows). The matrical granules are still visible (short arrows). These signs of cell injury, in addition to the absence of microvilli, are early signs of impending apoptosis (S: peritoneal space) (×54 600).

Inset. Intact mitochondrion (short star) showing normal cristae (long arrow) and matrical granules (short arrow) (×64 550).

merly called gp60 [60]. Other binding proteins, gp30 and gp18, appear to mediate the attachment, endocytosis and degradation of modified albumin. These vesicular carriers require key intracellular components that are sensitive to alkylation with N-ethylmaleimide. Indeed, this substance has been shown to substantially inhibit native albumin (MW: 67 kDa, $r = 36$ Å) and ferritin (MW $\sim$500 kDa, $r =$ 100–110 Å) uptake, both transcytosed by caveolae [77]. Additional experiments have shown that transcytosis and capillary permeability of insulin and albumin are selectively inhibited by filipin, a complex of polyene antibiotics obtained from *Streptomyces filipenensis,* but does not affect endocytosis mediated by the clathrin-coated vesicles [78]. This concept that identifies two different vesicular pathways is completed with the recent discovery of caveolin, the major structural caveolar protein [79]. This substance is a 22 kDa integral protein that represents a subcompartment of the plasma membrane [54, 80]. Basically, it is a component of the coating covering the luminal aspect of caveolae [81] that, when specifically stained by immunocytochemical methods, serves as a useful marker to draw the diagnostic line between caveolae and other pinocytotic related structures, e.g. coated vesicles [82–84].

Coated pits and coated vesicles (Fig. 15, left and right insets) remain the most extensively characterized transport vesicles. They are involved in the intracellular transport of membrane proteins between a variety of membrane components, mediate endocytosis of transmembrane receptors and transport newly synthesized lysosomal hydrolases from the trans-Golgi network to lysosomes [85]. The luminal coat contains at least six polypeptides, in addition to the above-mentioned 180 kDa polypeptide clathrin [86, 87]. This type of vesicle is also involved in receptor-mediated endocytosis. Cell surface mediators operate endocytosis clusters into clathrin-coated pits, which pinch off to form vesicles that transport the receptors and their ligand [88]. The complex process of invagination, constriction and budding of clathrin-coated vesicles employs the coordinated actions of several proteins. The best-characterized of them is the expanding family of dynamin guanosine triphosphate phosphatases (GTPase), essential for receptor-mediated endocytosis [89, 90]. This enzyme appears to be assembled around the necks of clathrin-coated pits, and assists in pinching vesicles from the plasma membrane [90]. Recently published information suggests that dynamins mediate both clathrin-dependent endocytosis and the internalization of caveolae in microvascular endothelial cells [91, 92].

Some 60 years ago [93], it was suggested that junctions between capillary endothelial cells should be considered the main pathway for exchanges across the microvascular wall. This concept was later extended to the peritoneal blood microvessels and mesothelium, and extensively analysed within the frame of the two [74, 75], and lately, the three [94] pore size model of capillary and/or peritoneal permeability. (Assumed pores size: large pore: >150 Å; small pore: up to 40–45 Å; ultra-small pore: 2–5 Å.) To date, physiological studies and mathematical models have failed to convincingly identify the morphological equivalents of the hypothetical cylindrical water-filled pores [73]. On the other hand, however,

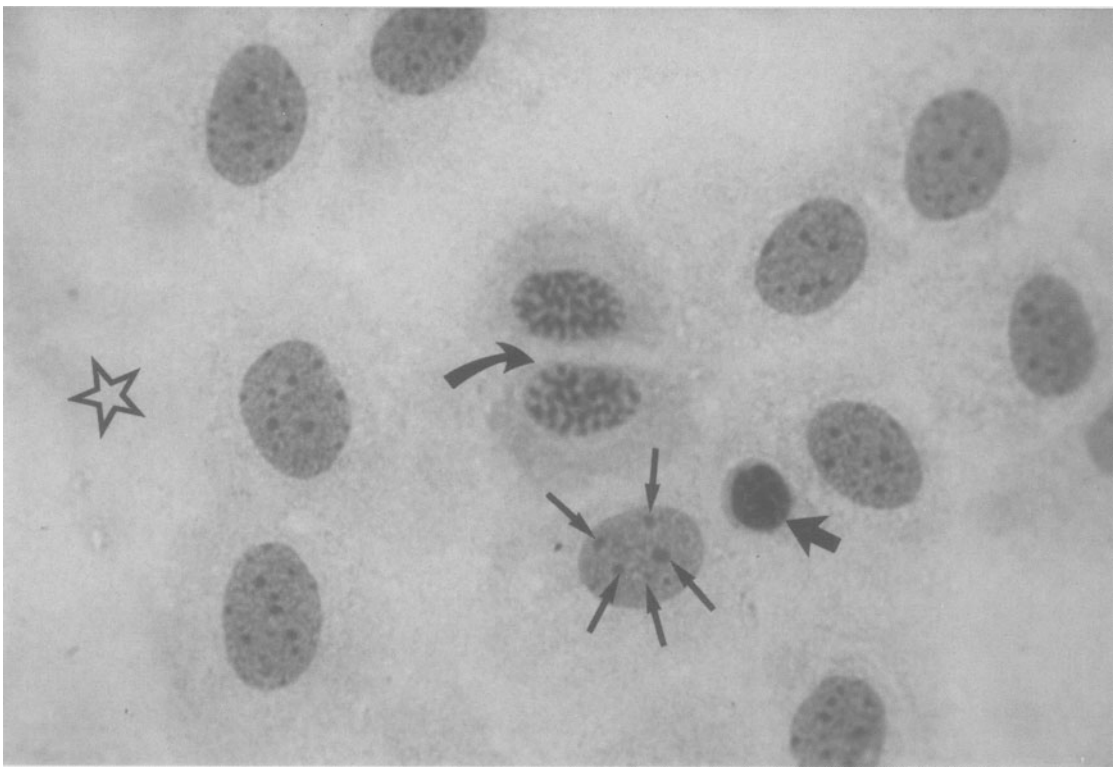

Figure 7. Sample from a mouse injected for 30 consecutive days with 4.25% glucose-enriched dialysis solution. The material was taken 7 days after interruption of the exposure to the dialysis solution (7 days of recovery). This photograph shows the two most critical moments in the life cycle of a mesothelial cell: mitosis (curved arrow), and apoptosis (short thick arrow). Open star shows an area of peritoneum where the mesothelial monolayer is absent (desertic peritoneum). Note the substantially reduced density distribution of cells (small arrows: nucleoli) (haematoxylin–eosin; ×1000).

this short review of the topic testifies that, at least for protein traffic, the vesicular carried hypothesis has been largely proven and accepted in the last few years [77].

Basically, that caveolae and transcellular channels function as a continuous operating conveyor belt, fusing with each other [46, 47, 95, 96], and moving through the cell [95, 96]. The source of energy fuelling vesicular movement remains one of the many questions still open [95–101].

Additionally, recently published evidence demonstrated not only the presence of aquaporin channels in mesothelial cells, but also that their expression can be modulated by both osmotic and non-osmotic stimulation [102]. The relevance of these channels for peritoneal permeability will be analysed in the section dealing with peritoneal microvasculature. Their presence in mesothelial cells is one more indication giving support to Henle's prediction that the essential anatomy and physiology of the peritoneum are located in its 'endothelia' [103].

Simionescu *et al.* [104] showed the existence of differentiated microdomains on the luminal surface of capillary endothelium where they found a distinct and preferential distribution of electronegative fixed charges, also called anionic sites. Cationic tracers, which did not bind to caveolae or to transcellular channels, decorated the luminal glycocalyx, coated pits and coated vesicles [95, 100, 104]. Recent studies applying cationic tracers such as ruthenium red and cationized ferritin in rat and mouse peritoneum, also showed a preferential distribution of negative charges at the level of the mesothelial cells luminal surface [33, 34, 41] (Figs 12 and 17). Density of these surface plasmalemmal charges is substantially reduced in cells undergoing apoptosis [38].

Mesothelial cell boundaries are tortuous, with adjacent cells often tending to overlap (Fig. 4, inset; Fig. 12). Tight junctions close the luminal side of the intercellular boundaries [11, 18, 29] (Figs 4 and 12). When studied in the horizontal plane by

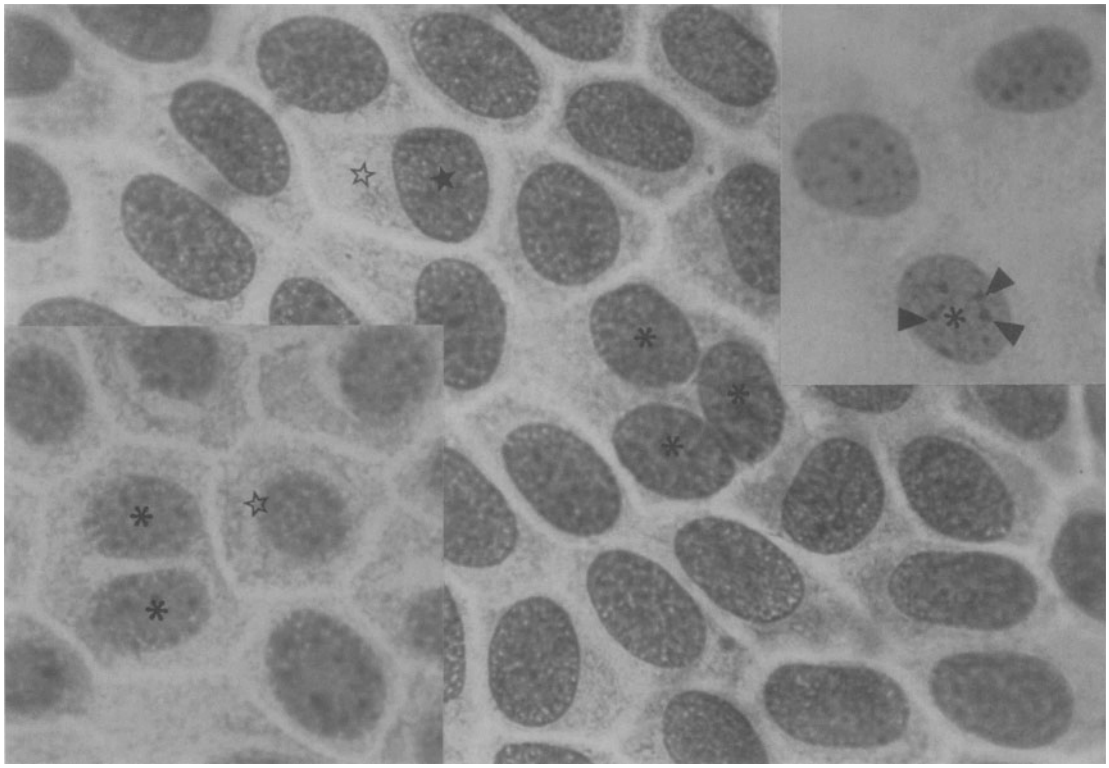

Figure 8. Normal density distribution of mesothelial cells observed in intact, unexposed animals. Asterisks indicate nuclei of a trinucleated cell, rarely seen in normal mesothelium (open star: cytoplasm of mesothelial cell; black star: nucleus). haematoxylin–eosin ×1000.

Lower left inset. Binucleated cells (asterisks) are seldom observed in intact, unexposed mesothelium. Note the polygonal shape of the cell (open star) (haematoxylin–eosin; ×1000).

Upper right inset. Arrow heads point at nucleoli of mesothelial cell nucleus (*) (haematoxylin–eosin; ×1000).

using the freeze–fracture technique these junctional contact areas were defined as cell extensions and finger-like processes, overlapping into the adjacent cell body. Cell processes were wedge-shaped and numerous, and the cell periphery appeared serrated [105]. Desmosomes have also been observed near the cellular luminal front [11, 20, 22, 29] (Fig. 18) and so have gap junctions [22]. The abluminal portions of cell interfaces usually show an open intercellular infundibulum (Fig. 18). Completely open intercellular interphases have not been observed in normal, resting mesothelium [11, 18, 29]. Even desquamated mesothelial cells showing severe degenerative changes can keep their junctional system almost intact (Fig. 19). These junctional morphological features are, however, different from those observed between mesothelial cells covering the diaphragmatic lymphatic lacunae, which are more cuboidal and prominent than mesothelial cells observed in other areas of the peritoneal surface.

The existence of stomata (open intermesothelial communications between the abdominal cavity and the submesothelial diaphragmatic lymphatics), predicted by William Hewson [1] 100 years before being discovered by Von Recklinghausen [106], have been the subject of a long and rich controversy along the years. Accepted by some [107–109] and denied by others [110–112], it was not until the advent of electron microscopy that their existence was demonstrated [41, 113, 114]. Scanning electron microscopy disclosed the patent intermesothelial junctions forming gaps whose average diameter ranged between 4 and 12 μm [113, 114] and circumscribed by cuboidal mesothelial cells. These gaps open into submesothelial lymphatics [41] and have not been observed in diaphragmatic mesothelium covering non-lacunar areas [114]. Additional studies have shown the passage of particles from the abdominal cavity into the submesothelial diaphragmatic lymphatics [115, 116]. These studies also con-

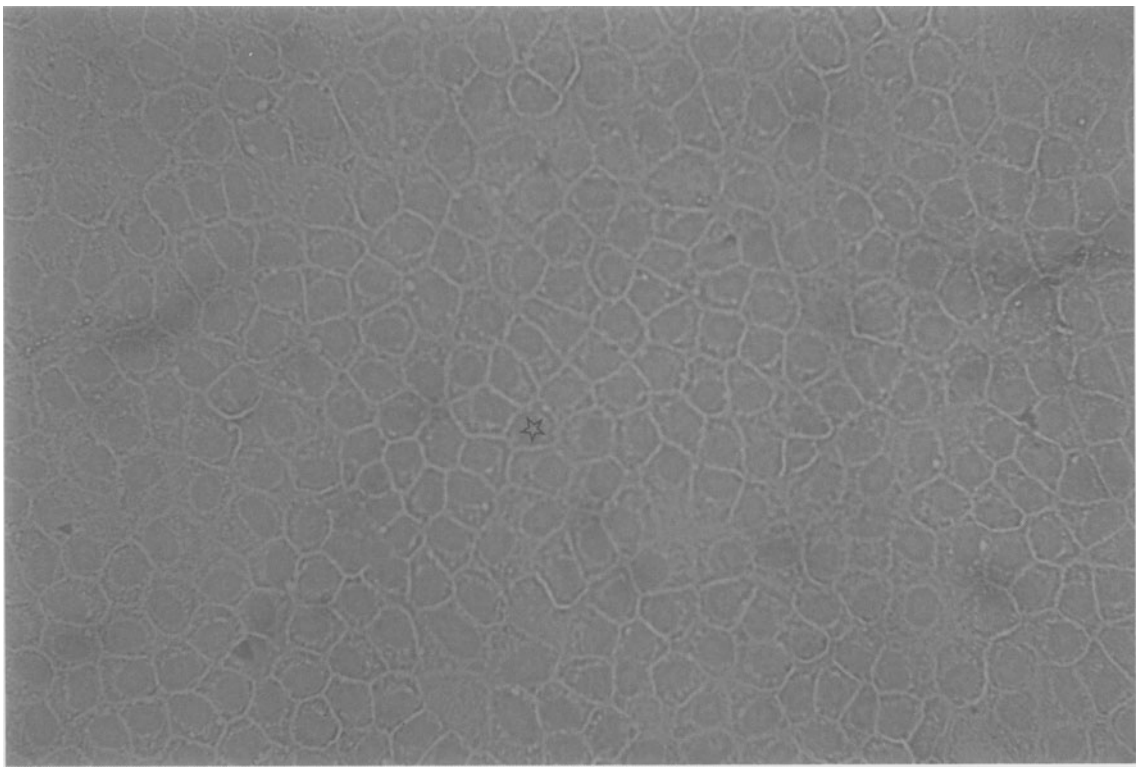

Figure 9. Cell viability evaluated on visceral mesothelium by Trypan-blue exclusion in an intact unexposed mouse. The stain did not permeate the cell membrane (open star: mesothelial cell) ($\times 400$).

firm the results of experiments performed by Allen [117], who demonstrated the passage of frog erythrocytes through stomata of the mouse diaphragmatic peritoneum, and their appearance within submesothelial lymphatics. This pathway paved the way for intraperitoneal blood transfusions that have been successfully performed in fetuses [118, 119], human adults [120], rats, mice, dogs and lambs [121, 122]. On the other hand, intraperitoneal malignant cells [123] and bacteria [124] also leave the abdominal cavity on their way to the central venous circulation, through diaphragmatic stomata. The same pathway applies for absorption of albumin–gold complexes injected into the peritoneal cavity (Fig. 16) [76]. These structures can be found only between mesothelial cells overlying lacunae.

At the sites of stomata and their channels, mesothelial and lymphatic endothelial cells contain actin-like filaments [125] assumed to induce cell contraction, opening the stomatal pathway for the passage of macromolecules and cells. Cationized ferritin has been observed decorating the glycocalyx of mesothelial and lymphatic endothelial cells located along the stomata, as well as the coated pits and coated vesicles of both types of cells [41, 126]. It should be noted that the presence of stomata has been recently detected in mouse mesenteric mesothelium [127], in omental, ovaric and pelvic peritoneum, as well as in that covering the anterior liver surface and the anterior abdominal wall [128, 129]. Therefore, it may be assumed that all these extradiaphragmatic openings contribute to the absorptive capacity of the entire peritoneal membrane. Albumin–gold complexes appear to be absorbed also from the peritoneal space through stomata [76] (Fig. 16), even though the capability of this pathway for the uptake of the probe did not seem to be much higher than that shown by non-stomatal mesothelial infundibular junctions that contained only 1% of the injected tracer.

Stomata have been ascribed the role of a preferential pathway for the output of fluids, cells, particles and bacteria from the abdominal cavity [130]. However, the luminal surface of mesothelial cells (which limits the gaps), after staining with cationized ferritin, displayed dense labelling of their cytoplasmic plasmalemma as well as coated pits and coated vesicles. The same cationic tracer also decorated the

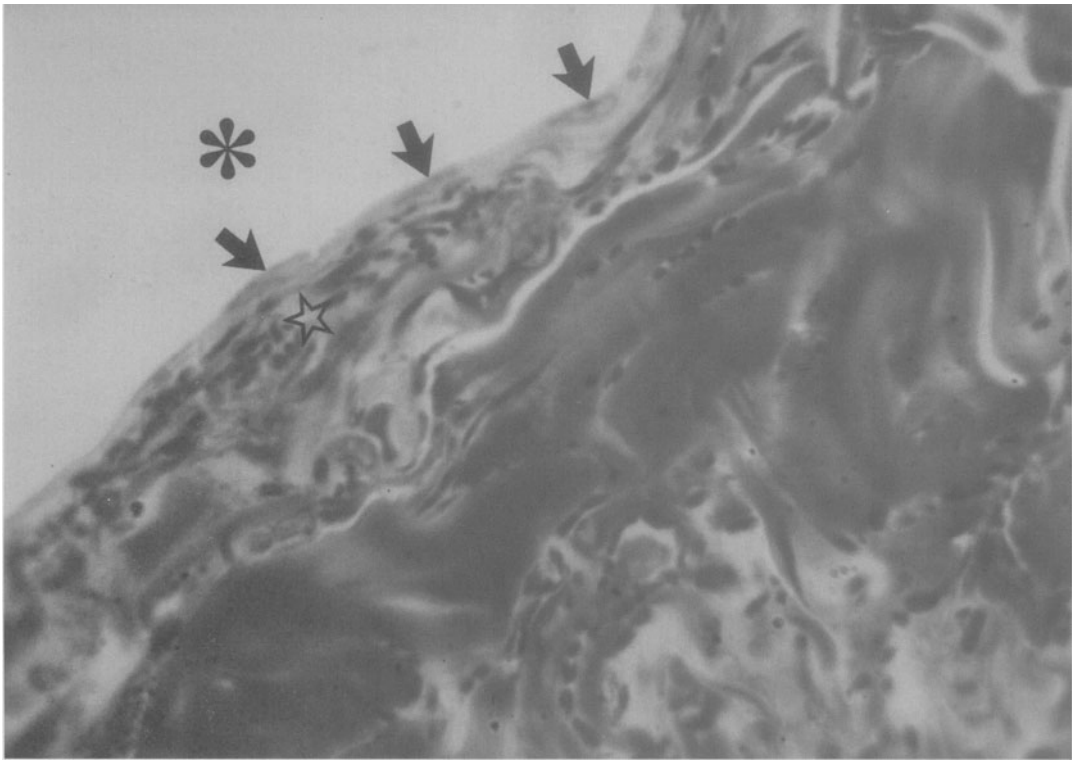

Figure 10. Biopsy of parietal peritoneum taken from a uraemic patient at the time of implanting the first dialysis catheter. Arrows point at nuclei of mesothelial cells. Open star was placed on the submesothelial interstitial tissue, the thickness of which ranges between 37 and 62 μm (*: peritoneal cavity) (toluidin blue; ×400).

lymphatic endothelial plasmalemma, which circumscribed the stomatal openings [41]. If this is so, the passage of solutes through stomata is most likely dependent not only on molecular weight, size and shape, but also on electric charge [41].

Studies in rat and mouse perfused with ruthenium red revealed that intermesothelial cell junctions were, in general, stained just at the level of their infundibulum, even though the dye now and then decorated the junctional complex, staining approximately 50% of its length [34] (Fig. 12).

Nuclei are generally located in the central region of mesothelial cells, showing an elongated, oval or reniform appearance with occasional irregularities in their outlines and sometimes protrusions and identations (Fig. 11). The chromatin is fine, evenly distributed and forms a dense rim around the nuclear membrane (Fig. 11). In normal unexposed mesothelium, around 2% of cells are binucleated [28] (Fig. 8, left lower inset; Fig. 20). Nucleoli have been reported both as present and absent [18, 29]. However, studies performed in imprints [28] showed that they are present and that their number ranges between 6 and 8 (Fig. 7). Rough endoplasmic reticulum and ribosomes are dispersed in the cytoplasm. Mitochondria and the Golgi complex are evident mainly in perinuclear areas (Figs 6 and 11). Although seldom observed, isolated cilia may emerge from the luminal aspect of mesothelial cells, showing in their cytoplasmic part the axial microtubule as well as the attached basal body (Fig. 4). More frequently observed in splenic mesothelium [131], their functional significance is still unknown [132].

The submesothelial basement membrane, originally described by Todd and Bowman [133], and later reported as hyaline, homogeneous, one-layered and continuous [107, 134], with an average thickness of approximately 40 nm for mouse and rabbit peritoneum [11, 19], normally appears lying under the mesothelial layer of visceral, parietal and diaphragmatic peritoneum [135] (Figs 11 and 18). As an exception, the functional significance of which is still unknown, the omental mesothelium of mice and humans lacks basement membrane [19, 136].

Submesothelial basement membrane of visceral, parietal and diaphragmatic peritoneum of rat and mouse, perfused with the cationic tracer ruthenium

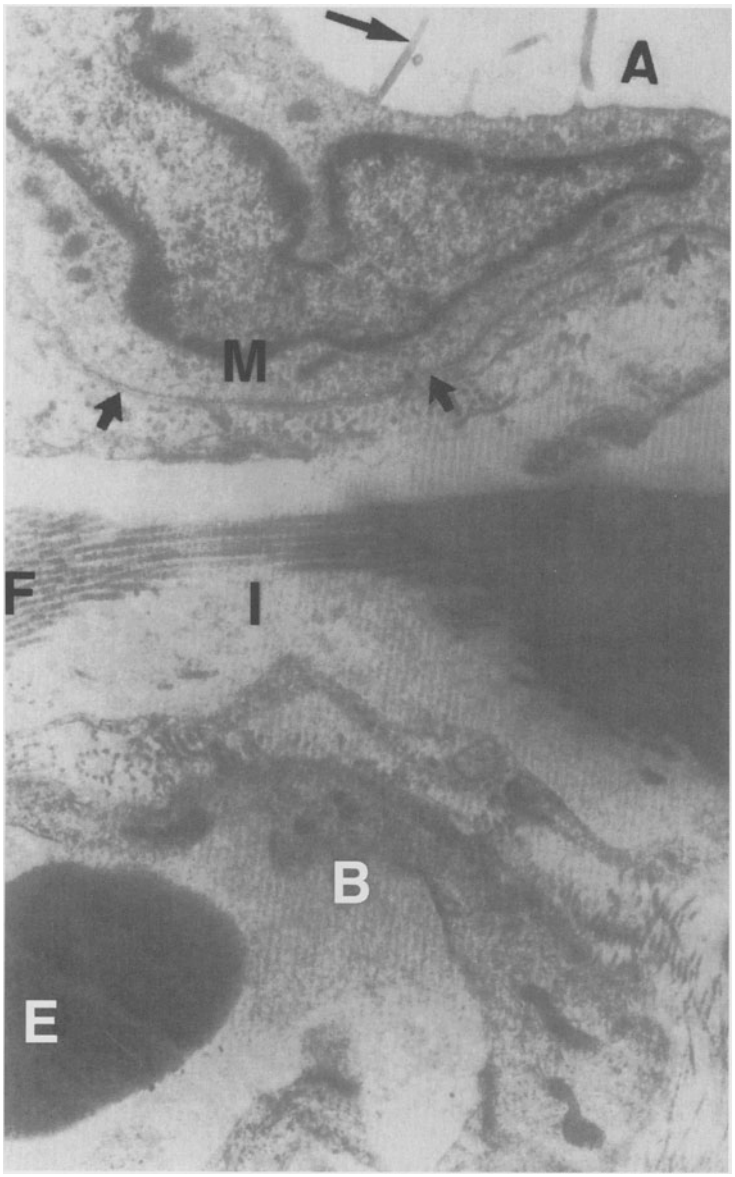

Figure 11. Rabbit mesentery: normal resting mesothelial cell (M) lying on a continuous basement membrane (short arrows) (A: abdominal cavity; long arrow: microvilli; I: interstitium; F: collagen fibres; B: blood capillary; E: erythrocyte) (original magnification ×27 500).

red, consistently showed anionic charges periodically distributed along the lamina rara externa and interna, most of the time, forming double rows [33, 34] (Fig. 12).

The reported average diameter of ruthenium red-stained particles in the basement membrane was 2.7 nm, whereas the average distance measured between the one-row oriented basal lamina dye particles ranged between 65 and 90 nm, not far from the interval value of 60 nm observed using the same tracer in rats [137] and human kidney glomeruli [138].

The fact that these charges are, as stated above, distributed along both aspects of the basement membrane implies that the charge-free interval is actually smaller than the mean distance calculated for each membrane layer. The electric field of each particle of ruthenium is around 8–10 nm, and charge discrimination for negative tracers is effective for substances with a molecular radius around 1 nm,

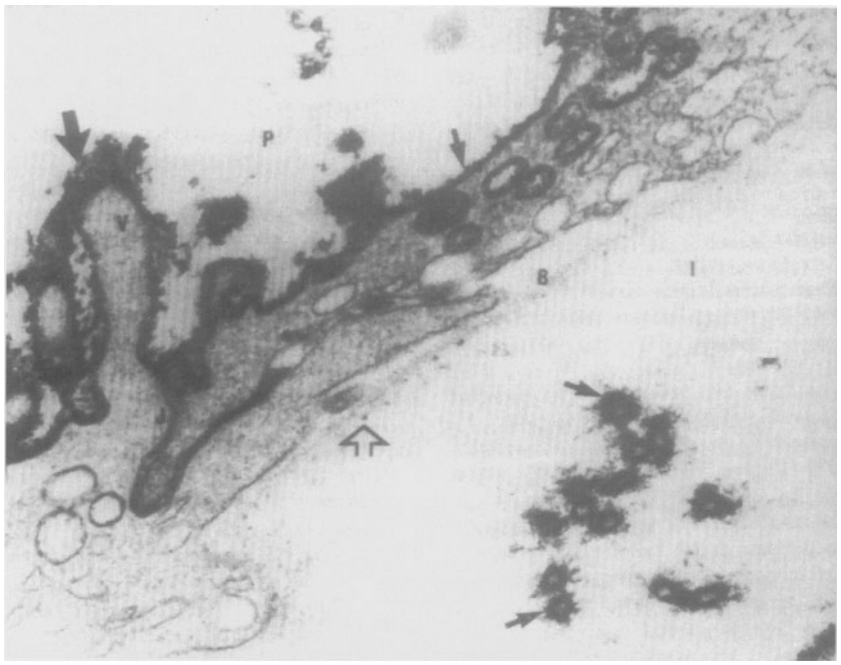

Figure 12. Section of rat mesentery showing microvilli (V) with heavily ruthenium-red decorated glycocalyx (large arrow), also evident on the mesothelial cell plasmalemma (small arrow). The cationic dye also stains a long portion of the intercellular junction (J). The basement membrane (B) shows quite regularly distributed anionic sites (open arrow) (P: abdominal cavity; I: interstitium). Original magnification $\times 50\,720$.

Inset. Rat mesentery: transversal section of microvilli showing the fibrilar ruthenium red-stained glycocalyx (arrows) ($\times 50\,720$).

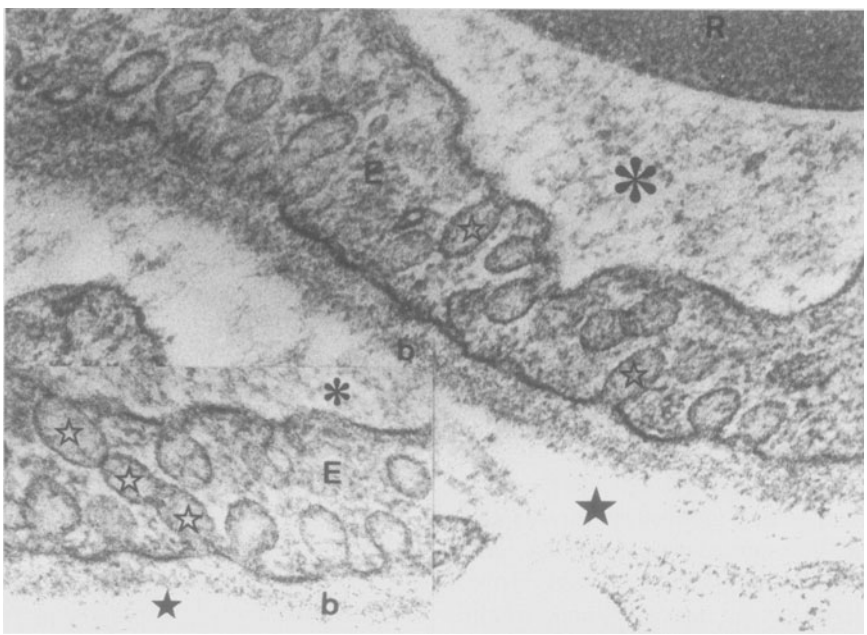

Figure 13. Continuous blood capillary of rat mesenteric peritoneum. Plasmalemmal vesicles (open stars) are open to both aspects of the endothelial cell (E) (R: red blood cell; *: microvascular lumen; b: subendothelial basement membrane; black star: interstitial space) ($\times 87\,000$).

Inset. Another capillary from the same sample, showing a transcellular channel made up by a chain of three plasmalemmal vesicles (open stars), connecting both aspects of the endothelial cell (E) (*: microvascular lumen; b: subendothelial basement membrane; black star: subendothelial interstitial space) ($\times 87\,000$).

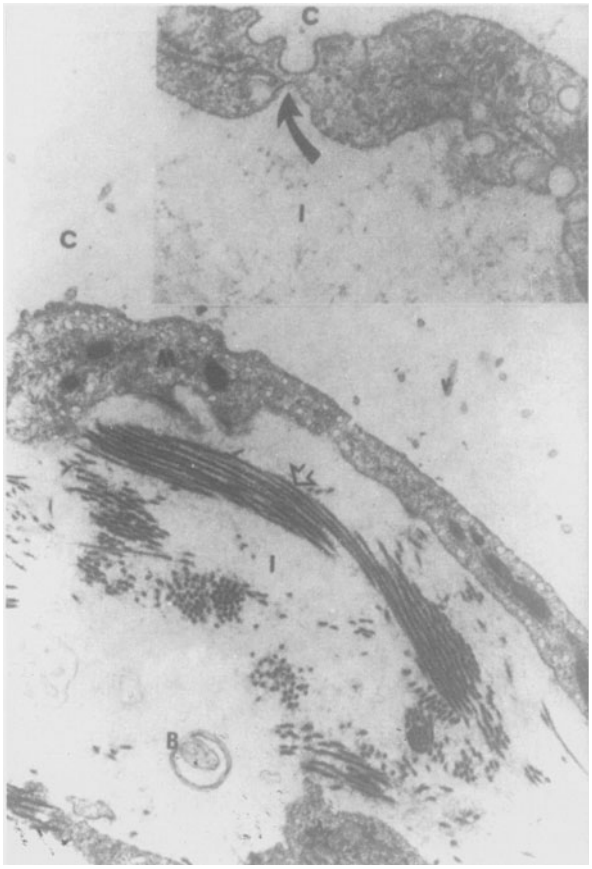

Figure 14. Sample of rat mesentery obtained after 13 intraperitoneal injections of 0.2% furfural, performed on a daily basis. Microvilli (V) are present. The elongated mesothelial cell (M) is lying directly on the connective tissue. The basement membrane is absent. Note the intensity of interstitial edema (I), which is evident even between the collagen fibres (open arrow) (B: myelinoid body; C: abdominal space) (original magnification ×15 400).

Upper right inset. A different area of the same sample showing a transmesothelial channel (black arrow) formed by two vesicles. Notice the lack of submesothelial basement membrane (I: edematous interstitium; C: abdominal cavity) (original magnification ×41 500).

corresponding approximately to a globular molecule showing a molecular weight of 2 kDa [139]. In this sense it should be taken into account that the radius of macromolecular anionic albumin is 3.6 nm, whereas its molecular weight is 67 kDa.

It should be noted that the density distribution of these anionic fixed charges of the basement membrane almost disappears during the acute inflammatory reaction secondary to septic peritonitis [140] (Fig. 21), and is substantially reduced in rats, soon after 4 months of streptozotocin-induced, uncontrolled diabetes [141] (Fig. 17).

The relevance of the electronegative charge of the mesothelial monolayer upon the peritoneal permeability to anionic plasma proteins will be discussed in the section dealing with microvascular permeability.

Reduplicated submesothelial basement membrane has been observed in diabetic and non-diabetic chronic uraemic patients treated by maintenance peritoneal dialysis [142, 143] (Fig. 22). It has been shown that perivascular basement membrane thickness increases with age [144, 145] as well as in the direction of head to foot [145, 146]. This same ultrastructural alteration has been observed in diabetics [145, 147]. It has been suggested that diabetes alone is not responsible for excessive accumulation of basement membrane associated with ageing [148]. Therefore, it could be claimed that the reduplication of basement membrane observed in human mesothelium is a by-product of cell renewal regardless of the cause of cell death that triggers the process of repopulation [142, 149]. However, the fact that this phenomenon was also detected in the submesothelial basement membrane of diabetic rats suggests that a high glucose content in the extracellular fluid appears to be related to the mechanism(s) leading to these changes [141].

Interstitium

Connective tissue, which originates from mesenchyma, is composed of cells and fibres embedded in an amorphous substance. The main connective tissue cell is the fibroblast and the main fibre is collagen [150].

The submesothelial connective tissue normally has a low cell population surrounded by high molecular weight intercellular material. Fibroblasts, mast cells in the proximity of blood microvessels (Fig. 23), occasional monocytes and macrophages (Fig. 2) are frequently observed.

Substantial amounts of quite compact bundles of collagen are usually interposed between the blood microvessels and the mesothelial layer (Figs 1, 2 and 3). The collagen density distribution in the different regions of visceral peritoneum is quite variable [144].

The macromolecular common denomination of connective tissues is a broad molecular class of polyanions: the tissue polyaccharides. They form a gel-like structure with the collagen fibres [151] which, when stained with ruthenium red, shows the presence of anionic fixed charges [34].

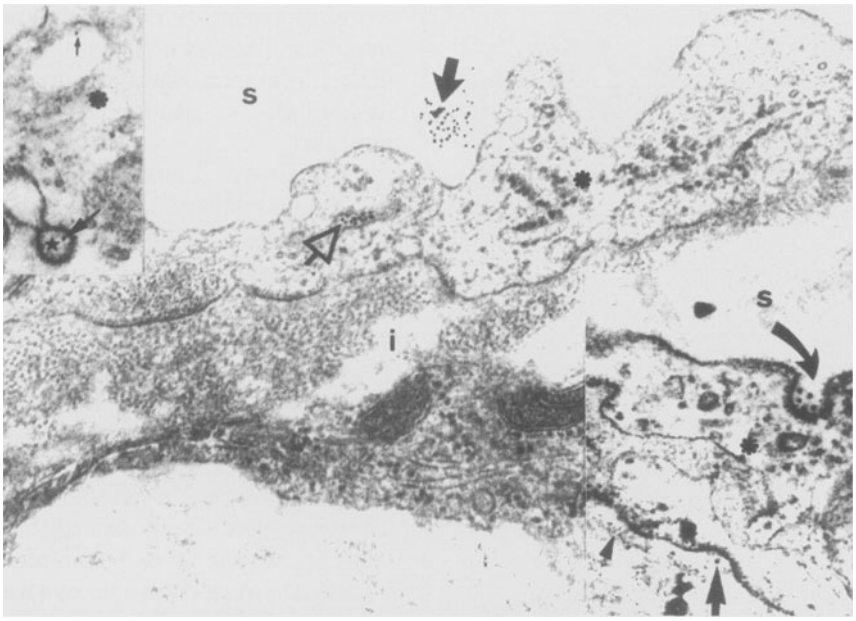

Figure 15. Diaphragmatic peritoneum of a mouse taken 10 min after intra-arterial perfusion with gold-labelled albumin. Some particles (black arrow) can be seen in the peritoneal space (s). The mesothelial cell (*) shows a multivesicular body (open arrow) containing particles of the tracer (I: interstitial space) (× 41 500).

Upper left inset. Cytoplasmic compartment of a mesothelial cell (*) showing albumin–gold complexes decorating the membrane luminal aspect of a pynocytotic vesicle (small arrow), as well as that of coated vesicle (big arrow) (× 64 550).

Lower left inset. Particles of the tracer decorating the luminal glycocalyx of a coated pit (curved arrow) of a mesothelial cell (*), seen in the same sample. The tracer is also present in the abluminal aspect of the mesothelial cell (straight arrow), between the plasmalemma and the submesothelial basement membrane (arrowhead) (× 64 550).

Thickness of the interstitial layer is extremely variable in the different portions of the peritoneum. This heterogeneity can also be applied to the distances separating the submesothelial blood vessels from the peritoneal cavity, ranging between 1–2 μm to ⩾30 μm (Fig. 1). It should be noted that restriction of molecular movement through the interstitial tissue and its progression from or to the microvasculature is affected not only by their molecular weight, shape and electric charge, but also by the length of the pathway. According to Fick's law of diffusion, it is the difference in concentration per unit of distance (the concentration gradient) which determines the rate of movement of the solute. If we double the distance over which the same concentration difference occurred, the gradient and, therefore, the rate of transfer, would be cut in half. Therefore, the relevance of the interstitial compartment thickness in the transperitoneal transfer of solutes may well be critical [75, 152], and diffusion of solutes coming out from capillaries far from the abdominal cavity could be rendered useful only in long-dwell exchanges, like those performed in CAPD.

The question of the interstitium in terms of plasma to lymph traffic of macromolecules has been basically investigated in lung interstitial tissue [153], which, at physiological pH, has the properties of a negatively charged membrane [154]. Therefore, the polyanionic glycosaminoglycans (mainly hyaluronan) and glycoproteins located in the interstitial ground substance have the capability of influencing the interstitial distribution volumes of plasma proteins coming out from the intravascular compartment, according to their molecular charge [155]. It has been suggested that these glycosaminoglycans restrict free diffusion through the interstitium [156] and can both reduce the interstitial distribution volume of anionic plasma proteins, and retard the plasma-lymph traffic of cationic macromolecules [153]. Anyway, the effect of protein charge on the interstitial hydraulic conductivity has been only partly clarified.

The extremely low and, at times, negative interstitial pressure (0 to −4 mmHg) [157–159] represents, together with the capillary permselectivity and the lymphatic drainage, one of the three key factors modulating the plasma-to-lymph fluid traffic, therefore, preventing the formation of interstitial oedema [160, 161]. Specifically, during peritoneal dialysis, studies by Flessner [162] have shown that transfer

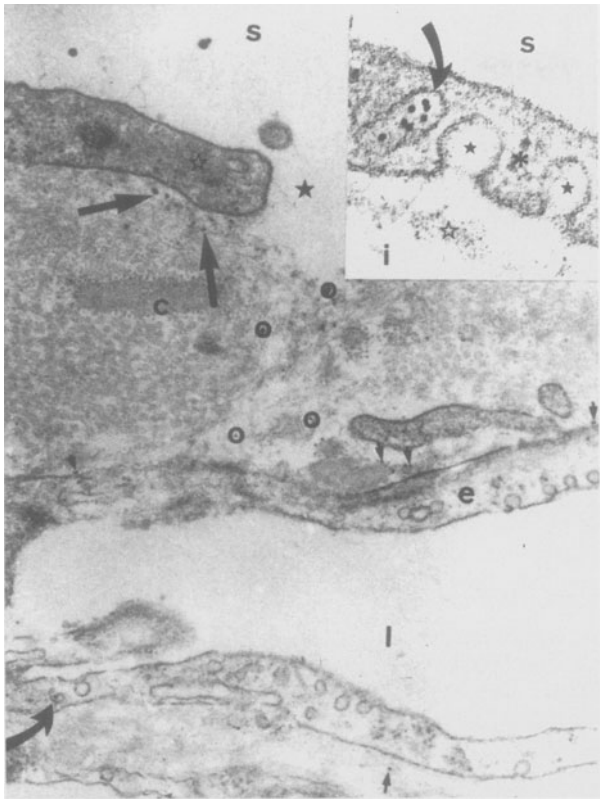

Figure 16. Diaphragmatic peritoneum of a mouse, taken 10 min after intraperitoneal injection of albumin–gold complexes. The black star points at stomata communicating the peritoneal space(s), and the submesothelial connective tissue (c). Albumin–gold complexes (large straight arrow) are present immediately under the mesothelial cell (open star), between collagen fibres (open circles), as well as in the submesothelial interstitial space, near the lymphatic lacuna (short straight arrows). The curved arrow points at a particle of the tracer included in an endothelial pinocytotic vesicle (l: lymphatic lacuna; c: interstitial space) (×30 740).

Inset. Mouse diaphragmatic mesothelium taken 10 min after intraperitoneal injection of albumin–gold complexes. Arrow indicates an endosome containing particles of the tracer (S: peritoneal space; *: mesothelial cell cytoplasm; black star: plasmalemmal vesicles; open star: submesothelial basement membrane; I: interstitial space) (×64 550).

Used with permission from *Kidney International*, **47**: 1274–84, 1995.

of small solutes through the tortuous interstitial pathways is primarily by diffusion, and that convection may contribute to overall transport in parietal tissue. As stated above, in normal conditions the interstitium has hydrostatic pressure near 0 [157, 162]. During clinical peritoneal dialysis the intra-abdominal pressure ranges between 4 and 10 cm H_2O [163, 164], thus creating a pressure gradient that drives fluid as well as solutes out of the peritoneal cavity to the interstitium. Thus, fluid loss from the abdominal cavity to the periperitoneal interstitial space is directly proportional to intra-abdominal pressures higher than 2 cm H_2O [164].

Blood microvessels

Capillaries of human and rodent parietal [165] and visceral peritoneum [40, 166] have been reported to be of the continuous type (Figs 1, 3, 24, 25 and 26), according to the classification of Majno [167]. However, the existence of fenestrated capillaries in human parietal and rabbit diaphragmatic peritoneum (Figs 1 and 27), as well as in mouse mesentery [168–170] has been reported. The incidence of fenestrated capillaries in human parietal peritoneum appears to be low (1.7% of the total number of capillaries) [170]. The reported density of fenestrated microvessels in mouse mesentery and rabbit diaphragmatic peritoneum ranged between 26% and 29% of the observed capillaries, whereas their presence in parietal peritoneum of non-dialysed uraemic patients was only 1.7%. It should be noted, however, that the anterior abdominal wall of humans comprises less than 4% of the peritoneal surface area [10]. Diameter of fenestrae, which ranged between 60 and 90 nm, is well within the range of fenestrae observed in other capillary beds: 40–70 nm in renal peritubular capillaries [171], glomerular capillaries [167], and rabbit submandibular gland [172]. The reported density of fenestrae counted along the capillary circumference of mice mesenteric microvessels is 3.4 fenestrae/micron [173]. This value is quite close to that of 3 fenestrae/micron of capillary circumference observed in renal glomerular capillaries [167]. Density of fenestrae per square micron of endothelial surface is 45–60/μm^2 in renal peritubular capillaries [174] and 20/μm^2 in renal glomerular capillaries [167], whereas their frequency in mouse mesenteric capillaries is approximately 12/μm^2 [169].

The density distribution of submesothelial microvessels along the different portions of the peritoneum is variable. In the rabbit the mesentery appears to be the most vascularized peritoneal segment (contributing 71.1% of the total number of observed capillaries). The reported diaphragmatic and parietal contributions to the total microvascular bed examined were 17.9% and 10.9% respectively [175].

In rabbit mesentery the main population of continuous blood microvessels is represented by:

1. True capillaries (without perithelial cells), the mean luminal diameter of which is 7.2 μm and

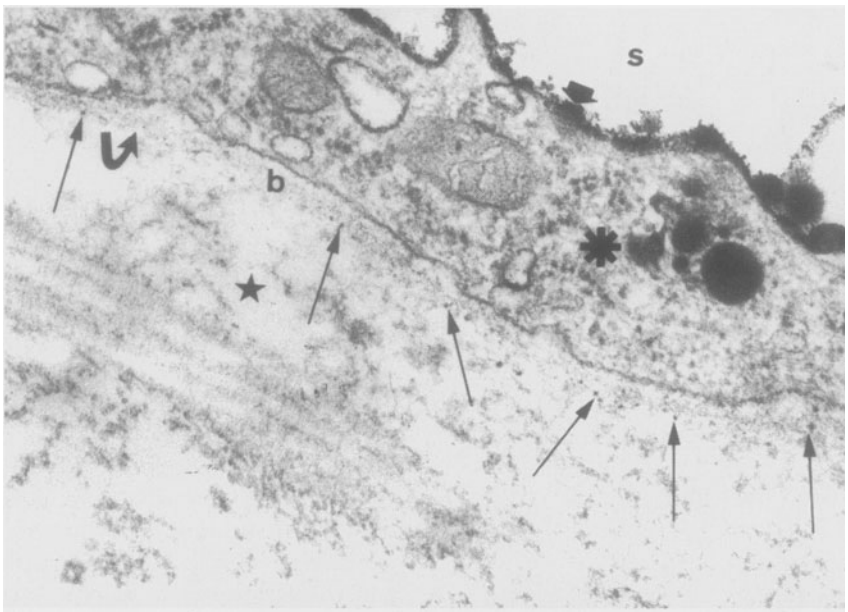

Figure 17. Mesenteric mesothelial cell of a diabetic rat (*). The animal was perfused with ruthenium-red 6 months after induction of the disease, with streptozotocin (glucose blood levels were higher than 500 mg/dl; glycated haemoglobin: 16.38 ± 0.57%). Glycocalyx covering the cavitary aspect of the mesothelial cell is heavily decorated by the cationic tracer (thick arrow). The submesothelial basement membrane (b) shows few dispersed anionic sites (long arrows), as well as areas where they are completely absent (curved arrow) (s: peritoneal cavity; black star: interstitial space) (×41 500).

whose mean wall thickness is 0.4 μm (Figs 11, 24, 25 and 26).

2. Venous capillaries usually formed by the confluence of two or three capillaries. These show a thin endothelial layer, occasional peripheral perithelial cells, and have a mean luminal diameter of 9.2 μm.
3. Postcapillary venules whose luminal diameter ranges between 9.4 and 20.6 μm [40].

With increasing luminal diameter there is a proportional increase in wall thickness due to the presence of more perithelial cells encircling the endothelial layer [176] (Fig. 25). The average ratio of luminal diameter to wall thickness is approximately 10/1 [176]. All aforementioned exchange vessels present at their luminal aspect a limiting area that separates the endothelial cell from the circulating blood and is formed by the plasmalemma with its trilaminar structure [16] (Fig. 26) and the glycocalyx (Fig. 26). The latter, originally described by Luft [35] in other vascular beds, has also been observed at the luminal aspect of peritoneal microvessels [36, 177] The presence of sialoconjugates, proteoglycans and acidic glycoproteins organized as a fibrous network provides the plasmalemmal glycocalyx with electronegative charge [178] (Fig. 28).

There is evidence that anionic plasma proteins (albumin and IgG) are adsorbed to the glycocalyx of microvascular endothelial cells [179]. The fibre-matrix model of capillary permeability envisages the glycocalyx as a meshwork of glycoprotein fibres which, after adsorbing circulating proteins, would tighten its mesh, thereby rendering the underlying endothelium less accessible to water and other water-soluble molecules [37]. Furthermore, it has been shown that the adsorption of circulating anionic plasma proteins to the glycocalyx renders the underlying endothelium relatively impermeable to large, electron-dense, anionic tracers such as native ferritin (MW ~450 kDa) [179].

The mean endothelial cell width of rabbit mesenteric capillaries is 0.4 μm, unless the cytoplasm bulges up to more than 1 μm at the site of the nucleus (compare Figs 3 and 24 with Fig. 26). The cytoplasm includes the usual cell organelles: mitochondria, rough endoplasmic reticulum and free ribosomes [11, 167].

The mitochondrial content of vascular endothelial cells in frog mesentery decreases gradually from arterioles towards venous capillaries and subsequently increases toward venules [180].

The Golgi complex displays variable degrees of development in biopsies taken from different

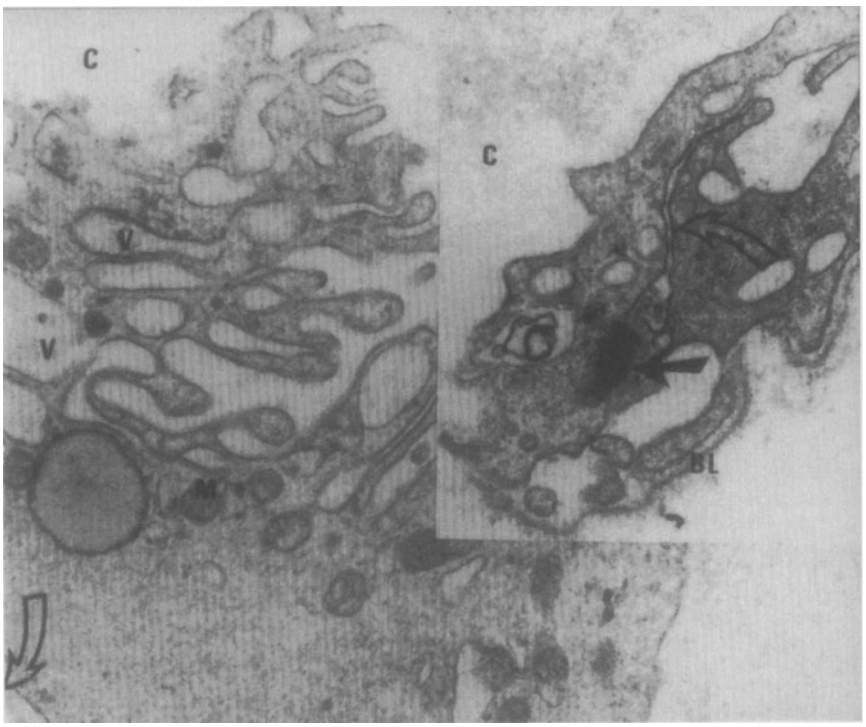

Figure 18. Biopsy of parietal peritoneum taken from a 67-years-old chronic uraemic patient, who was on IPD for a period of almost 2 years. A young mesothelial cell shows numerous vacuoles (V) giving a worm-like appearance, which is why this structure is called micropinocytosis vermiformis. The abluminal aspect of the mesothelial cell is lying on a hyaline basement membrane (open arrow) (C: abdominal cavity; M: mitochondrion) ($\times 26\,000$).

Upper right inset. Another area of the same biopsy. This electron micrograph shows the vacuolized cytoplasm of two adjacent mesothelial cells developing a new intercellular junction (open arrow). Note the presence of a typical desmosome (black arrow). The basement membrane (BL) is still discontinuous (original magnification $\times 30\,740$).

patients. This same variability was observed when comparing different peritoneal microvascular endothelial cells present in a single sample.

The cytoplasmic matrix of endothelial cells shows long filaments, parallel to the longitudinal cellular axis. Their diameter ranges between 20 and 100 Å [167], and at times they appear in bundles. These intermediate-size filaments seem to be a common component of the cytoplasmic matrix of vascular endothelial cells showing, however, a lower density distribution than that observed in other cell types [132].

Nuclei are generally oval, elongated (Fig. 24) or occasionally kidney-shaped with focal surface irregularities (Fig. 11). Their mean short-axis width in rabbit mesentery is 0.957 ± 0.417 μm [11].

Plasmalemmal vesicles, which can be found in most cell types, are particularly common in capillary endothelia [181], where they occupy approximately 7% of the cell volume [98] (Fig. 25). Their outer diameter is approximately 700 Å (it ranges between 500 and 900 Å) [11, 33, 47] and they have a round or oval shape surrounded by a three-layered membrane of 80 Å thickness (Fig. 26, inset).

According to their location in the cytoplasmic matrix, vesicles can be classified into three groups: (a) vesicles attached to the plasmalemma limiting the blood front of the endothelial cell; (b) free vesicles within the cytoplasmic matrix; (c) attached vesicles, but this time to the tissue front of the endothelial cell plasmalemma [47] (Fig. 25). The density population of plasmalemmal vesicles varies considerably from one vascular segment to another, even within the same microvascular territory [46, 47]. In the mouse diaphragm, arterioles show 200 vesicles/μm^2, true capillaries 900 μm^2, venular segments of capillaries 1200 μm^2 and postcapillary venules 600 μm^2 [46].

Most vesicles that open to the extracellular medium have necks whose diameter can be as small as 100 Å [47]. Transendothelial channels formed by a chain of vesicles opening simultaneously on both fronts of the endothelium have been described in capillaries of mouse diaphragmatic muscle [46] as

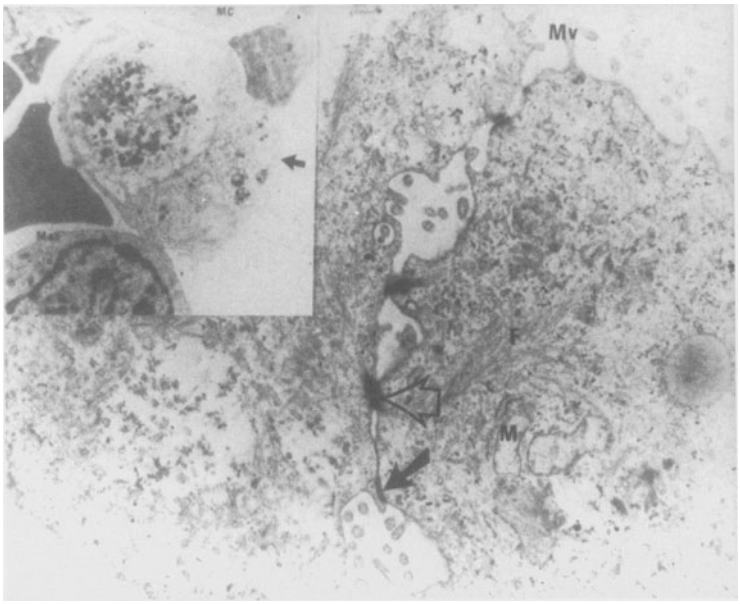

Figure 19. Effluent dialysate obtained from a non-infected patient on peritoneal dialysis. Two desquamated mesothelial cells show severe degenerative changes: swollen mitochondria (M) with broken membranes, sheaves of filaments (F), and swollen cytoplasm. Part of the tight junction is still present (black arrow), as well as a desmosome (open arrow) (M: microvilli) (original magnification ×15 400).

Upper left inset. Effluent dialysate obtained from the same patient. Note the presence of a signet-ring macrophage (arrow), as well as part of two floating mesothelial cells (Mc) (mac: macrophage) (original magnification ×8600).

well as in postcapillary venules of rabbit and rat mesentery (Figs 25 and 29) [11]. The relative frequency of transendothelial channels has been found to be higher in true capillaries than in arterioles and venules, with the highest density in the venular segment of capillaries [100]. Microvessels of frog mesentery showed a density distribution of three transendothelial channels for every 400 vascular profiles examined [180]. Just as in observations made on mesothelial cells, plasmalemmal vesicles and transendothelial channels do not bind cationic electron-dense tracers which, on the other hand, decorate the luminal aspect of coated pits and coated vesicles [95, 104] in the peritoneal microvasculature [34].

The functional significance of plasmalemmal vesicles or caveolae vesicles, transendothelial channels, coated pits and coated vesicles was discussed in the section on normal epithelium.

As stated above, in fenestrated capillaries, endothelial cells are pierced by fenestrae closed by a diaphram [182] (Fig. 24, inset; Figs 27 and 30). Fenestrae are not static structures. It has been shown that their prevalence can be increased under the effect of vitamin A metabolites [183], the influence of sexual hormones [166], thrombocytopenia [184], and by the acute inflammatory reaction [167]. In this sense a microvascular bed (capillaries and postcapillary venules), supplied with a continuous endothelium, can rapidly develop endothelial fenestrations under the influence of vascular endothelial growth factor (VEGF), a 34–42 kDa cytokine, released by different cell types (eosinophils, neutrophils, and others) during the acute inflammatory reaction [185–188]. This effect has been demonstrated *in vivo* [189, 190], after acute and chronic exposure of different microvascular beds.

High concentrations of negative fixed charges (heparin and heparan sulphate) have been found on the blood front of fenestral diaphragms in several microvascular beds [95, 104, 182, 191–194]. They are expected to discriminate against anionic macromolecules, essentially anionic plasma protein. Similarly, mesenteric fenestrated capillaries of mice perfused with the cationic tracer ferritin showed densely packed anionic fixed charges on the endothelial cell glycocalyx, on the luminal aspect of fenestral diaphragms, as well as along both sides of the subendothelial basement membrane [173] (Fig. 27).

What is the role of fenestrae and intercellular junctions in the still ill-defined mechanisms related to capillary permeability? For more than 25 years the fenestral pathway was ascribed a major role in the permeability capabilities of fenestrated capillar-

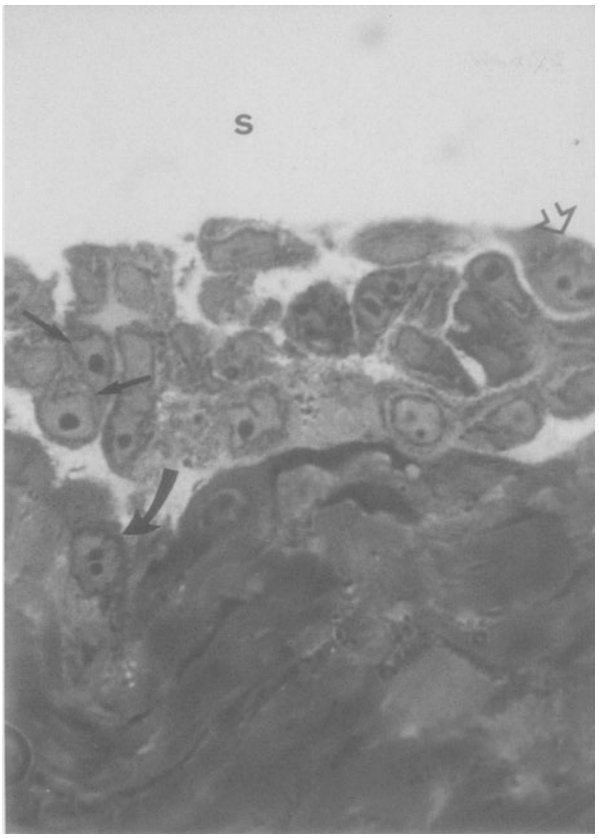

Figure 20. Peritoneal biopsy taken from a patient on CAPD (parietal peritoneum). Desquamating mesothelial cells (small arrows), one of them binucleated (open arrow). Curved arrow points at a binucleated mesothelial cell still forming part of the monolayer (s: peritoneal space) (haematoxylin–eosin; original magnification ×400).

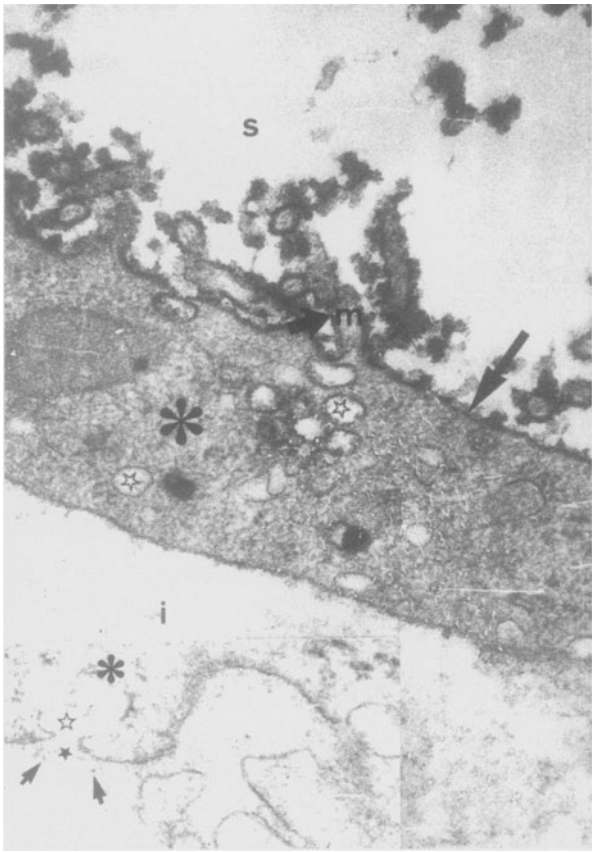

Figure 21. Rat mesenteric mesothelium. The animal was perfused with ruthenium-red, 24 h after experimental induction of *E. coli* peritonitis. Plasmalemmal vesicles or caveolae (open stars) can be seen in the cytoplasm of the mesothelial cell (*). The submesothelial basement membrane is absent, as well as the normally present anionic sites. The luminal aspect of microvilli (m) and that of the cellular membrane are decorated by the cationic tracer (short and long arrows respectively) (S: peritoneal space; I: oedematous interstitial space) (×41 500).

Inset. Another mesothelial cell (*) seen in the same tissue sample. Very few anionic sites (arrows) can be seen sporadically distributed along parts of the submesothelial basement membrane (black star). Open star: plasmalemmal vesicle or caveola, showing an open neck facing the abluminal aspect of the cell cytoplasm (I: interstitial space) (×84 530).

ies [195]. Some investigators suggested that, while open fenestrae could represent the ultrastructural equivalent of the large pore [74], fenestrae, closed by diaphragms (Fig. 27), could also provide a diffusive pathway for water- and lipid-soluble substances [196]. However, fenestral openings of 60–90 nm diameter are too large to be considered the structural equivalent of the hypothetical large pores, the radii of which range between 11 and 35 nm [74, 197]. Furthermore, the density of these pores, estimated at one every 20 μm^2 [47], is substantially lower than the density of fenestrae per square micron observed in microvascular beds.

At least from a theoretical point of view, the presence of anionic fixed charges at the level of fenestral diaphragms, as well as in the subendothelial basement membrane (Fig. 27), is a strong argument against the transfenestral passage of macromolecular anionic proteins [137, 198]. Indeed, previously reported physiological studies have demonstrated the selectivity and restriction of the fenestrated microvascular wall to the passage of electronegatively charged macromolecules [199–201]. Moreover, the permeability of fenestrated capillaries to anionic macromolecules is not higher than that of capillaries of the continuous type [202]. In this context Fig. 30 offers a descriptive account of the problem, observed in our laboratory [Shostak and Gotloib, unpublished observations]. Rat mesentery was perfused (*in vivo*) through the arterial tree with

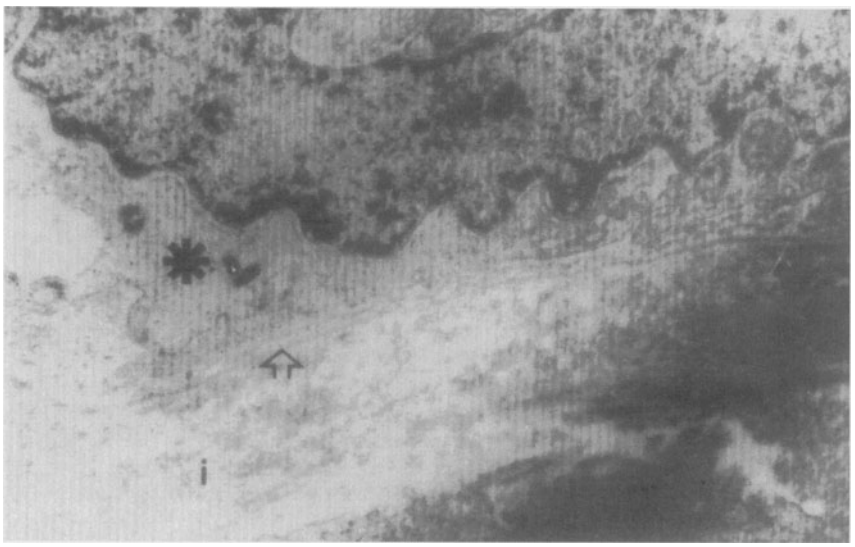

Figure 22. Parietal peritoneum taken from a 67-year-old patient on IPD. The open arrow shows the reduplicated submesothelial basement membrane (*: mesothelial cell; I: submesothelial interstitium) (original magnification ×24 600).

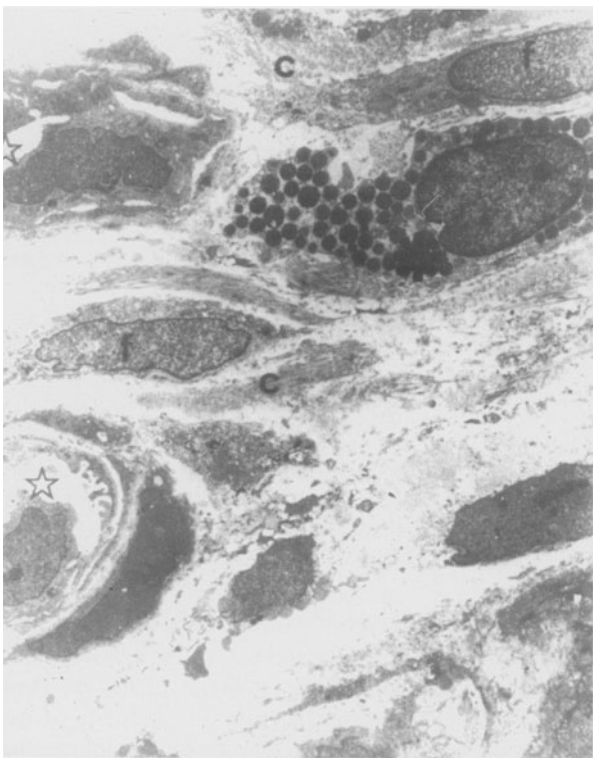

Figure 23. Interstitial tissue of human parietal peritoneum. Bundles of collagen (c) and fibroblasts (f) are interposed between the blood microvessels (open stars) and the mesothelial cells (not included in the electron micrograph). Mast cells (*) are frequently observed near blood microvessels (original magnification 42 900).

negatively charged albumin–gold complexes for a period of 30 min. As can be seen, substantial amounts of albumin–gold particles appear contacting the luminal aspect of the endothelial cell plasmalemma, as well as free into the capillary lumen. Particles of the tracer can be observed in close apposition to the luminal front of fenestral diaphragms. However, albumin–gold particles were not seen in the subendothelial space, even after 30 min perfusion. These observations support the hypothesis that fenestrae are not permeable to anionic plasma proteins. Consequently, it appears that fenestral openings are unrelated to the theoretically predicted large pore system [195, 198, 202, 203]. On the other hand, fenestrated endothelia have higher hydraulic conductivity, and are more permeable to small ions and molecules than continuous endothelia [204].

Capillary endothelial cells are linked to each other by tight junctions (zonula occludens), originally described by Farquhar and Palade [205–207] (Fig. 31). Communicating or gap junctions have been observed in arteriolar endothelium [206]. Postcapillary venules have loosely organized junctions with discontinuous ridges and grooves of which 25–30% appear to be open with a gap of 20–60 Å [47]. They also sometimes show gap junctions [11].

Cytoplasmic plasmalemma bordering both sides of junctions also shows anionic fixed charges [34]. Their functional significance in relation to the passage of charged molecules will be discussed later.

Research performed during the past 5–6 years revealed that interendothelial tight junctions appear

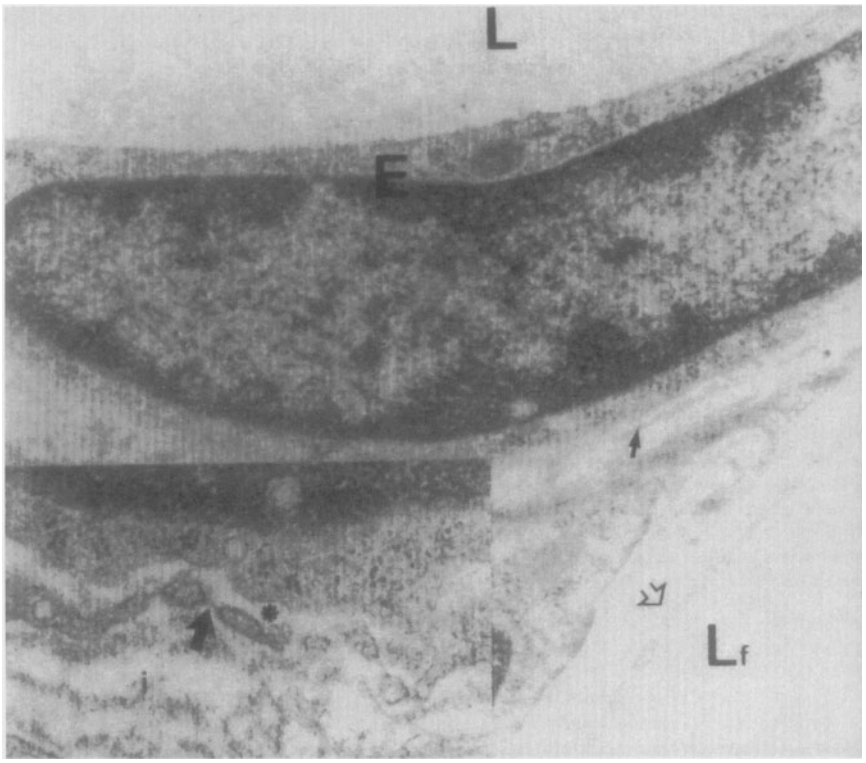

Figure 24. Continuous capillary of a blood mesenteric rabbit capillary whose endothelial layer (E) is lying on the basement membrane (black arrow). The lower right part of this electron micrograph shows a fenestrated capillary (open arrow) (L: lumen of continuous capillary; Lf: lumen of fenestrated capillary) (original magnification ×47 400).
Lower left inset. Fenestrated capillary of human parietal peritoneum. The arrow points to a fenestral diaphragm (I: interstitium; *: lumen of fenestrated capillary) (original magnification ×42 900).

as a set of long, parallel, linear fibrils that circumscribe the cell, with short fibrillar fragments interconnecting the main parallel array. The number of fibres correlates with junctional permeability: the more densely packed the fibrillar mesh, the lower the junctional permeability [208]. Therefore, the tight junction is not a simple fusion between the outer plasmalemmal leaflets of neighbouring cells [209]; rather, it consists of protein molecules such as occludins and cadherins in tight junctions, desmoleins and desmocolins in desmosomes, and connexins in gap juctions [210, 211].

Occludin is an integral membrane protein, exclusively localized at tight junctions in both epithelial and endothelial cells [210], and is directly involved in sealing the cleft, creating the primary barrier to the diffusion of solutes through the paracellular pathway as well as regulating, according to the modulation of occludin expression, the permeability properties of different microvascular beds [212]. Occludin is bound on the endothelial cytoplasmic surface to ZO-1, a 220 kDa membrane-associated protein likely to have both structural and signalling roles [213, 214].

Vascular endothelial cadherin, in turn, is an endothelial-specific cadherin that regulates cell to cell junction organization in this cell type, and provides strength and cohesion to the junction [215]. Cadherins are also implicated in junctional permeability, basically under the effect of inflammatory mediators such as tumour necrosis factor and histamine, which have been shown to induce a redistribution of these adhesion molecules to non-junctional regions and junctional disassembly [216, 217].

The role of tight junctions in the permeability capabilities of the microvasculature, during the situation of normal physiology, has been a topic for intensive research and controversy through the years. Whereas some groups considered the intercellular cleft as the main pathway for water, as well as for small and large solutes and electrolytes [218, 219], other groups developed the concept that tight junctions create a regulated paracellular barrier to the movement of water, solutes and immune cells

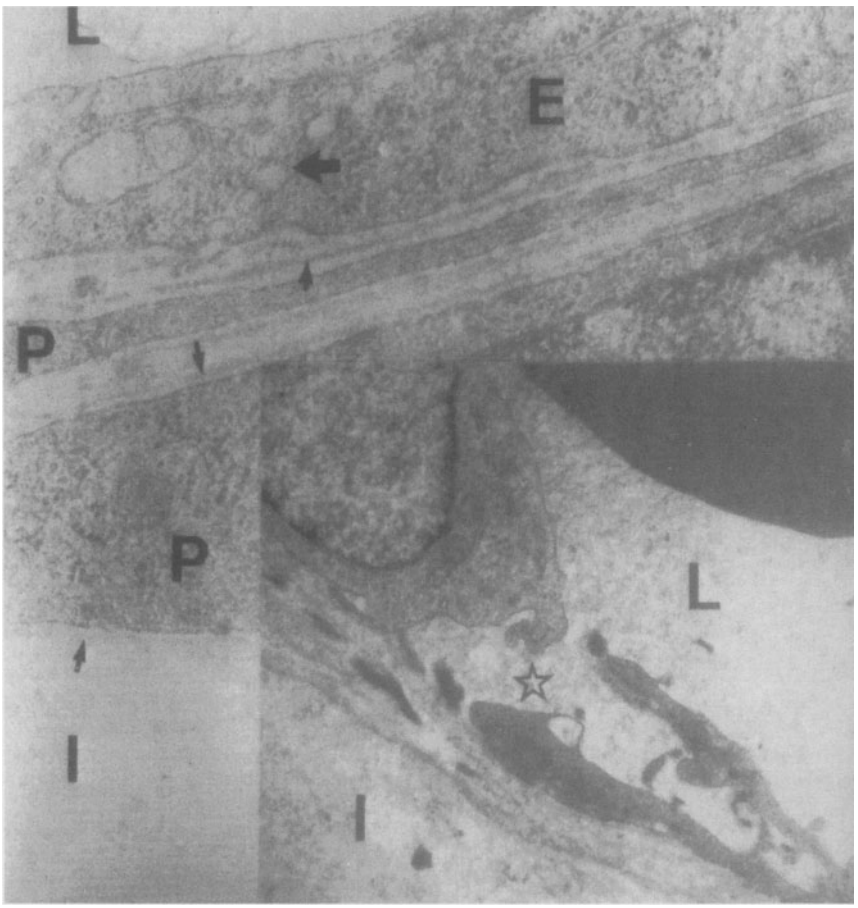

Figure 25. Postcapillary venule of rabbit mesentery. The large arrow shows a transcellular channel (L: microvascular lumen; E: endothelial cell; short arrow: subendothelial basement membrane; P: pericyte; small arrows: subperithelial basement membrane; I: interstitium) (×62 500).

Lower right inset. Human parietal peritoneum taken from a 21-year-old patient with *E. coli* peritonitis. The star shows an open interendothelial junction of a blood capillary. Note part of an erythrocyte in the upper right quadrant (L: capillary lumen; I: interstitium) (original magnification ×41 500).

between the microvascular compartment and the interstitial space, enabling the endothelial monolayer to create compositionally different fluid compartments [208, 220–222]. Recent progress indicates that the presence of tight junctions does not imply a foolproof seal of the intercellular cleft. Instead, this structure contains discrete ion-selective pathways through the extracellular portion of the junction, regulated, at least in part, by the activity of the cytoskeleton [208, 223]. As stated above, the transmembrane protein occludin is an excellent candidate for the sealing protein. Understanding the mechanisms involved in junction permeability will require both a more detailed molecular characterization of tight junction proteins and the regulation by the endothelial cells of their attachment to the perijunctional cytoskeleton [220]. As stated by Renkin [202] in 1977, identification of the tight junction with the diffusional pathway for macromolecular plasma proteins, in a situation of normal physiology, still remains questionable. Their role in capillary permeability is still debated.

As for blood cells, recent investigations showed that neutrophils preferentially migrate by crossing at tricellular corners, rather than passing through tight junctions that lie between two adjacent endothelial cells [224].

The basement membrane of true capillaries is normally a thin sheet at the interface between the abluminal aspect of the endothelial cell and the connective tissue (Figs 13 and 24). In postcapillary venules it is interposed between the endothelial and the perithelial cell (Fig. 25). Generally uniform for a given structure, its thickness varies among the

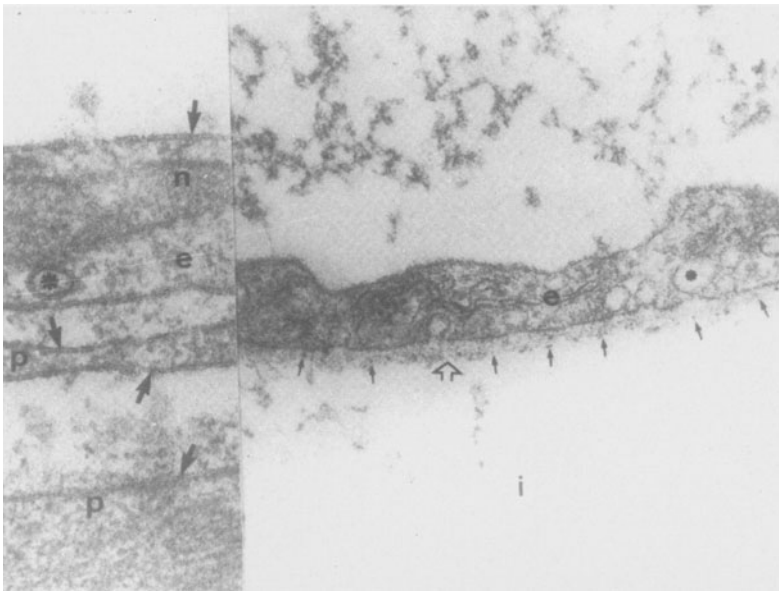

Figure 26. The right part of the figure shows part of a blood capillary wall observed in a sample of diaphragmatic peritoneum obtained from a normal rat. The luminal aspect (upper cell border) of the endothelial cell (e) shows a fine reticular glycocalyx stained by ruthenium red which, on the other hand, does not decorate pynocytotic vesicles (*). The subendothelial basement membrane (open arrow) is continuous and shows quite regularly distributed ruthenium-red stained anionic sites (small arrows) along both the lamina rara externa and the lamina rara interna (original magnification $\times 50\,720$).

Inset. Left part of the figure. Part of a postcapillary venule observed in mesentery of rat, 5 days after induction of peritonitis. The trilaminar structure of the endothelial (e) and perithelial cell plasmalemma is clearly observed (arrows), as well as that of the limiting membrane of the pinocytotic vesicle (*). Glycocalyx, basement membrane and anionic sites are absent (n: nucleus of endothelial cell) (original magnification $\times 84\,530$).

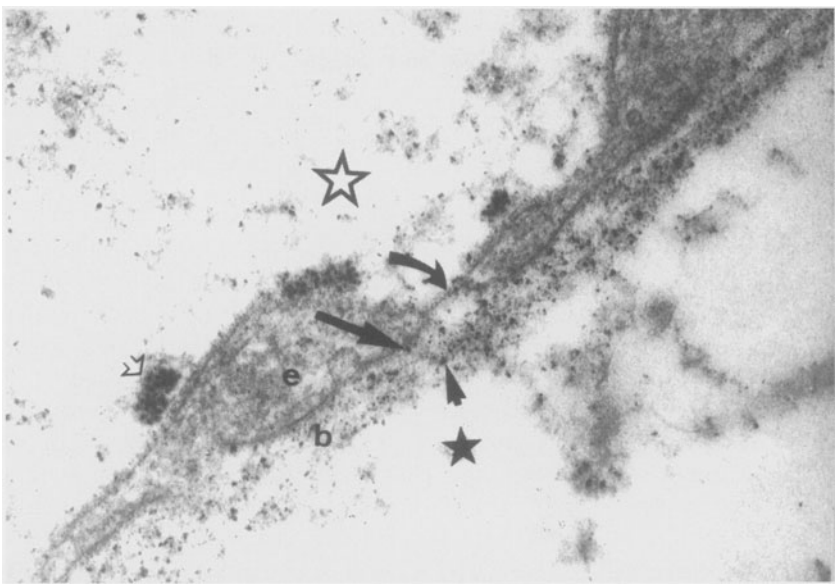

Figure 27. Fenestrated capillary of mouse mesenteric peritoneum. The animal was perfused with cationized ferritin. Particles of the tracer decorate the luminal (long straight arrow) and the abluminal (short black arrow) aspects of the basement membrane (b) laying under the endothelial cells (e). A fenestral diaphragm is also decorated on its luminal aspect by particles of cationized ferritin (curved arrow). Clumps of the tracer appear located on the luminal endothelial cell plasmalemma (open arrow) (open star: microvascular lumen; black star: subendothelial interstitial space) ($\times 41\,500$).

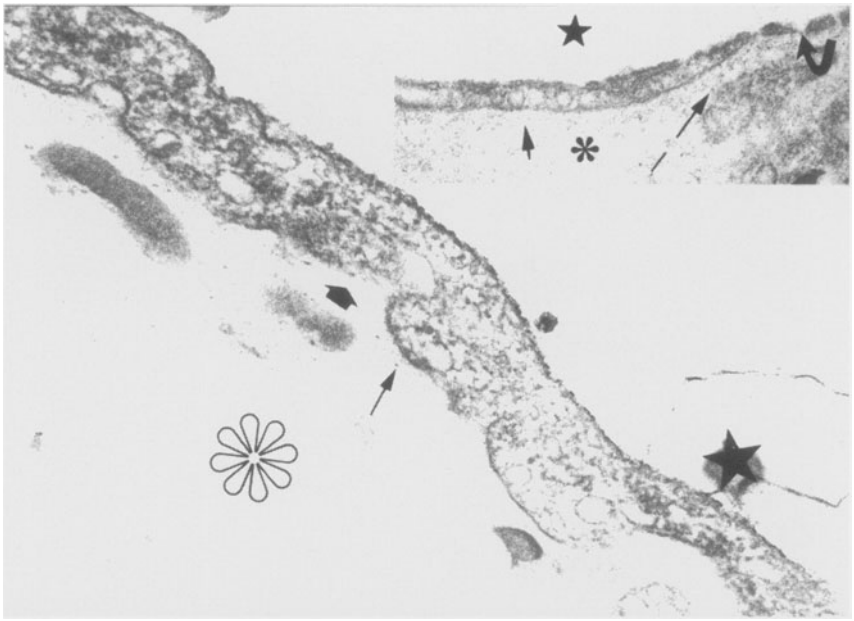

Figure 28. Continuous capillary of rat mesentery. The sample of tissue was recovered 24 h after induction of abdominal sepsis. Distribution of subendothelial anionic sites is irregular; at times they are totally absent (thick arrow), whereas in other portions of the basement membrane they can be seen, but showing an extremely low density (small thin arrow). The luminal aspect of the endothelial cell shows a black rim decorated by ruthenium red, indicating the still-present negative charges of the endothelial glycocalyx (star: microvascular lumen; *: edematous interstitial tissue) (ruthenium red; ×41 500).

Inset. Mesenteric fenestrated capillary taken from the same animal. Occasional anionic sites (long arrow) can be seen along the basement membrane. Most of its length is free from ruthenium-red decorated negative charges (short arrow) (*: structureless interstitial space; star: capillary lumen; curved arrow: fenestra) (ruthenium-red; ×30 740).

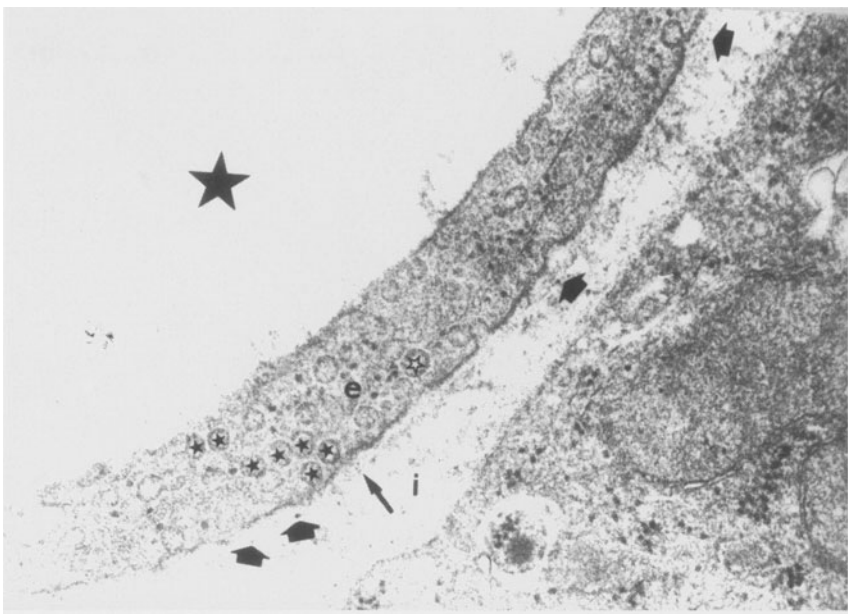

Figure 29. Mesenteric capillary of a rat 6 months after induction of diabetes with streptozotocin (glucose blood levels were higher than 500 mg/dl; glycated haemoglobin 16.38 ± 0.57%). The animal was perfused with ruthenium red. The basement membrane (long arrow), lying under the endothelial cell (e), shows few and occasional anionic sites (thick arrows) (large black arrow: capillary lumen; open star: pinocytotic vesicle; small black stars: transendothelial channel; i: interstitial space) (×41 500).

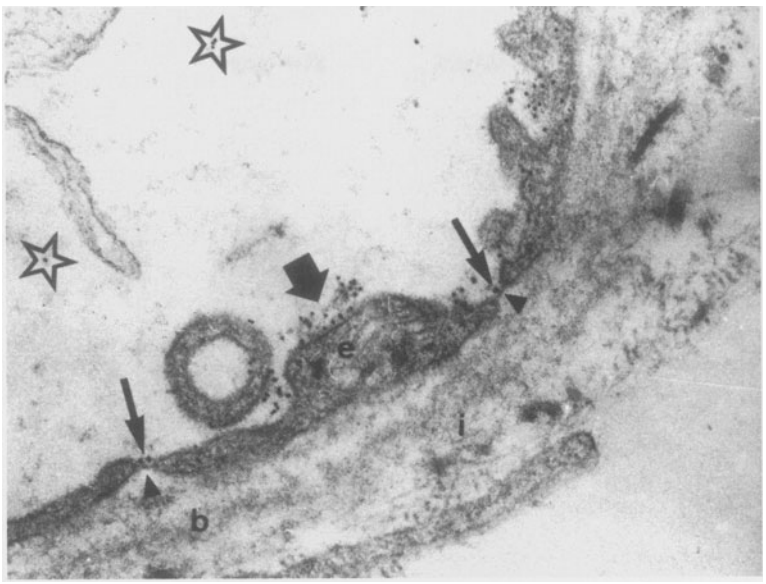

Figure 30. Fenestrated capillary of mouse mesentery taken 30 min after intra-arterial perfusion of the tissue with albumin–gold complexes. Particles of the tracer can be seen in the microvascular lumen (open stars), on the glycocalyx of the endothelial plasmalemma (short thick arrow), as well as on the luminal aspect (long arrows) of fenestral diaphragms (arrowheads). The tracer did not reach the subendothelial interstitial space (i) (b: subendothelial basement membrane) ($\times$ 50 720).

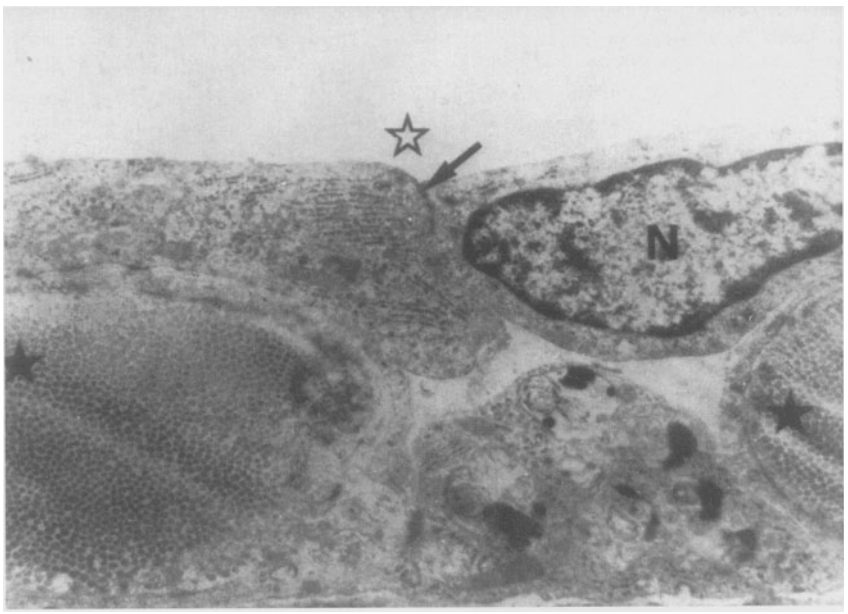

Figure 31. Blood capillary of rabbit mesentery. The black arrow points at a tight junction formed by two adjoining endothelial cells. A macrophage can be observed lying under the endothelial cells interposed between two bundles of collagen (black stars) (open star: capillary lumen; N: nucleus of endothelial cell) (original magnification $\times$ 85 000).

different parts of the body. True capillaries of normal rabbit mesentery have a mean basal membrane thickness of 0.234 ± 0.095 μm [11]. As described for the submesothelial basement membrane, that of human capillaries also exhibits a significantly increasing thickness in the direction of head to foot [145]. It has been suggested that these regional variations are secondary to differences in venous hydrostatic pressure effective on the capillary bed [145]. Diabetic and non-diabetic patients on long-term peritoneal dialysis, showing reduplicated submesothelial basement membrane, had similar alter-

ations on the capillary basement membrane of parietal peritoneum [142]. These changes were also observed in postcapillary venules and small arterioles of parietal peritoneum taken from diabetic uraemics on CAPD (Figs 32 and 33), as well as in skin capillaries (Fig. 34). Additionally, reduplication of mesenteric subendothelial capillary basement membrane has been recently reported in streptozotocin-induced diabetic rats, as early as after 4 months of uncontrolled hyperglycaemia [141], whereas thickening was seen in the same animals 6 months after induction of the disease. These structural alterations of diabetic basement membranes seem to be derived from a substantial increased presence of collagen IV [147, 225–229] which, according to *in-vitro* studies, appears to derive from extended exposure of cells to high concentrations of glucose [230, 231].

In rats, both thickening and layering of microvascular basement membrane can also develop as a consequence of ageing [149, 232], but not before completing the first year of life [232].

Figure 32. Subendothelial reduplicated basement membrane (small arrows) observed in a small venule of parietal peritoneum taken from a diabetic patient on CAPD (open star: red blood cells; *: vascular lumen; thick arrow: endothelial cell) (×15 400).

Inset. One arteriole from the same biopsy shows splitting of the subendothelial basement membrane (arrows) (e: endothelial cell) (×12 600).

So far it may be speculated that reduplication or layering of submesothelial and peritoneal microvascular basement membranes in non-diabetics on CAPD could result from their continuous and long exposure to high glucose concentrations.

Subendothelial basement membranes of both continuous and fenestrated capillaries (Figs 26 and 27), have regularly distributed anionic fixed charges along both aspects of the membrane [36, 173]. Their density distribution in continuous capillaries ranges between 31 and 34 μm of basement membrane [36, 141]. These values, shown in the section devoted to the mesothelial basement membrane, are not far from those detected in other microvascular basement membranes.

The chemical composition of the fixed electronegative charges linked to the subendothelial basement membrane has been explored in several microvascular beds. Studies have shown that their main structural components are glycosaminoglycans such as heparan sulphate and chondroitin sulphate [104, 233–235]. This is at variance with the biochemical and histochemical observations made on the glycocalyx cell surface charges, the main component of which is sialic acid and sialo conjugate. This pattern has been detected in microvascular endothelium [236–240], pleural, pericardial and peritoneal mesothelial cells [241], as well as in macrophages [242], erythrocytes [243] and platelets [244].

What is the functional significance of these electronegative charges? A strong body of literature supports the concept that the permselectivity of capillary walls to anionic macromolecules is basically dependent on molecular charge, besides size and shape [137, 139, 165, 203, 234, 245–251]. Investigations performed in *in-vivo,* whole organ studies [153], in isolated perfused frog capillaries [252] and in isolated rat hindquarters [246] have demonstrated their presence evaluating permeability of different endogenous proteins in a variety of microvascular beds. Indeed, similar results were observed in patients on CAPD comparing dialysate to plasma concentrations of amino acids, having almost the same molecular weight but quite different charge [253], as well as in rat peritoneum, using charged dextrans [254]. The fact that endogenous proteins of graded size are hetereogeneous with respect to their molecular charge [255] lead to some conflicting results [256]. The key to this problem was found investigating clinical and experimental situations, where the permselectivity was substantially reduced or neutralized, enabling the observer to evaluate changes in permeability, derived from the absence

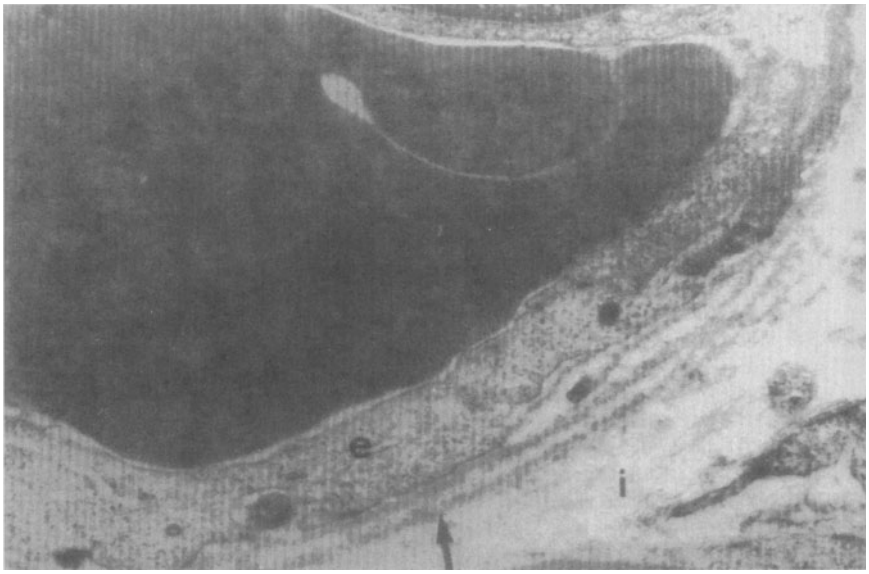

Figure 33. Blood capillary of parietal peritoneum taken from a 69-year-old uraemic patient on IPD for almost 3 years. The endothelial cell (e) is lying on a reduplicated basement membrane (arrow) (I: interstitium (× 24 600).

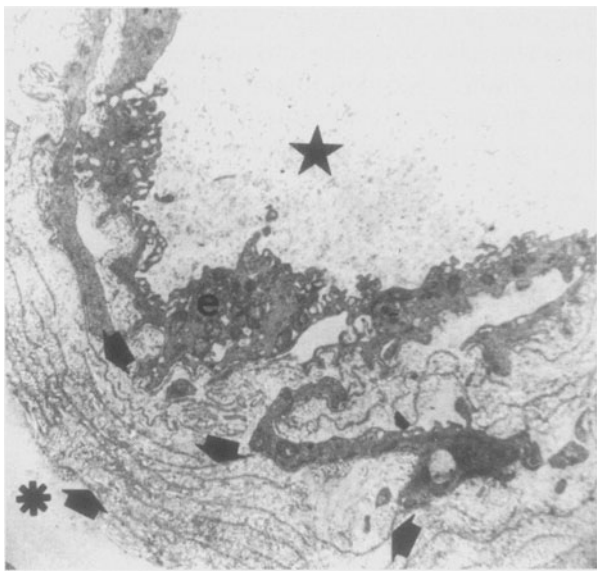

Figure 34. Blood capillary observed in a skin biopsy taken from the same diabetic chronic uraemic patient, whose parietal peritoneum was shown in Fig. 32. Arrows point at the multiple layers of basement membrane (star: microvascular lumen; e: endothelial cell; *: interstitial space) (× 5850).

of the normally present fixed electronegative charges. In the clinical set-up, type I diabetes [257], congenital [258, 259], and acquired nephrotic syndrome [260, 261] have been shown to expose the association of depleted glomerular negative charges and loss of the permselectivity of the capillary wall, leading to massive proteinuria. Experimental interventions performed in laboratory animals confirmed, in turn, the aforementioned findings. Enzymatic removal of sulphated (heparan sulphate) or non-sulphated (hyaluronic acid) glycosaminoglycans from the glomerular basement membrane resulted in a substantially increased permeability to bovine serum albumin [262]. Rats with streptozotocin-induced diabetic nephropathy showed reduced glycosaminoglycan contents in the glomerular basement membrane [263], decreased presence of their heparan sulphate-associated anionic sites [264], as well as significantly increased proteinuria [141]. Further observations made in the streptozotocin diabetic rat have shown a substantial reduction in the submesothelial and capillary subendothelial density distribution of anionic fixed charges (from 31 ± 2 to 12 ± 2 ruthenium red-decorated anionic sites/μm of basement membrane) and, at the same time, a significant increase of albumin losses in the peritoneal dialysis effluent, indicating a marked decrease of the permselective capabilities of the charged components of the peritoneal membrane (Fig. 17) [141]. Similar observations were made in intact rats after neutralization of the peritoneal negative charges with protamine sulphate [265].

The acute inflammatory reaction is the most spectacular experimental set-up to demonstrate the permeability changes derived from an acute reduction of the microvascular negative charge. This situation has been classically defined by the development of acute low hydrostatic pressure, high capillary perme-

ability, and albumin-rich interstitial oedema [161, 266]. In this sense the generalized acute inflammatory reaction derived from abdominal sepsis promotes a major erosion of the density distribution of the anionic fixed charges in several microvascular beds, diaphragmatic and mesenteric peritoneum (showing values as low as six anionic sites/micron of basement membrane) [267], myocardium [268], skeletal muscle, pancreas, renal peritubular capillaries [269], as well as in the submesothelial basement membrane of rat diaphragmatic and mesenteric peritoneum [140] (Figs 21 and 28). Additional studies in the same experimental model of abdominal sepsis in rats demonstrated abnormally increased albumin content in mesenteric, diaphragmatic and pancreatic interstitial fluid [270]. This drastic loss of the permselectivity of the capillary wall derives from a massive liberation and reduced inactivation of a host of mediators of inflammation triggered by acute inflammation [271–273], including tumour necrosis factor alpha, inlerleukins, platelet-activating factor, leukotrienes, thromboxane A2, activators of the complement cascade, kinins, transforming growth factor B, vascular endothelial growth factor, as well as many others already known, or still waiting to be identified [183, 274–277].

The role of intercellular junctions in macromolecular leakage during acute inflammation is still controversial. Some groups pointed to the endothelial tight junction as the main pathway for extravasation of macromolecular plasma protein. It was postulated that inflammatory mediators such as histamine, serotonin, bradykinin and leukotriene E4 induced junctional openings (Fig. 25, inset), by means of endothelial cells contraction [278–281] or by a loss of occludin and cadherin from the junctional complex [282, 283]. Unpublished observations from our laboratory (Shostak and Gotloib) made in intact rats, as well as in rats with *E. coli* peritonitis, by means of intra-arterial injection of albumin–gold complexes, showed that most particles of the tracer cross the endothelial barrier transcellularly, via plasmalemmal vesicles. In both experimental situations, intact and infected rats, the tracer was not seen beyond the junctional infundibulum (Figs 35 and 36); just the opposite: the tracer was present in plasmalemmal vesicles (Fig. 36, inset), and reached the subendothelial space in areas far from intercellular junctions (Figs 35 and 36). This concept of transcellular transport of albumin through the capillary wall, also during acute inflammation, is supported by recently published evidence postulating a significant role for plasmalemmal vesicles and even for fenes-

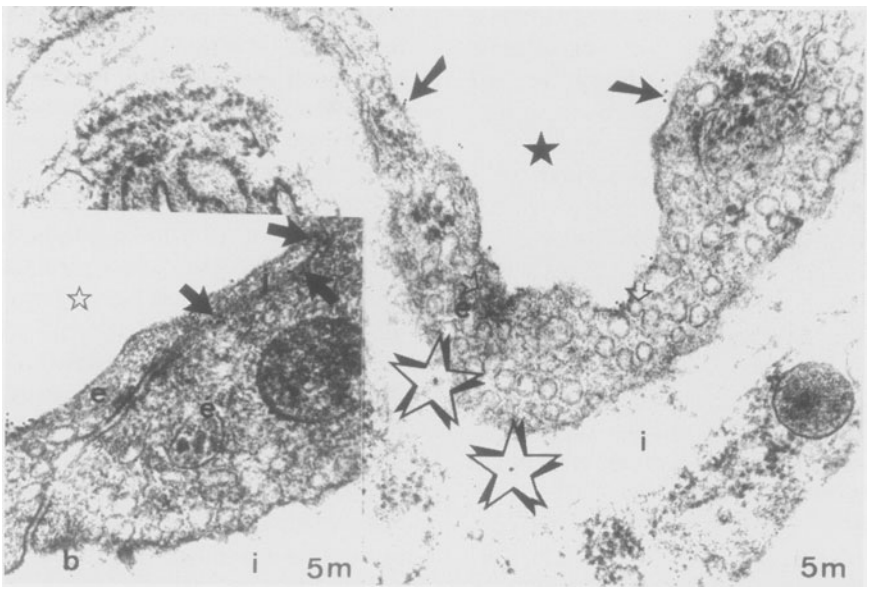

Figure 35. Blood continuous capillary of mouse diaphragmatic peritoneum. The material was taken 5 min after intra-arterial perfusion of the tissue with albumin–gold. Particles of the tracer decorate the luminal aspect (black arrows) of the endothelial cell, as well as that of pynocytotic vesicles (open arrows). Note the presence of albumin–gold complexes (open stars) in the subendothelial interstitial space (i), in an area free of intercellular junctions (× 41 500).

Inset. Another aspect of the same sample shows particles of the tracer (arrows) in the luminal side of the intercellular junction (j), whereas the interstitial space (i) is devoid of albumin–gold complexes (open star: microvascular lumen; b: subendothelial basement membrane; e and e′: adjacent endothelial cells) (× 41 500).

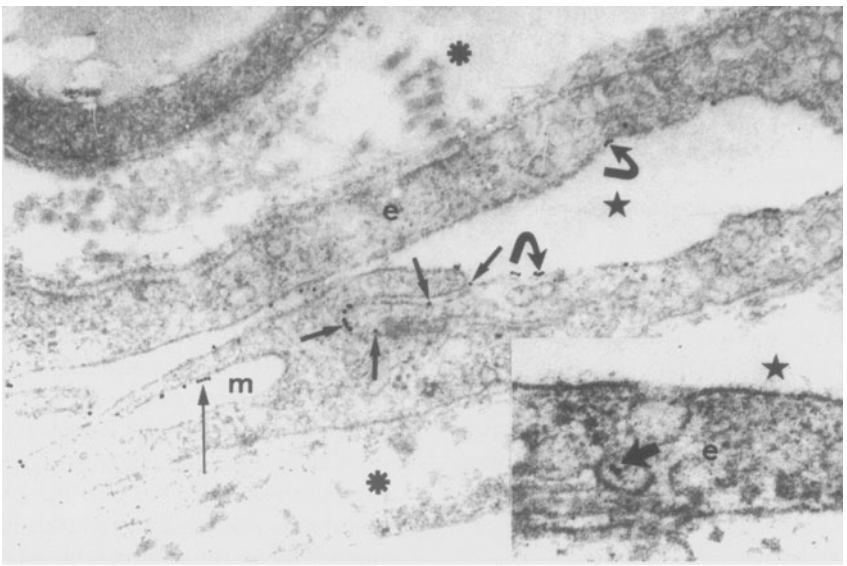

Figure 36. Mesenteric capillary of a rat with experimentally induced *E. coli* peritonitis. Intraarterial perfusion with albumin–gold was performed 24 h after provoking the disease. Particles of the tracer can be seen adsorbed to the luminal aspect of the endothelial cell membrane (curved arrows), as well as within the infundibulum of the interendothelial cell junction (short arrows). Some particles of the tracer (long thin arrow) are also present in a cytoplasmic multivesicular body (m) (*: interstitial space; e: endothelial cell; black star: capillary lumen) (×41 500).
Inset: Another aspect of the sample taken from the same animal. Albumin–gold complexes are also present in a pinocytotic vesicle (arrow) (star: capillary lumen; e: endothelial cell) (×84 530).

trations induced by vascular endothelial growth factor [284–286].

Water transport across endothelium of continuous capillaries was classically thought to occur almost completely via the paracellular pathway through intercellular junctions. Transcellular transport was considered to be nil.

However, the relevance of the transcellular pathway also for water has recently been brought to the forefront by the immunohistochemical identification of aquaporin-1 channels in peritoneal microvascular endothelium [287, 288], as well as in rat peritoneal mesothelium [102]. Expression of this transmembrane water channel protein in the endothelial cell surface of continuous capillaries appeared to be basically localized in plasmalemmal vesicles, and its concentration is quantitatively comparable to that seen in erythrocyte plasma membrane [289]. The presence of aquaporin–1 in microvascular endothelium provides a molecular explanation for the water permeability of some capillary beds [290], as well as a low-energy cost pathway [291] for almost 70% of the transmembrane transport of water [287]. Furthermore, this evidence confirms the predicted concept that, also during peritoneal dialysis, not less than 50% of the transperitoneal water flow occurs through ultra-small transcellular pores [94].

Summarizing the information obtained from ultrastructural and physiological studies, it can be stated that the microvascular endothelial cell should be considered a highly active structure, serving not only as a permeability barrier and an effective thromboresistant surface, but also as the location of important synthetic and other metabolic activities [180, 207].

Continuous capillaries are more permeable to larger molecules than are fenestrated capillaries [197]. Coated pits and coated vesicles are involved in receptor-mediated endocytosis, whereas the uncharged pinocytotic vesicles and transcellular channels are involved in the transfer of proteins and fluid-phase pinocytosis. The transcellular pathway plays a relevant role in the transmembrane transport of water and macromolecular plasma proteins. Additionally, all the resistances described by Nolph [75] along the pathway leading from the microvascular lumen to the abdominal cavity, are negatively charged [34, 36].

Lymphatics

The lymphatic system serves to drain, from the interstitial compartment, a range of materials such as

water, proteins, colloid materials and cells [292], all elements included in the interstitial fluid. Under normal conditions fluid crosses the microvascular endothelial membrane at a rate whose magnitude depends on the Starling forces acting at each aspect of the capillary membrane, as well as on the permeability properties of the endothelial microvascular monolayer. The local autoregulation of interstitial volume is provided by automatic adjustment of the transcapillary Starling forces and lymphatic drainage [159]. Therefore, an alteration in the aforementioned forces results in interstitial accumulation of fluid which will eventually be removed by the lymphatic flow that, in situations of high capillary permeability oedema occurring during acute inflammation, can increase by a factor of ten [293]. In the abdominal cavity, lymphatics have a relevant role in the prevention of ascites [294].

Work during the last 20 years has revealed relevant evidence characterizing lymphatic structure and organization. The first stage of lymph collection occurs through a system of interstitial non-endothelial channels, or low-resistance pathways known as pre-initial lymphatics [295, 296], which have been seen in the cat and the rabbit mesentery [297].

This most peripheral part of the lymph vessel system is a completely open net of tissue channels which drain, at least in the cat mesentery, mainly along the paravascular area of the venous microvasculature, into a network of 0.5 mm long, irregularly shaped endothelial tubes, approximately 20–30 μm width [298]. By the time these tubes are completely filled they can reach a maximal diameter of up to 75 μm [299]. A single endothelial layer (Fig. 37, inset) forms these endothelial tubes defined as initial lymphatics or lymphatic capillaries [297, 299, 300].

The subendothelial area is most of the time devoid from basement membrane, as well as from a smooth muscle layer present in larger lymphatic collectors [301]. The sporadically observed patches of basement membrane have, as in blood capillaries, anionic fixed charges that can be decorated by cationic tracers [302]. Due to the absence of muscular layer, lymphatic capillaries lack the capability for spontaneous contractility [303]. However, the fact that lymphatic endothelial cells contain an abundant supply of fine actin-like filaments, 40–60 Å in diameter, arranged in bundles parallel to the long axis of the cell, led some investigators to postulate that these filaments could function as a contractile element of the lymphatic capillary wall [304, 305].

Anchoring filaments, having histochemical and ultrastructural characteristics similar to those observed in elastin-associated microfibrils, form a uniform population of fibrous elements, leading to the development of structural and functional continuity between the abluminal aspect of the lymphatic capillary endothelial cell and the elastic network of

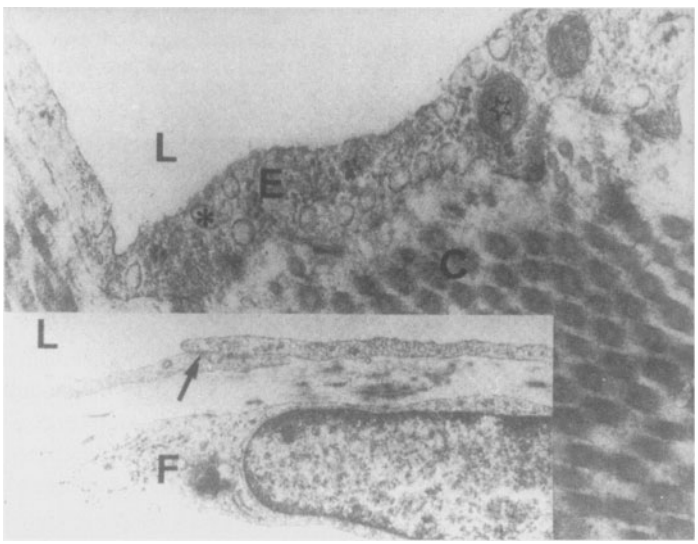

Figure 37. Partial view of a lymphatic lacuna observed in a sample of rabbit diaphragmatic peritoneum. The thin endothelial cell (E) shows numerous pinocytotic vesicles (*) and occasional mitochondria (star). Note the absence of subendothelial basement membrane (L: lacunar lumen; C: collagen fibres) (original magnification ×85 000).

Lower left inset. Lymphatic capillary of rabbit diaphragmatic peritoneum. Two adjoining endothelial cells, forming a tight junction (arrow), appear lying on the interstitial tissue. Basement membrane, as well as anchoring filaments, are not observed (L: capillary lumen; F: fibroblasts) (original magnification ×62 500).

the adjacent connective tissue [306]. The main role of these anchoring filaments is the prevention of capillary collapse, when the interstitial pressure gains strength as a consequence of expanded fluid content of the interstitial compartment [307]. This simple element enables the lymphatic system to launch a mechanism of fluid drainage that accounts for 25% of the safety factors that can prevent formation of interstitial oedema [307]. In this context it has been proposed that initial lymphatics directly sense and regulate the interstitial fluid volume [308].

The total surface area of pre-initial and initial lymphatics seems to be smaller than the total exchange area of blood microvessels [196]. Other studies on cat and rabbit mesentery showed the additional presence of flat, blind saccular structures up to 40 μm wide, with a wall made up of a simple layer of thin endothelial cells, devoid of basement membrane [196, 298].

Lymphatic endothelial cells are flat and elongated, showing an average thickness of 0.3 μm in non-nuclear areas [43, 304]. The luminal aspect of lymphatic endothelium, when exposed to cationic tracers such as cationized ferritin or ruthenium red, shows a high density of anionic fixed charges that, at times, can also be detected labelling the luminal aspect of the intercellular cleft (Fig. 38) [305, 309]. These charges prevent the adhesion of electronegatively charged blood cells to the endothelial luminal surface and may play a significant role in the movement of charged solutes from the interstitial compartment to the capillary lumen [309]. Furthermore, the absence of subendothelial and negatively charged basement membrane (Fig. 38) points at the asymmetry of the lymphatic capillary wall, that is at variance with the electric symmetry characteristic of blood capillaries.

Nuclei of endothelial cells are flattened and, on electron microscopy, appear elongated. Their irregular outline shows a thin peripheral rim of dense chromatin. Plasmalemmal vesicles [43, 310] and transendothelial channels, similar to those described for blood microvessels, are commonly observed [305]. Plasmalemmal vesicles have been shown to participate in the transcellular movement of albumin–gold complexes, from the submesothelial interstitial space to the lumen of capillary lymphatics [76] (Fig. 39). Furthermore, the endocytotic pathway has been shown up by the presence of the same tracer into cytoplasmic endosomes (Fig. 40).

Several types of interendothelial junctions have been described. Approximately 2% of the whole

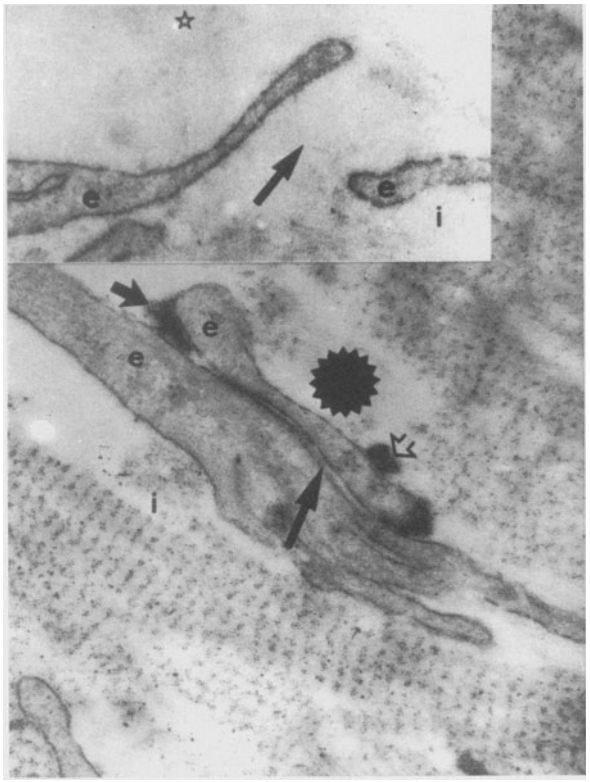

Figure 38. Mesenteric lymphatic capillary of a mouse perfused with cationized ferritin. The long arrow points at the intercellular junction formed by two adjacent endothelial cells (e). The short black arrow indicates the presence of the electropositive tracer on the luminal aspect of the intercellular junction, whereas the open arrow shows particles of ferritin decorating the endothelial luminal plasmalemma. Note the absence of subendothelial basement membrane (*: microvascular lumen. i: subendothelial interstitial space) (×41 500).

Inset. Mesenteric lymphatic capillary of an intact mouse. The arrow points at an open intercellular cleft formed by two adjacent endothelial cells (e). The junction serves as a valvular structure sensitive to the hydrostatic gradient between the interstitial space (i) and the microvascular lumen (open star) (×41 500).

junctional system consists of open junctions, showing gaps up to 100 nm width, that can, at times, be as wide as 1000 nm [305, 311]. These openings serve as a way in for macromolecular solutes such as gold-labelled albumin (Fig. 40) or cationized ferritin (Fig. 41). At times two adjoining endothelial cells overlap each other, forming a kind of valvular junction that can be easily opened by an eventual increase of interstitial pressure (Fig. 38, inset). Junctional infundibuli show anionic fixed charges similar to those observed in the luminal endothelial glycocalyx (Fig. 38). Around 10% of junctions are zonula

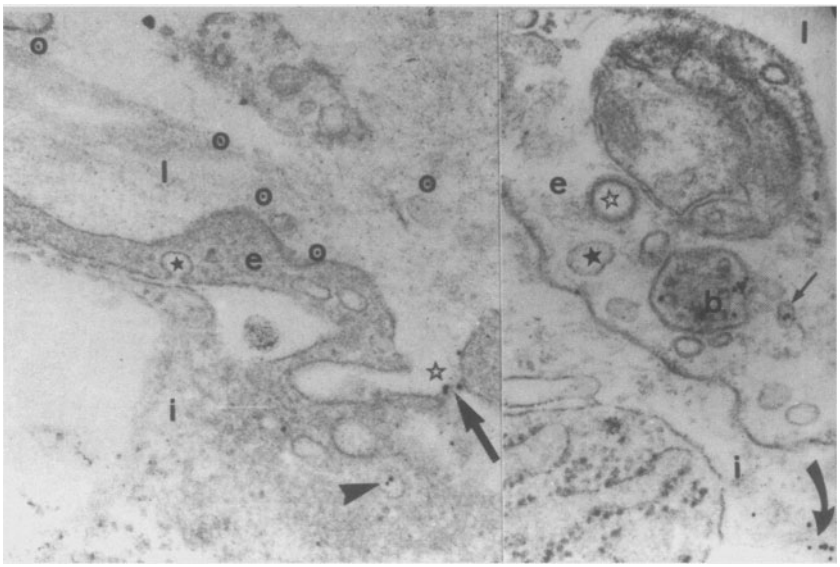

Figure 39. Diaphragmatic submesothelial lymphatic capillary taken from a mouse 10 min after intraperitoneal injection of albumin–gold complexes.

Left inset. Albumin–gold complexes (long arrow) can be observed in their pathway through an open interendothelial cell junction (open star). More particles of the tracer are seen (open circles) within the luminal space (l) of the microvessel. Arrowhead points at albumin–gold included into a pinocytotic vesicle (i: subendothelial interstitial space; black star: plasmalemmal vesicle) (× 41 500).

Right inset. Lymphatic capillary endothelial cell (e). Albumin–gold complexes appear in an endosome (b) as well as in a pinocytotic vesicle (straight arrow). Curved arrow points at albumin–gold complexes present in the interstitium (i). Notice the absence of subendothelial basement membrane (black star: plasmalemmal vesicle; open star: coated vesicle) (× 64 450).

Used with permission from *Kidney International*, **47**: 1274–84, 1995.

adherens, whereas the rest are tight junctions [299, 312]. It has been proposed that, in addition to the organized prelymphatic system [313], a small percentage of open junctions (1–6%) can account for a substantial proportion of the lymphatic pathway for fluid and small and large molecule drainage [299].

The diaphragmatic lymphatic capillary net is organized as a plexus along the submesothelial surface [314], which drains, through an intercommunicating microvascular system, into a plexus on the pleural side of the diaphragm [130]. The distribution of the whole diaphragmatic network is irregular, and varies in different species.

A prominent feature of diaphragmatic lymphatics is the presence of flattened, elongated cisternae or lacunae, approximately 0.3–0.6 cm length, with a long axis that is parallel to the long axis of the muscle fibres [314–316] (Fig. 42). The monolayer endothelial lining of the lymphatic lacunae is thin and shows no tight junctions. Adjacent cells usually overlap, forming valve-like processes, leaving an open interface that can be as wide as 12 μm. The cytoplasm of endothelial cells, basement membrane, and anchoring filaments of lymphatic lacunae are similar to those structures described for lymphatic capillaries. While anionic sites have not been observed, the glycocalyx of cisternal endothelium, when exposed to ferritin, is heavily decorated by the cationized tracer, which also appears along the open intercellular clefts [41, 317].

Diaphragmatic lymphatic lacunae, regularly connected by transverse anastomosis [115], and capillaries from the whole peritoneal lymphatic network, including the rich omental plexus [318], drain into a system of precollector, small-calibre lymph vessels that have a poorly developed smooth muscle layer underlying the endothelium. These vessels, which have semilunar valves [1, 319], drain, in turn, into the larger collecting vessels, whose diameter ranges between 40 and 200 μm [320]. The luminal aspect of the endothelial layer shows a sequence of valvular segments, with a semilunar bicuspidal valve at the distal end of each [130, 320]. The smooth muscle layer underlying the subendothelial basement membrane shows a spiral arrangement around the endo-

Figure 40. Diaphragmatic lymphatic capillary of a rat. The sample was taken 15 min after starting intraarterial perfusion with albumin–gold complexes. Endosome (e) present in the cytoplasm of the endothelial cell (open star) shows particles of the tracer. This may well represent the endocytotic pathway for degradation of the complex. Note the absence of subendothelial basement membrane (black star: microvascular lumen; *: interstitial tissue) (× 87 000).

thelial tube that becomes more pronounced towards the downstream end of the intervalvular segment [303, 321, 322]. Distances between adjacent valves range between 0.1 and 0.6 mm [322]. Thereby, the anatomical and functional unit (lymphangion) is established, consisting of one valve and the following intervalvular segment, which measures 2–3 mm in length [323]. This collecting segment, limited by two-one way valves and an intrinsic smooth muscle layer, compresses the lymphatic lumen driving the intravascular fluid centrally into the next compartment, making up an escalated system of drainage which has, in the proximal part of each lymphangion, a valve which prevents retrograde flow [303]. The presence of valves also enables this part of the system to reach differential intraluminal pressures around 1–2 cm of water [324].

Capillary lymph that flows from the interstitium slowly moves downstream (average velocity for particles with diameter up to 5 μm = 1 μm/min) [301], drains into large collecting channels (40–200 μm diameter), and proceeds in the direction of the central venous circulation, propelled by peristaltic and rhythmic contractions of consecutive lymphangions [290, 301, 320, 325], with frequencies ranging between four and 12 contractions/minute [320, 325]. Within each lymphangion, hydrostatic pressure increases to a threshold of approximately 12 cm of water, after which the proximal valve is closed, and the downstream valve is opened. The cycle is repeated in the following segment. Contractility of lymphangions is modulated by a pacemaker site of spontaneous activity, apparently located, at least in bovine mesenteric lymphatics, in the vessel wall near the inlet valve of the unit. Activity propagates at a speed of 4 mm/s, and the ejection fraction was evaluated at 45–65% [326].

Contractions are generated by myogenic stimuli (hydrostatic pressure of 5–7 cm water) [326], and influenced by activation of α and β adrenoreceptors [327–329], histamine, leukotriene C4 and D4, platelet-activating factor [330, 331], PGF2 alpha, PGA2, PGB2 [332], bradykinin [333], and vasoactive intestinal peptide [334]. It should be noted that all the aforementioned vasoactive substances are mediators of inflammation present in high concentrations in blood and tissues during the localized or the generalized acute defense reaction [274].

Lymph flows from collectors to the thoracic duct and the right lymph duct, and finally drains into the subclavian veins. Lymphangions join larger collecting lymphatic vessels, forming a dichotomous tree that drains entire tissue regions. This arrangement has been described in the diaphragm as well as in mesentery [303, 324, 335].

Innervation of lymph vessels has been studied in the dog and cat mesentery, by means of silver stains [319]. It was shown that large lymphatic collectors have myelinated nerves that remain on the adventitial area, and non-myelinated nerve fibres that penetrate into the region of valve attachment and are considered to be the motor supply to the smooth muscle. Bovine mesenteric lymphatics show adrenergic nerve fibres in the media, as well as in the adventitia. Human mesenteric lymph collector neurotransmitters are both adrenergic and cholinergic, the former being prevalent. Lymphatic capillaries are devoid of innervation [336].

Since Starling [337, 338], it has been accepted that, besides the removal of excess interstitial tissue,

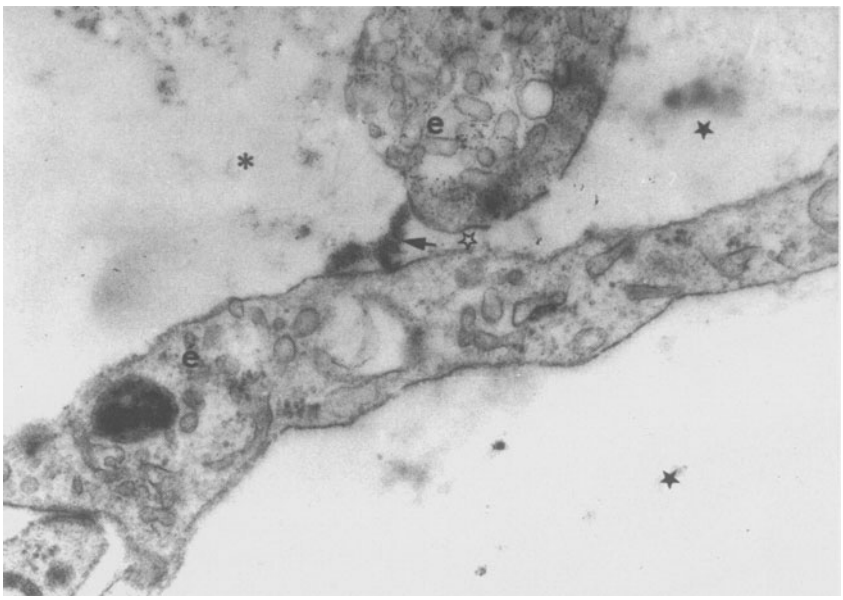

Figure 41. Mesenteric lymphatic capillary obtained from a mouse intraperitoneally injected with cationized ferritin. Particles of the tracer (arrow) can be seen entering the microvascular lumen (*) through the open interendothelial cell junction (open star). Again, note the absence of subendothelial basement membrane and anionic sites (e and e': lymphatic endothelial cells; black stars: interstitial space) (×41 500).

the lymphatic system has the special function of absorbing protein. Normally, blood capillaries leak protein, which will not re-enter the blood vessels unless delivered by the lymphatic system [339]. It is generally accepted that the rate of lymph formation is equal to the net capillary efflux under normal physiological conditions, in order for the interstitial fluid volume to remain constant [308]. However, the mechanisms involved in the formation of lymph, at the level of the most peripheral part of the lymphatic system, are still controversial. According to Allen [340], who formulated the hydraulic theory, lymph formation is the end-result of hydraulic forces acting across initial lymphatics. Assuming that the interstitial hydrostatic pressure is zero, or even negative [157, 341], any rise will also increase the initial lymphatic flow, and oedema will eventually develop if and when the lymphatic drainage capabilities are exceeded [342–344]. This concept of increased hydrostatic pressure as the main factor in the process of lymph formation was extrapolated to the lymphatic absorption from the peritoneal cavity [345, 346]. In this context it was postulated that, during peritoneal dialysis, the intra-abdominal pressures [347, 348] modulated lymphatic drainage from the abdominal cavity well within the range of values observed in dialysed patients [163, 349]. This concept has been substantially challenged by a series of elegant studies performed by Flessner *et al.* [164, 350], who showed that a significant proportion of the intra-abdominal fluid is lost to the abdominal wall, the rate of which is also dependent on the intra-abdominal pressure. This fluid, after being incorporated to the tissues surrounding the abdominal cavity, will be drained through the lymphatic circulation [351]. The eventual influence of the intrathoracic negative pressure upon the lymphatic downstream circulation [352] may well be an additional component of the hydrostatic forces involved in lymph progression to the venous-blood compartment.

The osmotic theory of lymph formation [353] postulates the existence of a protein-concentrating mechanism at the level of the initial lymphatics, the main result of which would be that only 10–40% of the fluid initially entering within the lymphatic network would flow downstream, back to the blood compartment, and the remaining fluid would be filtered out from the lymphatics as a protein-free solution. This process would eventually cause a high protein concentration, and an oncotic gradient between the contents of the initial lymphatics and the surrounding interstitial fluid. Other investigators have proposed a vesicular theory of lymph formation, which holds that plasmalemmal vesicles provide the major route for transendothelial transport

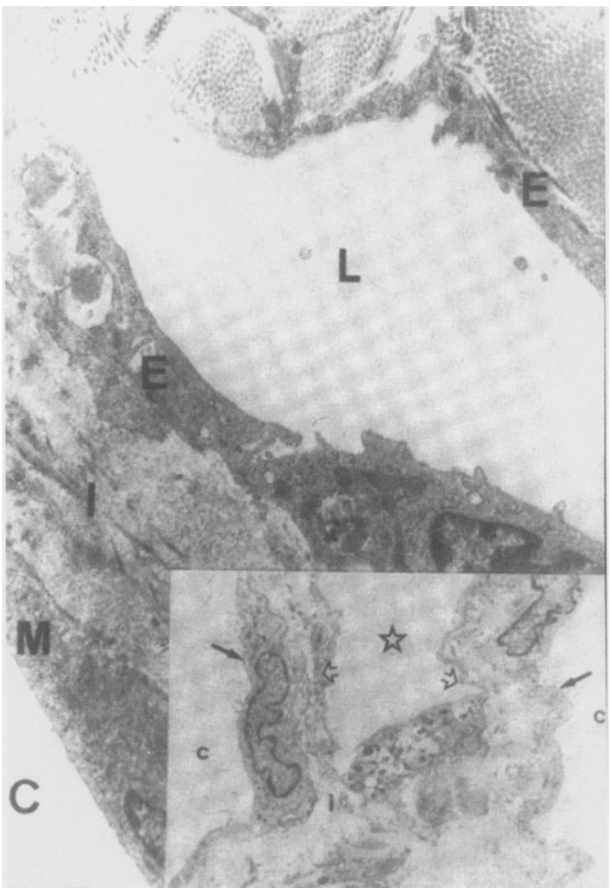

Figure 42. Lymphatic lacuna of rabbit diaphragmatic peritoneum. The wide lacunar lumen (L) is surrounded by the lymphatic endothelium (E). Connective tissue (I) is interposed between the lacuna and the mesothelial cell layer (M) (G: abdominal cavity) (original magnification ×17750).
Lower right inset. Lymphatic lacuna of rabbit mesentery. The open star shows the lacunar lumen surrounded by a thin endothelial layer (open arrows). Mesothelial cells (black arrows) are covering both aspects of the mesenteric peritoneal surface (I: interstitium. C: abdominal cavity) (original magnification ×4750).

of protein, thereby creating the oncotic gradient needed for further fluid flow between adjacent cells or through transendothelial channels [354, 355]. This hypothesis is supported by recent studies that have shown active transendothelial transport of albumin in plasmalemmal vesicles [57, 356]. Figure 39 shows gold-labelled albumin transported by plasmalemmal vesicles of a mouse diaphragmatic lymphatic capillary.

On the other hand, it has been suggested that the postulated mechanisms may not necessarily be exclusive in the sense that some or all could function simultaneously. However, the relative influence of each one could vary in different areas of the initial lymphatic network [357].

The relevance of peritoneal lymphatics, as well as their impact upon ultrafiltration during peritoneal dialysis, is addressed in Chapter 6.

Peritoneal innervation

The first report announcing the presence of nerves in the peritoneal interstitium was made by Haller in 1751 [358] and confirmed during the nineteenth century by Ranvier and Robin who, using osmic acid and silver nitrate, described nerve trunks, branches and nerve endings accompanying arteries and veins. Robinson [1] described the peritoneum as being richly supplied with myelinated and non-myelinated nerves (Fig. 43).

In rat mesentery, networks of adrenergic axons innervate the principal and small arteries and arterioles. Precapillary arterioles, collecting venules and small veins are not innervated, and are most likely under the influence of humoral vasoactive substances [359]. Lymphatic innervation was described in the previous section.

In 1741 Vater observed that the submesothelial connective tissue of cat mesentery contained oval corpuscles with a diameter of approximately 1–2 mm. In 1830 Paccini rediscovered and gave a systemic description of this corpuscle, known as the Vater–Paccini corpuscle [1]; it takes the form of a non-myelinated nerve ending which, in transverse section, appears as a sliced onion. In humans it has been observed in the peritoneum of mesentery and visceral ligaments, functioning as the main receptor for perception of pressure.

Cytology of the peritoneal fluid

The peritoneal fluid of laboratory animals has classically been a favoured site for experiments dealing with the inflammatory response [360], as well as for those designed to analyse the biological reaction to infection [361].

More than 50 years ago Josey and Webb realized that fluid shifts into and out of the peritoneal cavity could change the concentration of cells without affecting their absolute number [362–365]. The methodological answer to this question was given by Seeley and colleagues, who weighed peritoneal fluid and measured the cellular concentrations, and so were able to estimate the absolute number of cells [366]. Padawer and Gordon [364], after analysing

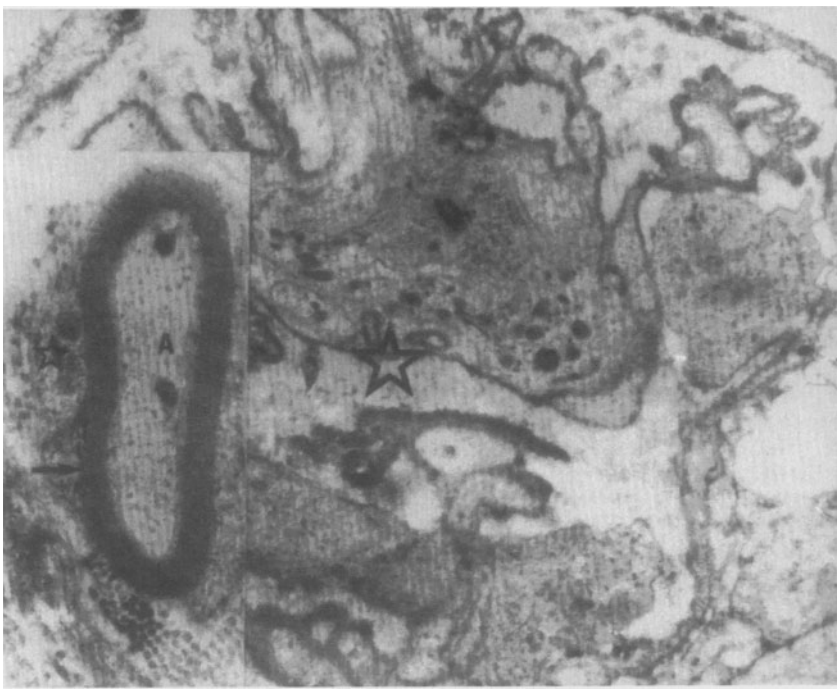

Figure 43. Parietal peritoneum taken from a 67-year-old chronic uraemic patient on IPD, showing a transversal section of an unmyelinated nerve (star) (× 12 600).
Inset. Rabbit mesentery showing a myelinated nerve fibre (star: Schwann cell cytoplasma; arrow: myelin; A: axon) (original magnification × 47 400).

the cellular elements present in peritoneal fluid of eight different normal mammals, concluded that the most frequently observed cells were eosinophils, mast cells and mononuclears (including lymphocytic and macrophagic elements). Total cell numbers, as well as percentages of the different cells, varied greatly among the species examined. Neutrophils were never observed in normal animals. Total absolute counts were higher for females than for males, as well as for older animals compared with younger ones. In the individual animal, under normal conditions, the number of cells present within the abdominal cavity was constant [364].

Observation of peritoneal fluid obtained from healthy women showed that macrophages and mesothelial cells contributed more than 70% of the whole cell population, whereas lymphocytes and polymorphonuclears contributed to a lesser extent (18% and 7% respectively) [367]. Other investigators observed that at the midphase of the menstrual cycle, macrophages, which comprised 82–98% of the peritoneal cells, showed morphological as well as biochemical heterogeneity and were seen to be involved in phagocytosis of erythrocytes [368] (Fig. 44). However, other studies showed up to four different types of cytological patterns in peritoneal fluid of women during the course of the menstrual cycle, in all of which mesothelial cells contributed substantially to the total cell counts. The paramenstrual type was in most cases haemorrhagic and highly cellular [369]. Ciliocytophtoria, anucleated remnants of ciliated mesothelial cells, can be occasionally observed in effluent dialysate, basically in young women. Inability to identify these structures can mislead the laboratory team as well as the physician to search for parasitic or fungal contamination [370].

The apparently puzzling effect of intraperitoneal saline inducing substantial influx of neutrophils into the abdominal cavity, which was observed long ago [361], was not confirmed when the experiments were carried out using sterile techniques. Bacterial lipopolysaccharides proved to be very effective in producing intraperitoneal exudate rich in cells [365]. This phenomenon was inhibited by prior intraperitoneal injection of cortisone [371].

In humans, sterile inflammatory effusions are characterized by a rich cellular content including neutrophils, lymphocytes, macrophages, mesothelial cells, eosinophils and basophils; usually in that order

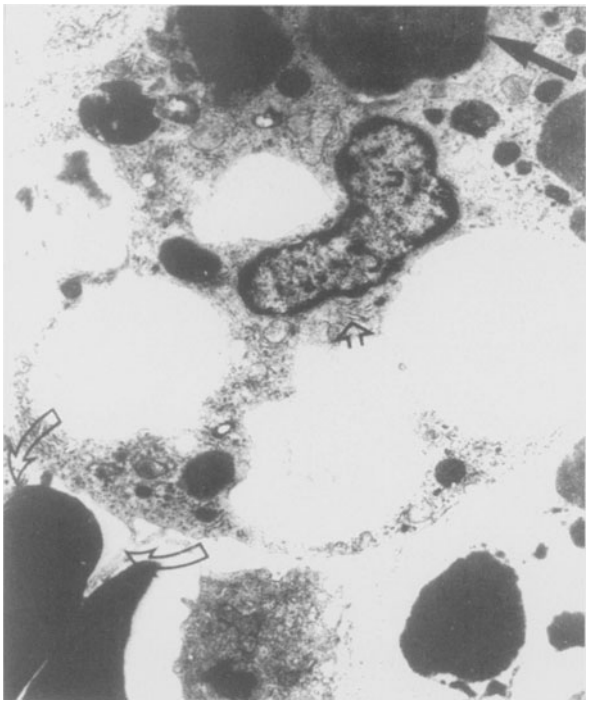

Figure 44. Peritoneal effluent obtained from a chronic uraemic patient on peritoneal dialysis. The macrophages depicted in the figure show phagolysosomes digesting erythrocytes (black arrow). Note the presence of rough endoplasmic reticulum (short open arrow) near the nucleus (n). The former normally appears in macrophages when the cells are involved in phagocytic activity. The curved open arrows are pointing to cell processes engulfing red blood cells ($\times$ 8600).

of frequency [372]. The presence of macrophages, mesothelial cells, lymphocytes, eosinophils and even plasma cells has been confirmed by electron microscope studies [373–375].

Peritoneal eosinophilia (eosinophils $>$10–50%) has been experimentally induced by intraperitoneal injection of iodine, chalk, nucleic acids, pilocarpine, haemoglobin or red blood cells, egg albumin, gold salts, mineral and vegetable oils, hydatidic fluid, and saline [372, 376]. On the other hand, intraperitoneal injection of bacteria and/or bacterial endotoxins induces a massive migration of neutrophils and monocytes into the peritoneal cavity [364, 377, 378].

The information presented above suggests that the cell content of effluent peritoneal dialysate is likely to be modified by so many factors that a concise description of a standardized cytological pattern becomes extremely difficult. There are, however, a few aspects of peritoneal effluent dialysate which have been defined: (a) patients on CAPD have total cell counts up to 50 cells/ml [379]. (b) The population of resident peritoneal cells observed in patients on long-term peritoneal dialysis is basically made up by macrophages (around 50% of the population), and lower prevalence of lymphocytes, mast cells and mesothelial cells [379–382]. (c) During infection there is a substantial increase in total cell number [383], as well as in the proportion of neutrophils [379–382]. (d) Fluid eosinophilia is a basic component of the still ill-defined eosinophilic peritonitis [384–386].

Ultrastructure of peritoneal fluid cells

Free-floating mesothelial cells are round or oval in shape and show a central, round nucleus (Fig. 45). Occasionally, binucleated mesothelial cells can be observed (Fig. 46). Nuclear chromatin is quite evenly distributed (Fig. 47, inset) and a small nucleolus may be observed. Numerous slender and sometimes branching microvilli emerge from the cytoplasmic membrane [373, 375, 387–389]. Branching microvilli, similar to those observed in human embryos [14], can be quite crowded in some cells, whereas in others they are scarce [375] (Fig. 47, inset). The glycocalyx covering the luminal aspect of the plasmalemma is endowed with electronegative fixed charges as shown in preparations exposed to the cationic tracer ruthenium red (Fig. 48). Mitochondria, numerous cisternae of rough endoplasmic reticulum and free ribosomes are mainly located in the outer part of the cytoplasm, and so are pinocytotic vesicles [373, 389]. The presence of intermediate-size filaments, perinuclear or irregularly scattered along the cytoplasm, has been documented in young free-floating mesothelial cells [372, 374], as well as in those recently implanted on the peritoneal surface (Fig. 49). These free-floating mesothelial cells should be distinguished from desquamated, degenerating mesothelial cells wandering in the peritoneal fluid (Fig. 46) [390]. Free-floating mesothelial cells in culture undergo mitotic activity [155].

Macrophages, which can be observed in large numbers, usually show an irregular and, at times, kidney-shaped nucleus with distorted masses of chromatin concentrated along the nuclear membrane (Figs 44 and 45). The cytoplasmic outline of macrophages is irregular, with thin processes of variable length which, at times, engulf degenerated cells (Fig. 44) or take the form of signet-ring macrophages (Fig. 5, inset). Mitochondria, a small Golgi complex and phagolysosomes are more evident when the cell is involved in phagocytic activity (Fig. 44).

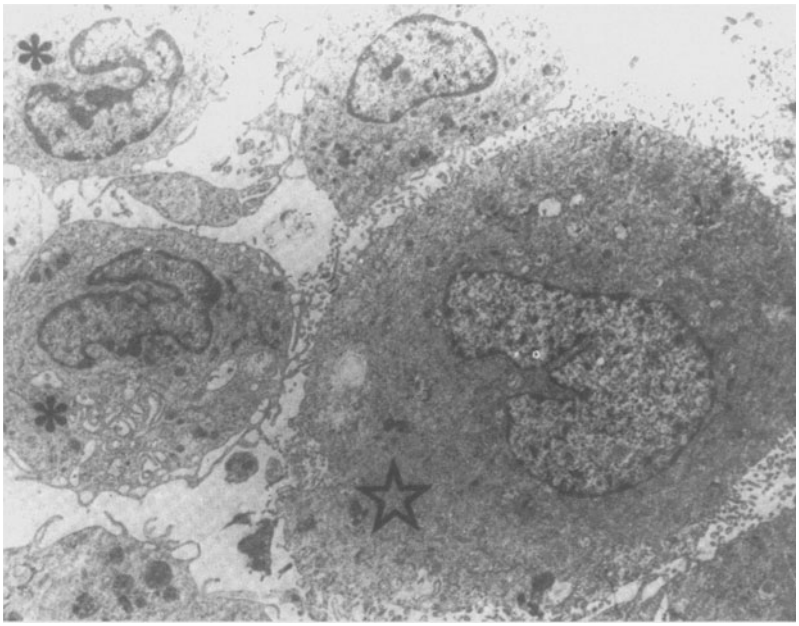

Figure 45. Effluent dialysate obtained from a non-infected uraemic patient, showing a floating mesothelial cell (star), as well as macrophages (*) (× 6900).

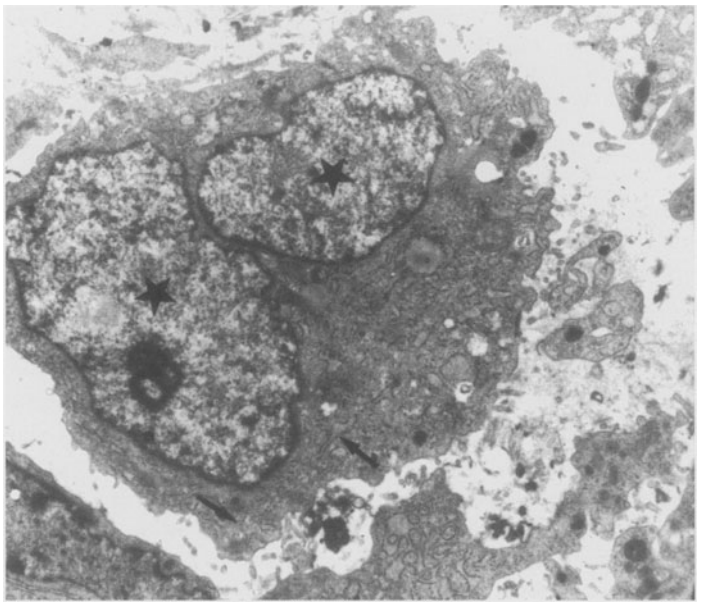

Figure 46. Binucleated mesothelial cell observed in effluent fluid from a patient on CAPD. Note the abundance of rough endoplasmic reticulum (arrows) (stars: nuclei of mesothelial cell) (× 8600).

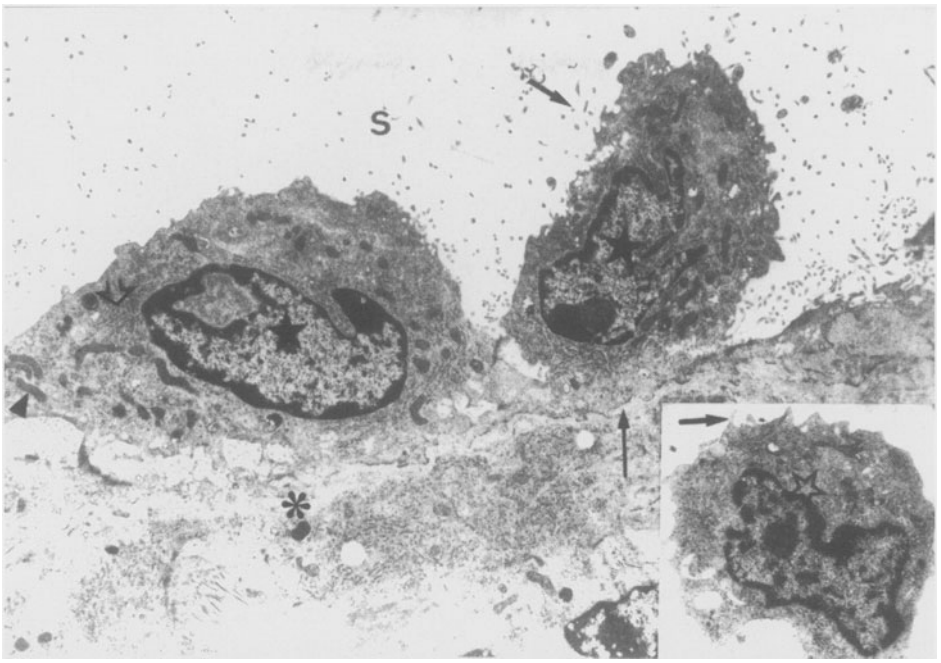

Figure 47. Sample taken from the parietal peritoneum of a patient on CAPD. Two recently implanted young and active mesothelial cells (black stars), showing numerous mitochondria (arrowhead), rough endoplasmic reticulum (open arrow) and microvilli (short arrow). The cell on the right is forming its own basement membrane (long arrow) (*: submesothelial connective tissue; S: peritoneal space) (× 6900).

Inset. Free-floating mesothelial cell (open star), seen in effluent dialysate of a CAPD patient (arrow: microvilli) (× 5600).

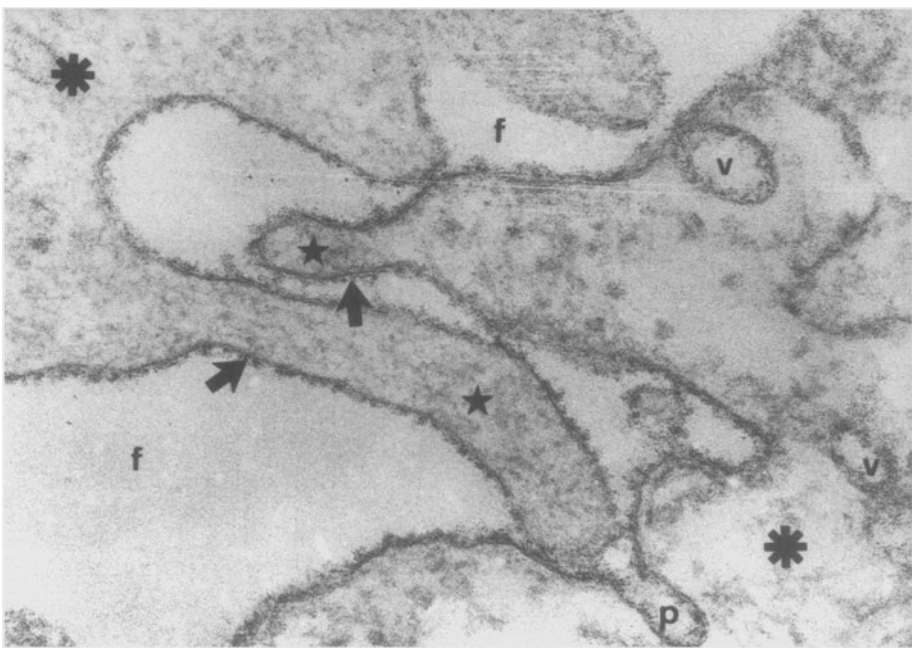

Figure 48. Wandering mesothelial cells (*) recovered from effluent dialysate of a CAPD patient. Ruthenium red decorates the electronegative plasmalemmal glycocalyx of microvilli (thick arrows), as well as that covering the internal aspect of a coated pit (p) and a pinocytotic vesicle (v) (f: peritoneal fluid) (× 87 000).

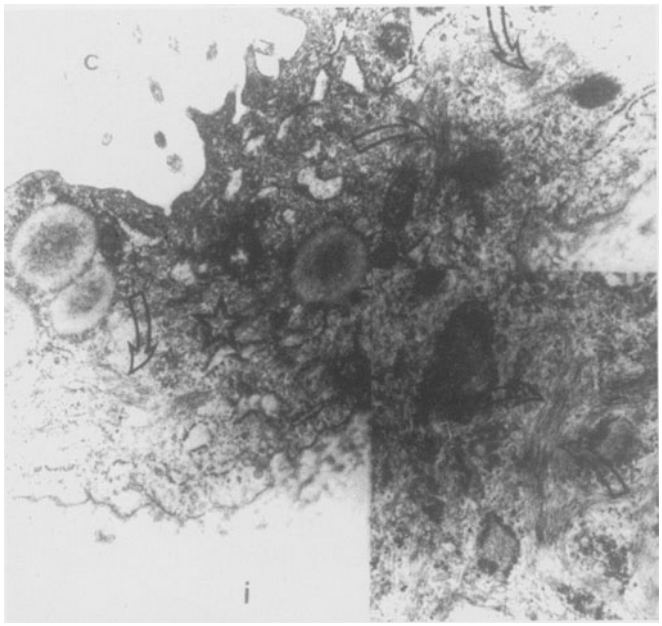

Figure 49. Biopsy of parietal peritoneum taken from a chronic uraemic patient 16 h after interruption of peritoneal dialysis. This recently implanted (~4–5 days) mesothelial cell (star) shows microvilli on its luminal aspect facing the abdominal cavity (c). The open arrows point to intermediate-size filaments. The basement membrane is still lacking (i: interstitium) (×15 400).
Lower right inset. Intermediate-size filaments at higher magnification (open arrows) (×24 600).

The ultrastructural aspect of inflammatory cells that eventually appear in the peritoneal fluid is similar to that classically described for other tissues.

Peritoneal ultrastructural changes during long-term peritoneal dialysis

Mesothelial cells are extremely sensitive to minor injury. Mild drying or wetting of rat caecal peritoneum for 5 min induced mesothelial cell degeneration and detachment, and severe interstitial oedema [391, 392]. Biopsies taken from CAPD patients also showed detachment of mesothelial cells (Fig. 20) and similar severe degenerative changes: widened intercellular spaces (Fig. 50) between mesothelial cells [393] and variable degrees of interstitial oedema (Figs 51, 52 and 53) [393, 394, 395].

In one of the deepest analyses of this topic, Di Paolo and colleagues described the (at that time) unexplained focal absence of microvilli, intercalated with areas where the other cells show a normal prevalence of these cytoplasmic prolongations (Figs 6 and 54) [23, 393]. This change is an early manifestation of impending apoptosis [25, 396–398], the prevalence of which has been shown to be increased in mesothelial cells exposed *in vitro* [399] as well as *in vivo* (Fig. 7) to glucose-enriched dialysis solutions.

Cell organelles are also affected by the dialysis solutions. Mitochondria frequently show a condensed appearance with increased material density, blurring of cristae and fusions of the inner membrane (Fig. 6), rating as stage III in the classification of Trump describing mitochondrial profiles following cell injury [400]. This situation of cell injury is still compatible with cell survival [401], even though it indicates impaired ability for ATP synthesis. Mitochondrial stage III can be observed in cells undergoing either necrosis or apoptosis [402]. Lamellar bodies (Fig. 55, right inset) described in human mesothelium not exposed to dialysis solutions [403], as well as lipid droplets (Fig. 46) are frequently observed in the mesothelial cytoplasm of patients treated by CAPD, and in that of animals exposed to high glucose concentration fluids (Fig. 56).

Substantial hypertrophy of the rough endoplasmic reticulum (Fig. 57, left inset) is an additional pattern commonly seen in samples of mesothelium taken from CAPD patients. This same material observed under electron and light microscopy revealed the presence of large binucleated cells in the mesothelial monolayer (Fig. 20; Fig. 57, right inset), some of

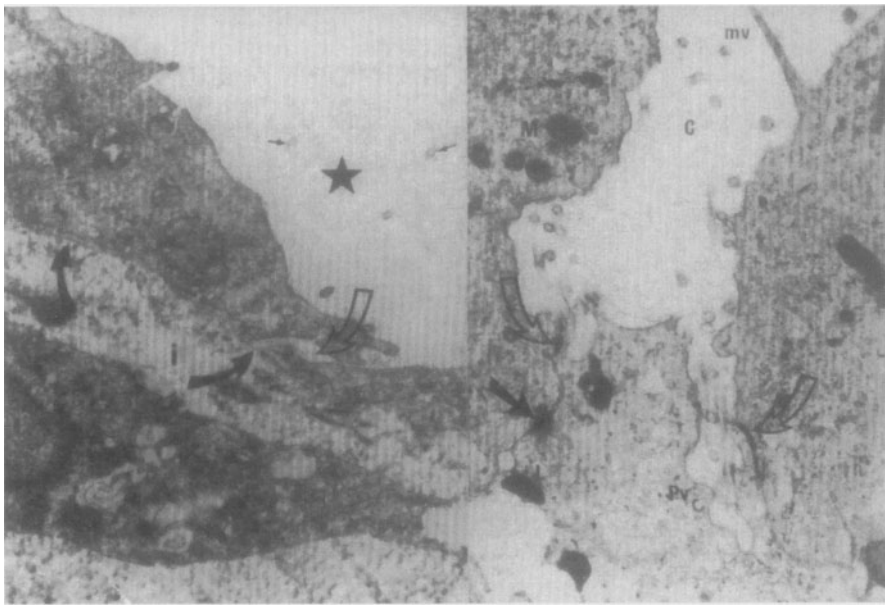

Figure 50. *Left.* Parietal peritoneum taken from a chronic uraemic patient, approximately 14 h after interruption of peritoneal dialysis. A few transversally sectioned microvilli (small arrows) can be seen in the peritoneal cavity (star). Two young adjacent mesothelial cells are separated by an open intercellular junction (open arrow). The basement membrane (black arrows) is, at times, interrupted (i: interstitium) (original magnification ×16 250).

Right. Another area of the same biopsy. The general appearance of the tissue is quite close to that observed in normals and to that reported by Ryan and Majno in rats, 7 days after injury. Note the presence of microvilli (mv), tight junctions (open arrows) and a desmosome (black arrow) (Pv: pinocytotic vesicles; M: mitochondria: L: lysosome; C: abdominal cavity) (original magnification ×16 250).

them exfoliating at times from the peritoneal luminal aspect (Fig. 20).

Furthermore, studies in rats treated for 6 weeks with daily intraperitoneal injections of a high-glucose-concentration dialysis solution showed a substantially increased mesothelial cell thickness [404]. These morphological alterations were interpreted as a reaction of the exposed cells to the continuous and long-term contact with unphysiological dialysis solutions. This concept was supported by evidence indicating that cultured mesothelial cells acutely [405–409] or chronically [410] exposed to dialysis solutions showed evidence of substantial functional and structural damage.

New challenges appeared after the early years of CAPD: biocompatibility of the dialysis solutions [411–416], the role of mesothelial cells in the defense mechanisms of the peritoneal cavity [417–419], and the eventual relevance of the mesothelial monolayer in the mechanisms of peritoneal permeability. On the other hand, research based only on ultrastructural observation of the mesothelium (electron microscopy) and light microscopy performed in biopsies taken from patients, carries some limitations. In patients, sequential observations (biopsies) cannot be performed, the population of patients will be characterized by a substantial heterogeneity, and the circumstances and timing prevailing when the biopsy is obtained will also make difficult the evaluation and classification of data. In this sense the obtained information will deal mainly with reactions of the entire peritoneum as an organ in response to the detrimental effects of the dialysis solution, and the effects of infection and other complications inherent in the therapeutic procedure. Furthermore, electron microscopy provides information on a limited number of cells. On the other hand, studies on cultures examine specific reactions of cells that are exposed for minutes, or a few hours, to experimental solutions, the physicochemical composition of which remains constant. This situation is much different from the continuously changing steady-state characteristic of peritoneal dialysis [420]. Therefore, having the feeling that a complementary approach was to be found, we developed the experimental method of population analysis of mice mesothelium, based on the method of imprints originally designed by Efskind [27], and later refined by Raftery and Whitaker [421, 422]. This experimental model, in which animals receive daily

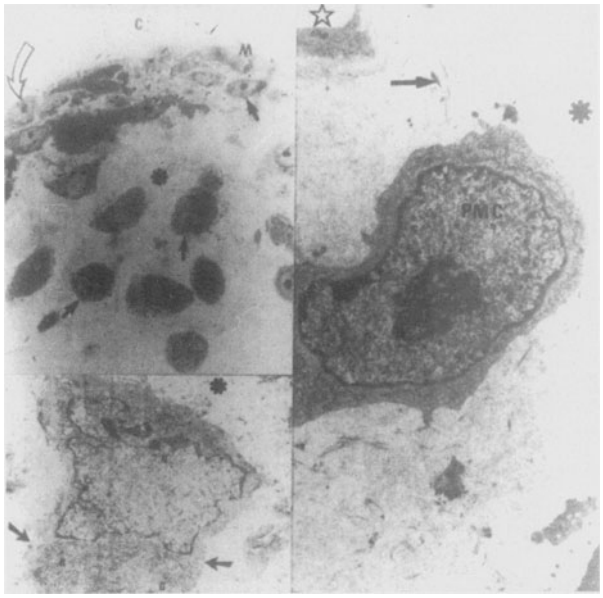

Figure 51. Biopsy taken from a chronic uraemic patient, 14 h after interruption of peritoneal dialysis.

Upper left. Mesothelial cell precursors (black arrows) appear to be progressing towards the peritoneal surface facing the abdominal cavity (C). One of these cells (open arrows) is already implanted on the luminal surface of the peritoneum. The elongated mesothelial cell (M) shows a nucleus quite similar to that of the precursors. The interstitium (*) is oedematous. This situation is similar to that observed by Ryan and Majno 3 days after experimentally induced severe mesothelial injury (original magnification ×400).

Lower left. This submesothelial interstitial cell (arrows) is interpreted as a mesothelial cell precursor. The cytoplasm shows protrusions and indentations. The irregularly shaped nucleus (N) shows fine and evenly distributed chromatin with a dense rim along the nuclear membrane. The presence of numerous cisternae of rough endoplasmic reticulum (R) indicates the high metabolic activity of this cell. The Golgi complex (G) is poorly developed as is usually observed in stem cells and fast-growing cells (*: interstitium) (original magnification ×10 450).

Right. This cell is interpreted as a primitive mesenchymal cell (PMC). The nucleus is oval, with some irregularities and shows a granular and even distribution of chromatin. A fine chromatin rim underlines the nuclear membrane. The nucleolus is prominent. These cells are usually arranged along interstitial blood capillaries (star). Note collagen fibres (arrow) between the cell and the blood capillary (*: interstitium) (×4400).

intraperitoneal injections of a dialysis solution, provides the possibility of *in-vivo* exposure and practically *in-situ* observation of the mesothelial monolayer at any given time, during the period of exposure and that of recovery [28]. Studies using this experimental set-up concluded that mesothelium exposed to glucose-enriched dialysis solutions develops a hypertrophic phenotype, characterized by increased enzymatic activity at the level of the cell membrane: Na,K,ATP-ase (Fig. 58), alkaline phosphatase and 5-nucleotidase, and cytoplasmic enzymes such as acid phosphatase, cytochrome oxidase (Fig. 59) and glucose-6-phosphatase (Figs 60 and 61) [423]. Additional parameters indicating the hypertrophic change were reduced density distribution of the mesothelial cell population derived from increased mean cell and cytoplasmic surface area, and the substantially high prevalence of large (up to three times) multinucleated cells (up to seven nuclei) (Fig. 62) [28, 276, 424]. This pattern of increased mean cellular surface, in addition to the fact that Slater *et al.* [404] reported an increased mean cell thickness in mesothelium of mice exposed for 6 weeks to daily intraperitoneal injections of 4.25% glucose lactated fluid, suggests that after long-term exposure to this dialysis solution cells had a substantially higher volume. Large multinucleated cells have been also described in effluent fluid of rabbits dialysed with high glucose concentration solutions [425]. These hypertrophic changes showed a dose-dependent relationship with the concentration of glucose: the higher the concentration of the aforementioned osmotic agent, the more marked the manifestations of cell hypertrophy [28, 276]. These changes bore no relationship to the pH [28, 276], or with the osmotic pressure of the solution, since they were not observed in mesothelial cells of mice exposed to dialysis fluid, having mannitol in iso-osmolar concentration the same as the osmotic agent [426]. Furthermore, exposure of the mesothelial monolayer to a glucose-free, lactated dialysis fluid, using the same experimental set-up, failed to induce any of the hypertrophic changes observed during exposure to glucose-enriched solutions [427].

The mitotic rate observed in intact mice (0.33%) was not far from the 0.25% prevalence previously reported by another laboratory using a different methodological approach [428]. However, in one of our early studies [28], we detected a substantial increase in the prevalence of mitosis only after a short (2 h) exposure to high glucose concentration (4.25%) dialysis solution (Figs 63 and 64), whereas at the end of the following period the mitotic rate was nil. This intriguing development was further investigated using the same experimental model of population analysis, injecting a high glucose concentration fluid (4.25%) for 30 consecutive days [429]. Samples were taken before and 2 h after one daily intraperitoneal injection of the high glucose concentration (4.25%) lactated-experimental solution. As

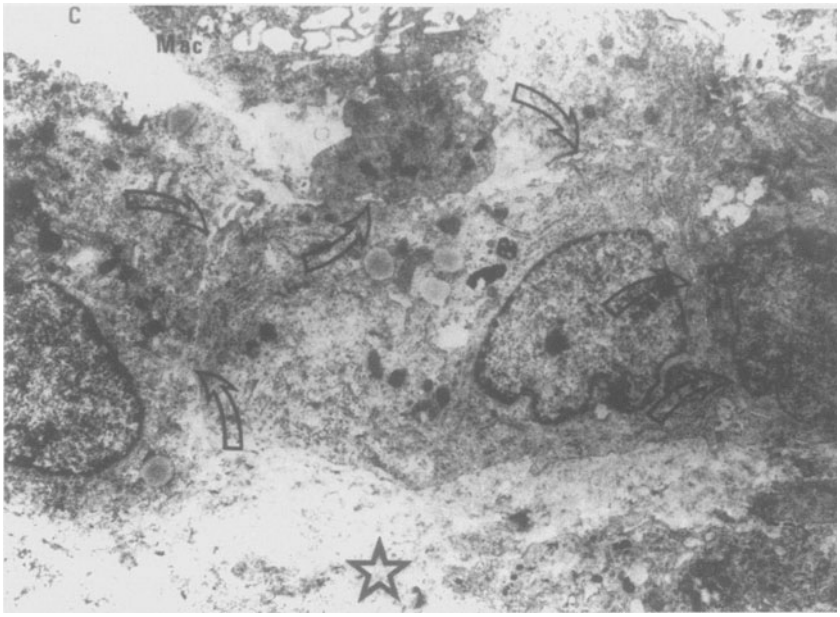

Figure 52. Biopsy of parietal peritoneum taken from a chronic uraemic patient 13 h after interruption of peritoneal dialysis. Note adjacent recently implanted mesothelial cells touching one another (open arrows), forming new intercellular junctions. There is no evidence of basement membrane. This situation is similar to that experimentally observed by Ryan and Majno 3–4 days after severe mesothelial injury (C: abdominal cavity; Mac: macrophage; star: interstitium) (original magnification $\times 5600$).

Figure 53. Biopsy of parietal peritoneum taken from an IPD patient (14 months on IPD). The young fibroblast depicted in the figure shows irregular cytoplasmic outline. The nucleus (N) is large, irregular with faint, widely distributed chromatin, which is concentrated at the nuclear periphery, forming a thin rim. Note a large, granular and central nucleolus (open arrow). The interstitium shows bundles of collagen fibres (open stars) as well as large areas of oedema (I) (R: endoplasmic reticulum) ($\times 8600$).

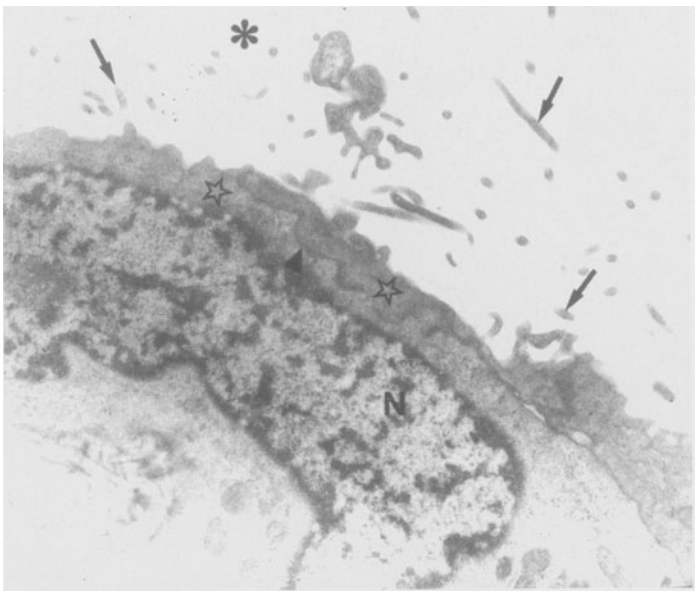

Figure 54. Parietal peritoneum of a patient on CAPD. Two adjacent mesothelial cells (open stars) show the normal presence of microvilli (arrows) (*: peritoneal space; arrowhead: intercellular junction; N: nucleus of mesothelial cell) (× 15 400).

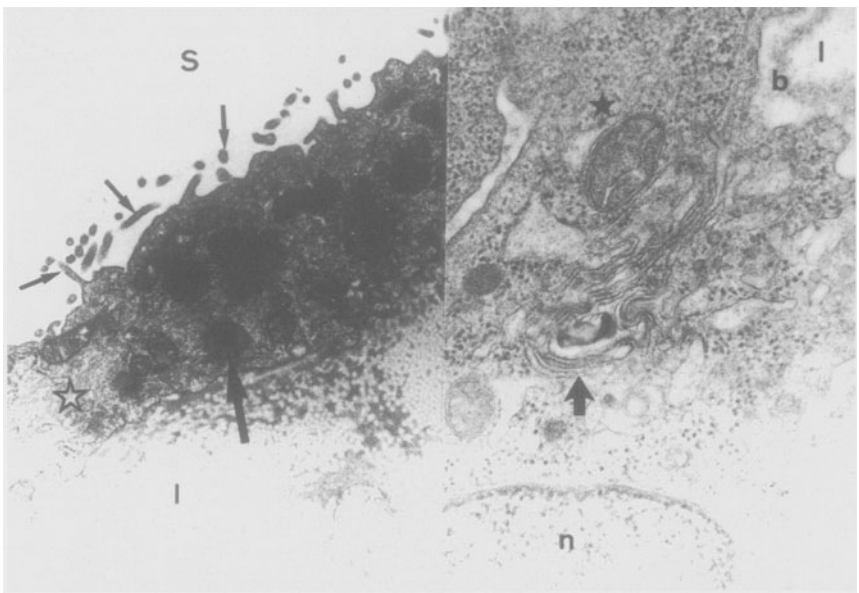

Figure 55. *Left.* Mesothelial cell (open star) observed in a biopsy of parietal peritoneum taken from a patient on CAPD. Note the presence of lipid droplets (long arrow) in the cytoplasm (S: peritoneal space; small arrows: microvilli; I: submesothelial interstitial space) (× 24 600).

Right. Lamellar body (arrow) in the cytoplasm (star) of a mesothelial cell seen in parietal peritoneum of another CAPD patient (n: nucleus of mesothelial cell; b: submesothelial basement membrane; I: interstitial space) (× 35 000).

shown in Fig. 65, this early acceleration of the cell cycle was maintained only during the first 3 days of exposure, reaching a prevalence of mitosis near zero on the 4th day (eight per 10 000 cells). This low prevalence lasted during the rest of the follow-up period (30 days). Additionally, mice exposed to lactate-free, high glucose concentration showed the same hypertrophic changes observed in animals treated with the commercially available high glucose solutions. This hypertrophied appearance, coupled to an extremely low mitotic activity observed *in vivo* as well as *in vitro* after long-term exposure [410],

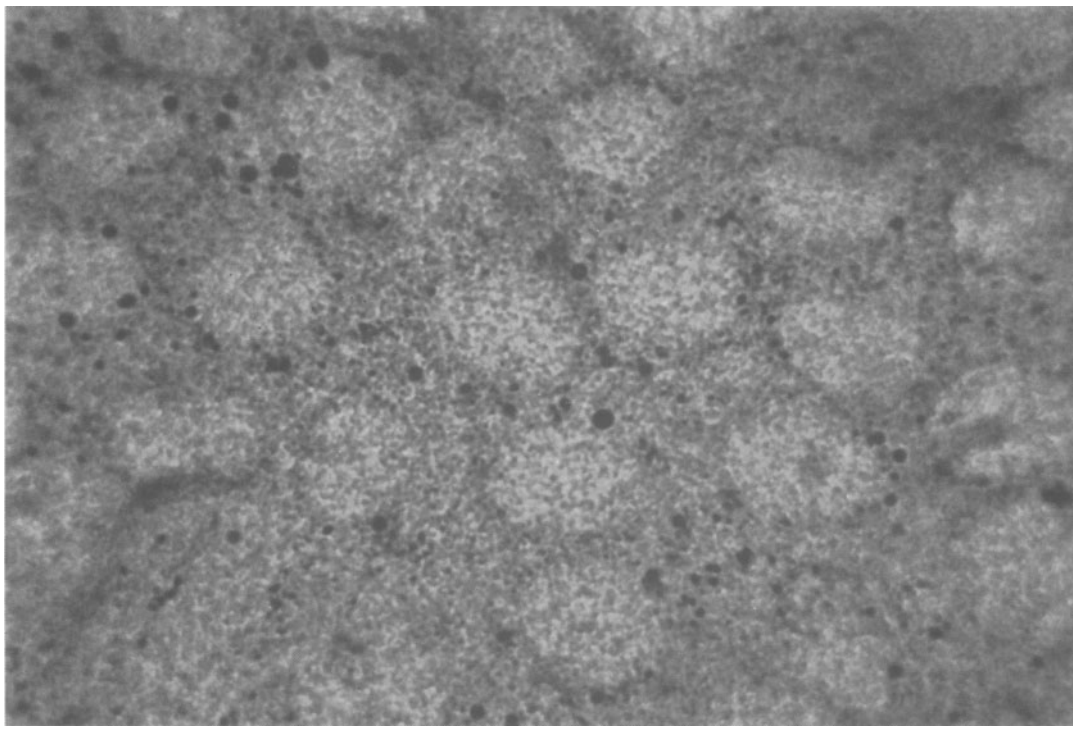

Figure 56. Mesothelial imprint taken from a mouse treated for 30 days with one daily intraperitoneal injection of high glucose (4.25%) dialysis fluid. The black dots are lipid droplets (Sudan black; ×1000).

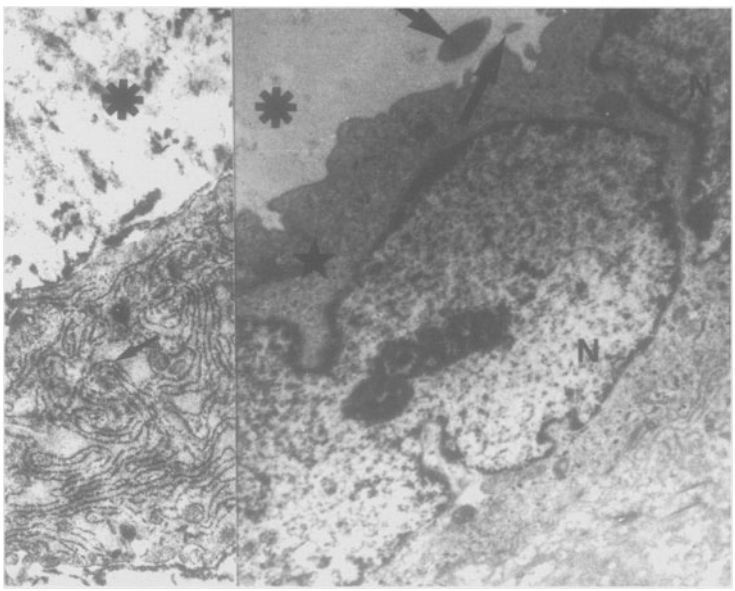

Figure 57. *Right.* Large binucleated mesothelial cell seen in parietal peritoneum of a CAPD patient (N and N′: nuclei of mesothelial cell; star: cytoplasm; arrows: microvilli; *: peritoneal space) (×24 600).

Left. Another mesothelial cell from the same biopsy. The arrow points at hypertrophic endoplasmic reticulum (*: peritoneal space) (×24 600).

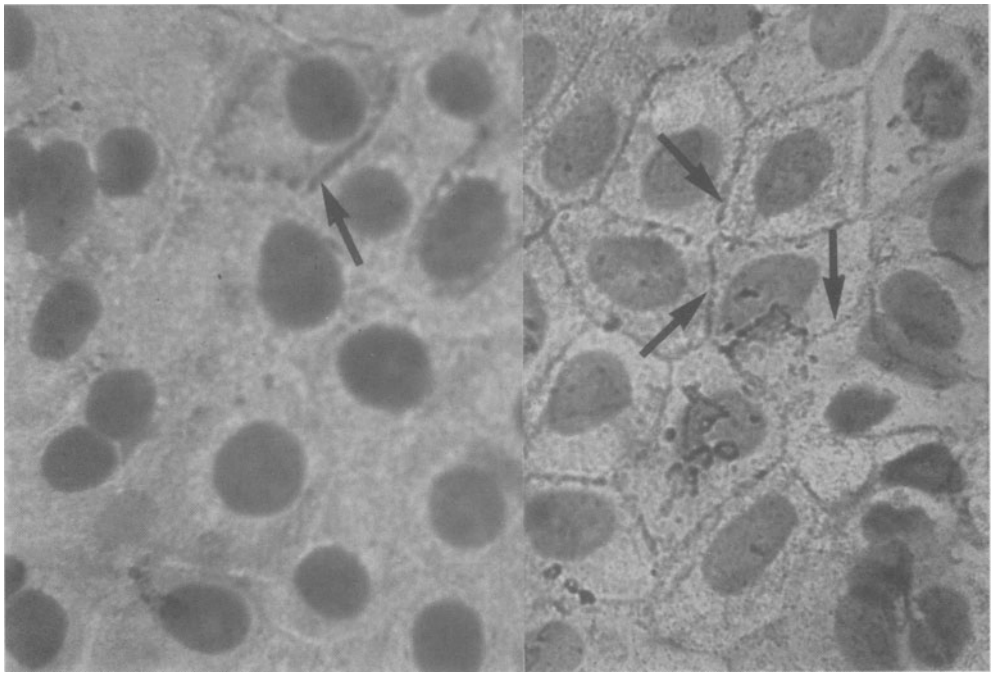

Figure 58. *Left.* Imprint taken from an intact mouse. Arrow points at the cell membrane of one mesothelial cell, showing positive staining for Na,K,ATPase.

Right. This sample was taken from a mouse exposed to 4.25% glucose-enriched dialysis fluid for 30 consecutive days. Note the substantial increased enzymatic activity (arrows) (Guth and Albers staining; ×1000).

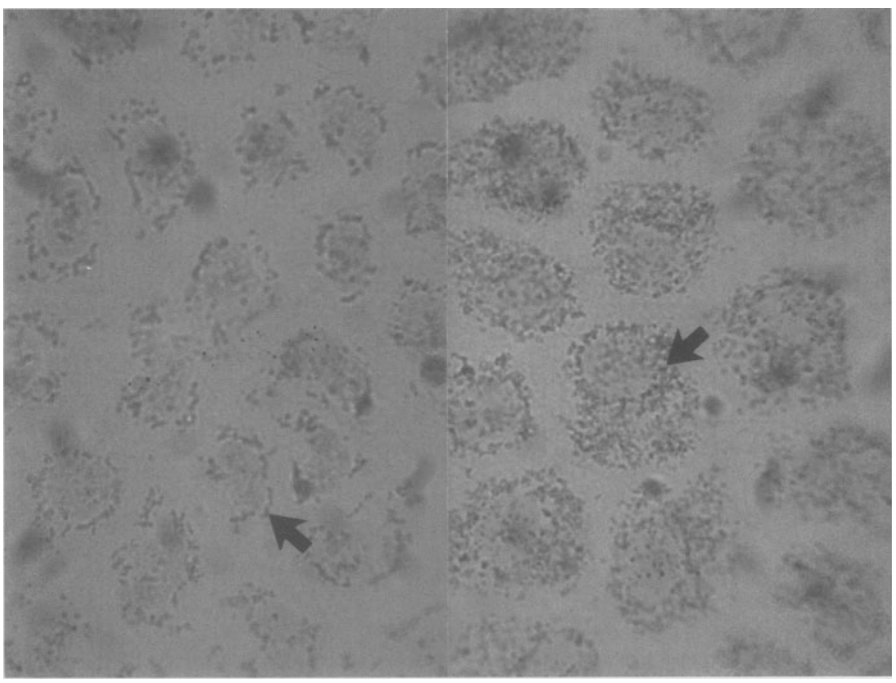

Figure 59. *Left.* Cytochrome-oxidase cytoplasmic activity (arrow points at granules) in a mesothelial cell imprint taken from an intact unexposed mouse (anterior liver surface) (DAB method of Seligman *et al.*; ×1000).

Right. This imprint was recovered from a mouse exposed to 4.25% glucose-enriched dialysis fluid for 30 consecutive days. Note the substantial increase of both the enzymatic activity (arrow) and the size of the cytoplasmic compartment (same staining and magnification).

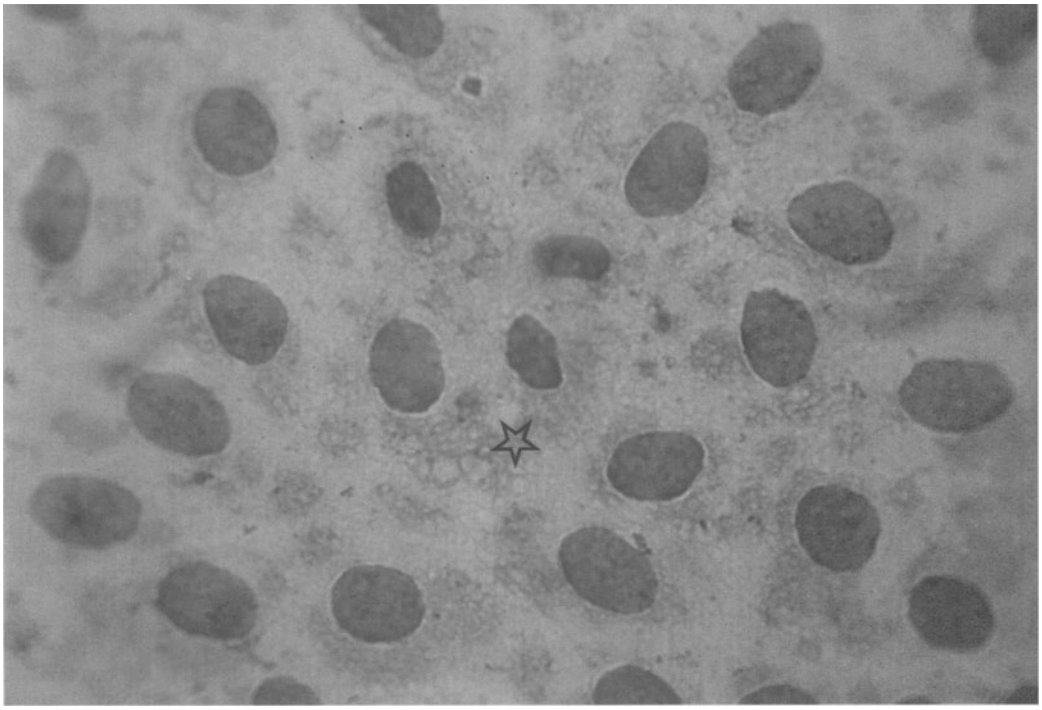

Figure 60. Visceral mesothelium of an intact mouse. Open star indicates staining of cytoplasmic glucose-6-phosphatase (lead method of Wachstein and Meisel; ×1000).

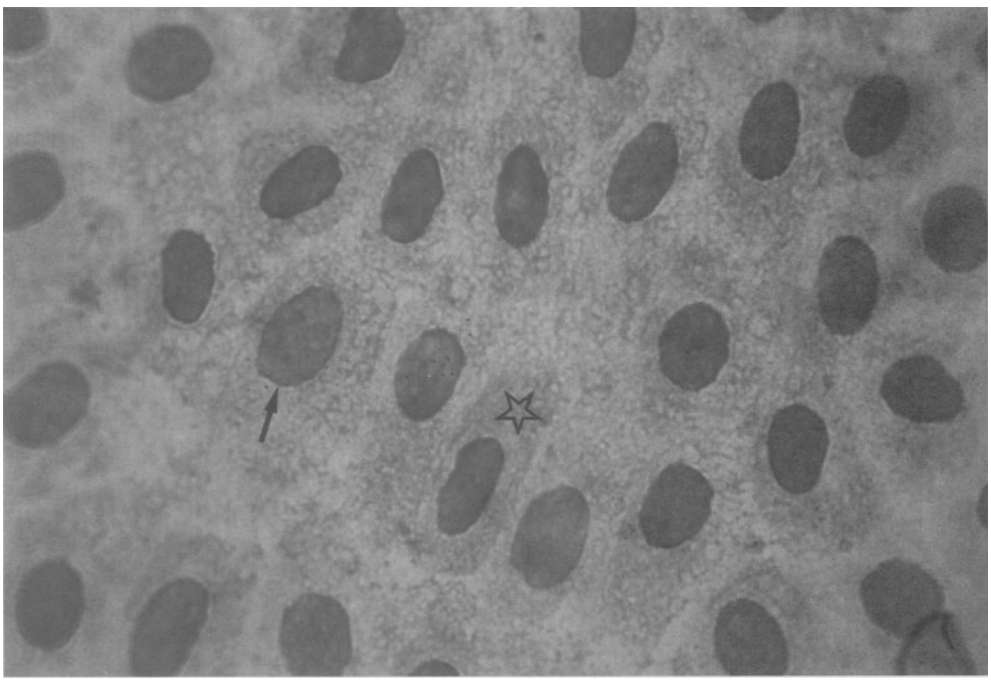

Figure 61. This material was obtained from the mesothelial monolayer covering the anterior liver surface of a mouse treated for 30 days with intraperitoneal injections of 4.25% glucose-enriched dialysis solution. Note the increased activity of the cytoplasmic glucose-6-phosphatase (open star pointing to the granules) (arrow: nucleus of mesothelial cell) (lead staining method of Wachstein and Meisel; ×1000).

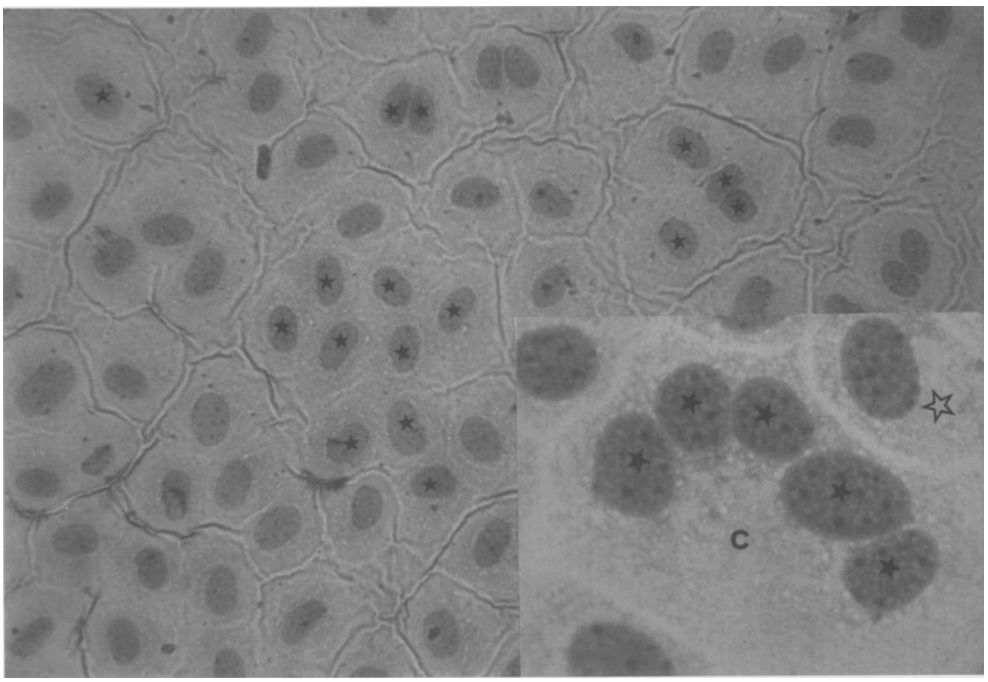

Figure 62. Mice exposed to high glucose concentration (4.25%) dialysis fluids for long periods of time (at least 30 days) can show as much as 50% of multinucleated cells (one star: mononuclear cell; two stars: binucleated cell; three stars: trinucleated cell; four stars: cell with four nuclei; six stars: cell showing six nuclei) (haematoxylin–eosin; ×400).

Inset. Imprint taken from the same mouse. Huge mesothelial cell (c) showing five nuclei. Compare with the normal size of a mononuclear cell (open star) (haematoxylin–eosin; ×1000).

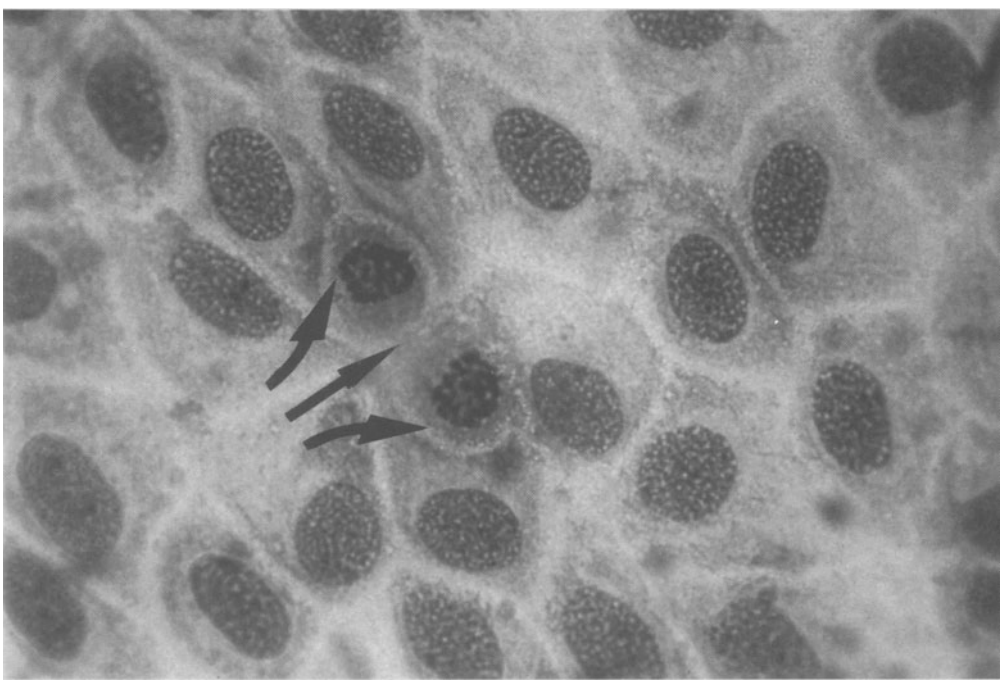

Figure 63. Normal, unexposed and unstimulated mesothelium shows a very low proportion of cells in mitosis at any given time. This photograph shows a mitotic cell at the time of cytokinesis (arrows) (haematoxylin–eosin; 1000).

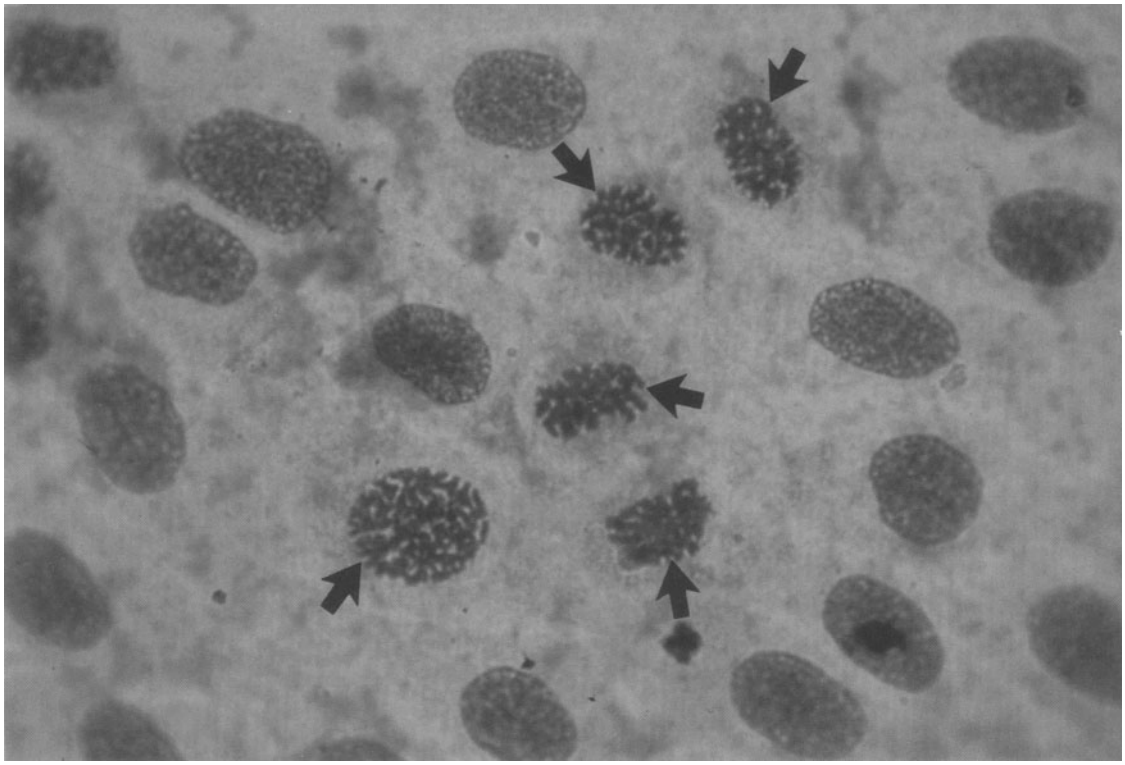

Figure 64. Sample of visceral mesothelium recovered from a mouse 2 h after one intraperitoneal injection of 4.25% glucose-enriched dialysis fluid. The photograph shows a substantial increase in the prevalence of cells in mitosis (arrows) (haematoxylin–eosin; ×1000).

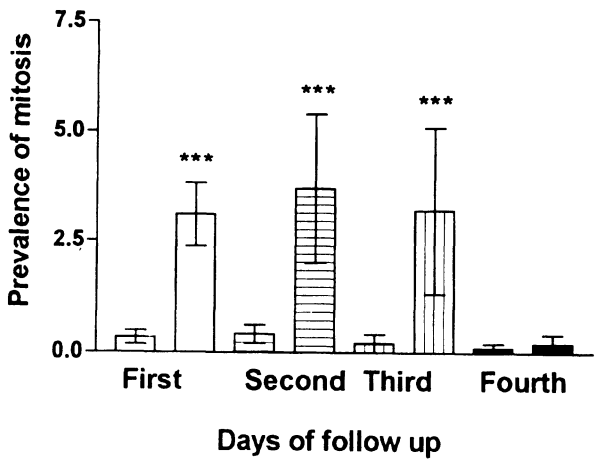

Figure 65. Bars at each time interval show prevalence of mitosis on each group of 10 mice, before and 2 h after the once-a-day intraperitoneal injection of the high glucose concentration (4.25%) lactate-free dialysis solution. The early acceleration of cell growth lasted only 3 days, after which the prevalence of mitosis remained of nil during the rest of the follow-up period (30 days).

indicates that glucose, in high concentration, induces in the exposed mesothelial monolayer the development of an hypertrophic phenotype of multinucleated (derived from defective cytokinesis) senescent cells, with low regenerative capabilities. This substantial change in the cell cycle of the mesothelial cell population was not related to the low pH, the presence of lactate, or to the high osmolality of the dialysis solution, but appeared specifically connected to the high concentration of glucose in the dialysis solution [28, 276, 426, 427]. Additionally, use of high glucose concentration in dialysis solutions is associated with a significant reduction of mesothelial cell viability (Figs 9 and 66).

What could be the link of high glucose concentration to these substantial changes of the cell cycle? Several reports have shown evidence indicating that different cell types, exposed to hydrogen peroxide, display a reduced rate of proliferation, increased multinucleation, expanded cell size, higher protein content indicating cellular hypertrophy, premature senescence, as well as higher prevalence of apoptosis

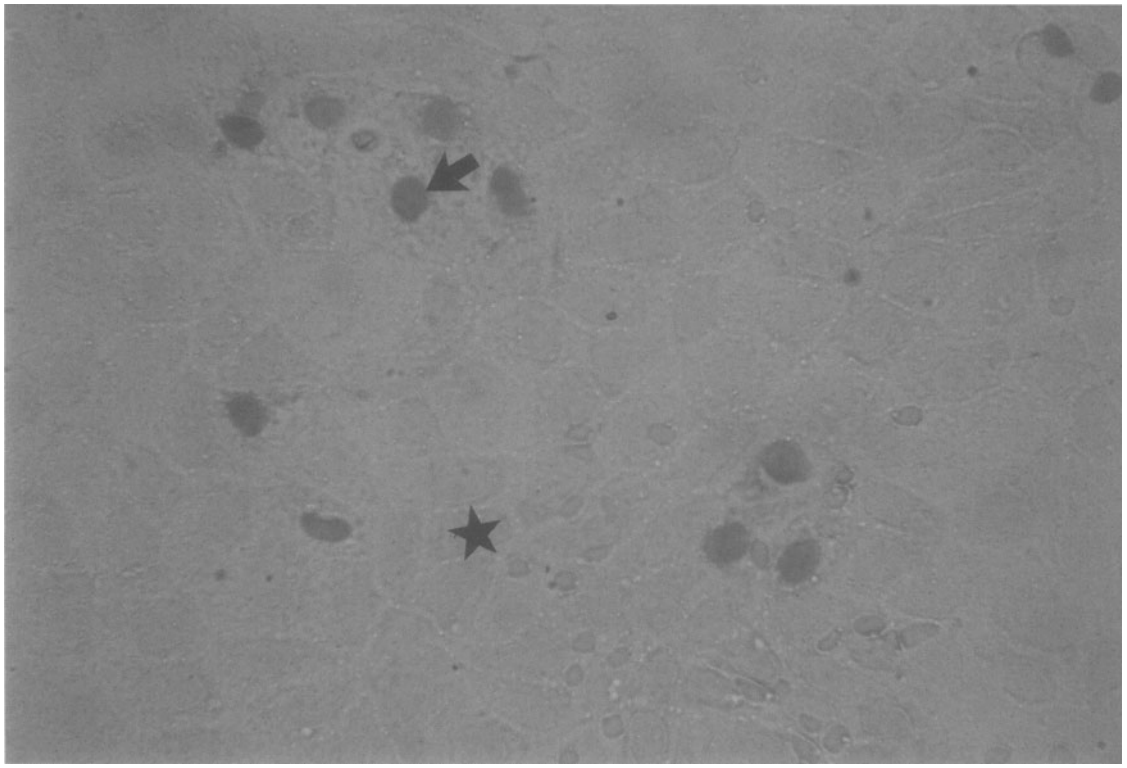

Figure 66. Trypan-blue exclusion performed in a sample of visceral mesothelium (anterior liver surface) recovered from a mouse after being injected for 30 consecutive days with high glucose (4.25%) dialysis fluid. The prevalence of non-viable cells (arrow) is higher than that seen in controls. Compare with Fig. 9 (star: viable cell) ($\times 400$).

[430–432]. Additional studies have shown the existence of a dose-related effect. Indeed, low levels of oxidants potentiate cell growth signals and enhance proliferation, whereas higher oxidant concentrations can block cell proliferation which, in turn, results in premature senescence and the consequent activation of the mechanisms leading to apoptotic cell death [433–435].

High glucose concentration (20 mmol/L), and the subsequent increased generation of oxygen-reactive species derived from glucose auto-oxidation, has been shown to induce a delayed replication of human endothelial cells in culture [436]. In this sense, the fact that mesothelial cells in culture significantly increased the generation of hydrogen peroxide when exposed to high glucose concentration (24 mmol/L), coupled to the observation that 24–27 mmol/L concentration of D-glucose (432–480 mg/100 ml), and not equimolar concentrations of L-glucose or raffinose, induced a substantial impairment of hydrogen peroxide degradation by human endothelial and mesothelial cells [437, 438], are further arguments pointing at the D-glucose-specific metabolism, and the subsequent increased generation of reactive oxygen species, as being the more suitable candidates to be blamed for the altered mesothelial cell cycle observed in our experimental animals. Therefore, it may be hypothesized that the D-glucose-dependent cell damage is a function of both the reduced production of scavengers, and the increased generation of reactive oxygen species [439], not only by the mesothelial cells, but also by the peritoneal phagocytes [440]. The fact that Amadori and AGE products are a source of H_2O_2 formation *in vitro* [441], and that glycation of peritoneal tissues is rapidly increased after 2 h of exposure to a 2.5% glucose dialysis fluid [442], suggests that these substances may well be an additional source of oxidative stress, acting on the exposed mesothelium.

All these elements, premature senescence due to accelerated cycle of the cell population, in addition to reduced viability, can be at the origin of areas of the peritoneal surface devoid from the normally present mesothelial monolayer observed in CAPD patients [443], as well as in experimental animals (Fig. 67). It may well be that a failure of the regenerative capabilities of the mesothelium can lead to

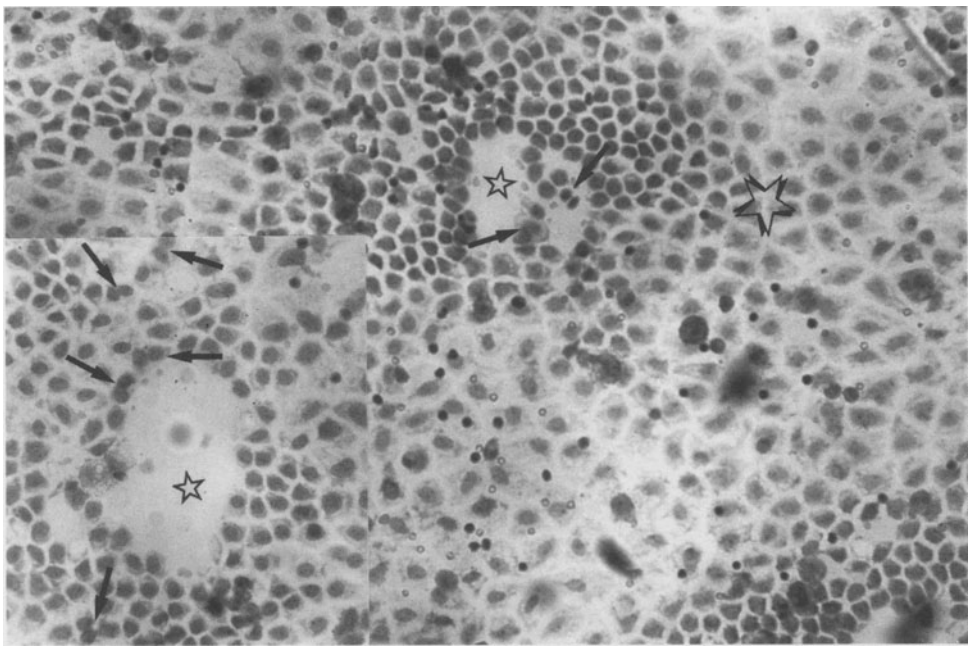

Figure 67. Imprint taken from a mouse after 7 days of recovery. The peritoneal cavity was exposed for 30 days to a high glucose (4.25%) dialysis solution. Open small star was placed in an area of the sample devoid of mesothelium. Arrows point at mitotic cells. Compare the higher density distribution of small cells in the mesothelial surface surrounding the area free from mesothelium, with the lower density observed in other part of the sample (double large star) (haematoxylin–eosin; ×160).

Inset. Another part of the same preparation. Several mitotic cells can be seen surrounding the area free from mesothelium (arrows) (haematoxylin–eosin; ×160).

repair the desertic peritoneal area, by means of fibrous tissue [444, 445]. This complication covers a wide range of morphological alterations starting from peritoneal opacification, passing through the tanned peritoneum syndrome, and finally reaching replacement of the serosal layer by fibrous tissue. This situation develops, in some patients, in the fearful syndrome of sclerosing encapsulating peritonitis (Fig. 68) [446, 447], in which a thickened, fibrous sheet of tissue envelops the small intestine. Fibrous bands may be present compromising spleen, liver and stomach, as well as pelvic organs. Light microscopy in both situations reveals serosal fibrosis and its worst consequence, sclerosing peritonitis, total absence of the mesothelial monolayer, replaced by a thick layer of connective fibrous tissue. Sclerosing peritonitis has been reported as idiopathic [448], associated with the use of some β-blockers such as practolol [449], propranolol [450], or timolol [451], as well as to metroprolol [452], and intraperitoneally administered antibiotics such as tetracycline [453]. In CAPD patients the origin of this complication is still ill-defined. Many possible factors have been invoked (acetate, hyperosmolarity, recurrent peritonitis, glucose, antiseptics, intraperitoneal antibiotics, bacterial endotoxins), even though there is no available evidence clearly demonstrating specific relevance for any of them [444, 454]. Experimental studies have suggested that a substantial decrease in the mesothelial fibrinolytic activity could be the most likely initiating mechanism [455–457]. Increased thickness of the submesothelial collagenous layer, apparently leading to a decreased peritoneal ultrafiltration potential, has also been reported [395].

Some researchers have reported small plastic particles [393, 395] as well as cytoplasmic inclusions of crystals (Fig. 69), both probably resulting from the use of contaminated dialysis solutions or defective lines and/or bags.

It has been shown that the mesothelium has powerful regenerative capabilities [391, 392]. Comparison of experimental observations with those obtained from patients on maintenance peritoneal dialysis suggests that most of the observed peritoneal ultrastructural changes are the end-results of two processes occurring simultaneously: mesothelial injury and regeneration [458].

Biopsies taken from IPD patients approximately 14–16 h after completion of peritoneal dialysis showed peritoneal areas denuded of mesothelium and covered only by smooth muscle cells. Round,

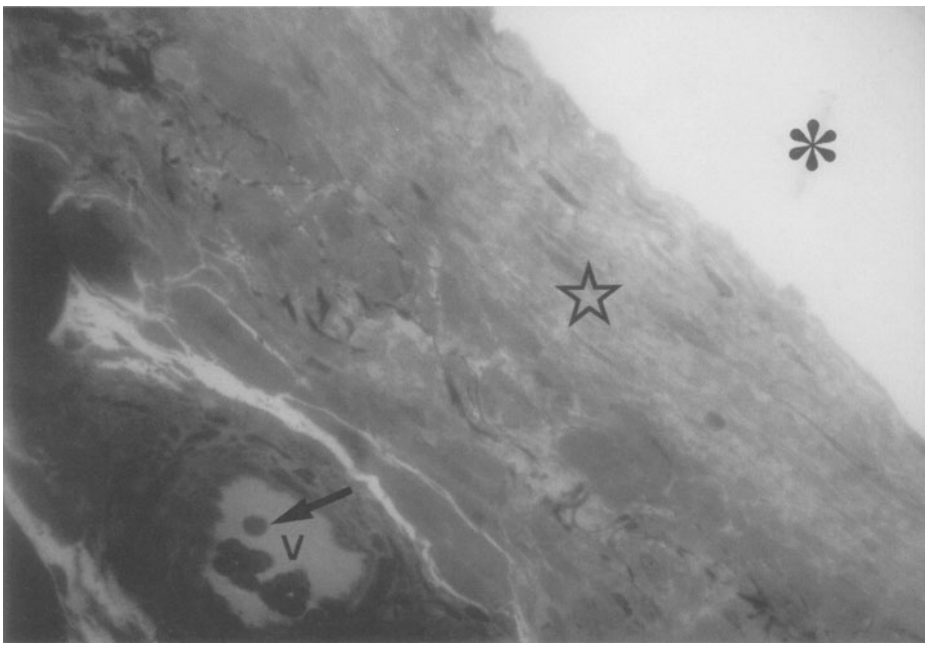

Figure 68. Biopsy of parietal peritoneum. The patient developed total membrane failure after being treated with CAPD for 39 months, at the time the biopsy was taken. Note the absence of mesothelium on the peritoneal surface facing the abdominal cavity (*). Huge amounts of fibrous tissue replaced the missing monolayer (open star). Thickness of the repair tissue ranges between 163 and 175 μm. Distance between the peritoneal cavity and the venule (v) is around 190 μm. With the diagnosis of peritoneal sclerosis the patient was referred to haemodialysis (compare with Fig. 10) (haematoxylin–eosin; ×400).

Figure 69. Biopsy of parietal peritoneum taken from a chronic uraemic patient, 10 days after interruption of peritoneal dialysis. This patient was on peritoneal dialysis for 7 months. The mesothelial cell (star) depicted in the figure shows crystalline inclusions (open arrows), mitochondria (M), smooth endoplasmic reticulum (framed by the open star), as well as microvilli (black arrow) (C: abdominal cavity) (×50 720).

mononuclear, wandering mesothelial cells coming up from the peritoneum and, at times, macrophages were observed settling at the injured areas (Fig. 5; Fig. 70, inset). These findings resemble those made by Ryan *et al.* [391] 24 h after experimental mesothelial injury. Other areas of the same biopsies showed recently implanted young mesothelial cells (Figs 47 and 70). Both the mesothelial basement membrane and microvilli were absent. Adjoining mesothelial cells occasionally appeared forming new intercellular junctions which were still more or less open (Fig. 50, left; Fig. 70). The submesothelial interstitium was grossly oedematous (Figs 52 and 53). Similar ultrastructural features were observed experimentally 3 days after mesothelial injury [391, 392].

Figure 70. Parietal peritoneum of a patient on IPD. The biopsy was taken 13 h after peritoneal dialysis was interrupted. This electron micrograph shows two recently implanted new mesothelial cells, still separated by a wide intercellular space (open arrows). The cytoplasm is rich in rough endoplasmic reticulum (black arrows) and mitochondria (open star) (N: nucleus) (×19 200).

Lower right inset. Wandering mesothelial cells (arrows) coming from the peritoneal space (c) are repopulating the denuded peritoneal surface. The smaller round cells are macrophages (original magnification ×400).

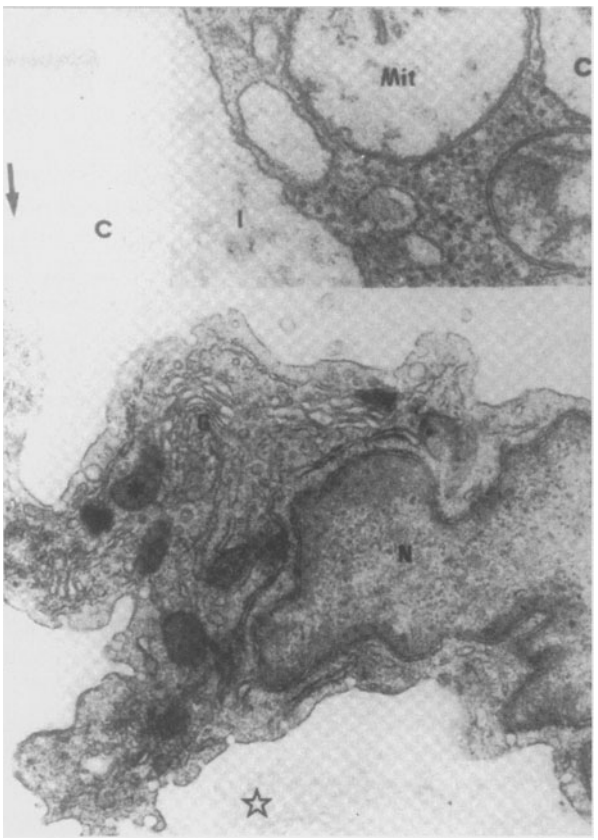

Figure 71. Mesentery of rat. The animal was sacrificed after 14 consecutive intraperitoneal injections of 0.2% furfural, on a daily basis. The young mesothelial cell appearing in this electron micrograph shows some microvilli (black arrow), an irregularly shaped nucleus (N), hypertrophic Golgi complex (G), and mitochondria (*). The normally observed submesothelial membrane is absent. The interstitial space (I) is grossly oedematous. A few collagen fibres (star) can be seen at the bottom (original magnification ×24 600).

Upper right inset. A different mesothelial cell of the same sample showing marked mitochondrial swelling (Mit) as well as absence of basement membrane (C: abdominal cavity; I: interstitium) (original magnification ×50 720).

Other specimens, taken from patients approximately 14–16 h after peritoneal dialysis, showed young mesothelial cells building a new basement membrane (Figs 18 and 50), as well as new microvilli which sometimes took on the worm-like appearance of micropinocytosis vermiformis (Fig. 18). These were reminiscent of the branching microvilli observed in mesothelial cells of human embryos in the 5th–6th week of gestation [14]. This sequence of mesothelial regeneration is compatible with that observed 4–5 days after experimental mesothelial injury [391]. Biopsies taken 10 or more days after the last peritoneal dialysis had a normal mesothelial lining which,

in one case, showed intracytoplasmic crystalline inclusions (Fig. 69).

In summary, studies performed on PD patients disclosed that different blocks taken from one biopsy of parietal peritoneum showed each of the above-mentioned steps of mesothelial regeneration taking place simultaneously in different areas of the peritoneal surface [458]. From these observations it can be inferred that the currently used peritoneal dialysis solutions induce a situation of continuous mesothelial injury, which is restored by a continuous process of regeneration and/or repair. Similar ultrastructural changes were experimentally induced by intraperitoneal injections of furfural, one of the many substances resulting from the non-enzymatic degradation of glucose (Fig. 14) [459].

The detrimental effects of the dialysis fluids do not spare the peritoneal microvasculature. Small venules show specifically fibrosis and hyalinization of the media. Immunofluorescence microscopy revealed extensive deposition of type IV collagen and laminin in the microvascular wall, whereas electron microscope observation detected substantially increased presence of collagen fibres and degenerative changes of smooth muscle cells [460].

Interstitial oedema (Figs 49 and 51) results from the inflammatory reaction after injury. The presence of wide-open intercellular channels (Fig. 50) occurring after mesothelial injury would reflect a specific stage in the process of building new junctions by the new mesothelial cells [388, 392, 461, 462] (Figs 50 and 52). Ultrastructural studies on mouse embryo [13] revealed that mesothelial cells directly derived from mesenchymal cells showed increasing numbers of microvilli according to the extent of the differentiation. Therefore, the aforementioned lack or scarcity of microvilli in recently implanted cells could also denote the presence of less mature, regenerating mesothelial cells at the peritoneal luminal surface [22].

The origin of the new mesothelial cells

It has been experimentally shown that small and large mesothelial wounds heal at the same rate within 7–10 days after injury [463]. The basal, normally observed mitotic rate of mesothelial cells, as measured in the rat by ^{3}H-thymidine incorporation, is approximately 1%/day. This rate is significantly increased during peritonitis, reaching maximal values of up to 19% between 1 and 3 days after injury, and returning to the basal activity on the 4th or 5th day [464]. It should be noted, however, that proliferations of fibroblasts, as well as mesothelial cell regeneration, are substantially inhibited in experimental uraemic animals [464–466].

The origin of the new mesothelial cells repopulating denuded areas of injury is still controversial. Four different hypotheses have been proposed:

1. The repopulating cells originate from the bone marrow [99]. Other experimental studies showed, however, that whole-body irradiation sufficient to depress peripheral white blood cell count as well as cell replacement by the bone marrow did not prevent mesothelial healing [467]. Therefore, the existence of a circulating mesothelial precursor originating from the bone marrow seems unlikely.
2. Mature mesothelial cells from adjacent and/or opposed areas proliferate, exfoliate and migrate to repopulate the affected surface [462, 463, 468]. Other investigators [465, 469, 470] have not accepted this hypothesis.
3. Other studies [387, 465, 471] suggested the sequence of a two-stage process; during the first 24 h, macrophages forming the first line of defence [472] and coming from the peritoneal fluid repopulate the wound surface (Fig. 5, inset; Fig. 72). Later, during the second stage, new mesothelial cells, arising from metaplasia of mesenchymal precursors located in the interstitial tissue well below the site of injury, migrate to the surface and differentiate into mature mesothelial cells (Fig. 51). This hypothesis has not been universally accepted [22, 391, 392, 461, 463]. It has also been suggested that the early implanted macrophages are gradually transformed into mesothelial cells [461]. However, Raftery [473], after labelling peritoneal macrophages with polystyrene spheres, presented strong evidence against the hypothesis that peritoneal macrophages could be transformed into mesothelial cells.

   Primitive mesenchymal cells which have been observed deep in the interstitial tissue [474] (Fig. 51, right) are multipotential and can give rise to a wide variety of cells, including mesothelium [469, 475].

   Mesothelial cell precursors coming up from the submesothelial connective tissue were also observed under the damaged areas. The nuclear and cytoplasmic aspects of these cells were identical to that shown by new mesothelial cells already implanted on the peritoneal surface (Fig. 51, upper left). This approach is supported by observations made in imprints taken from

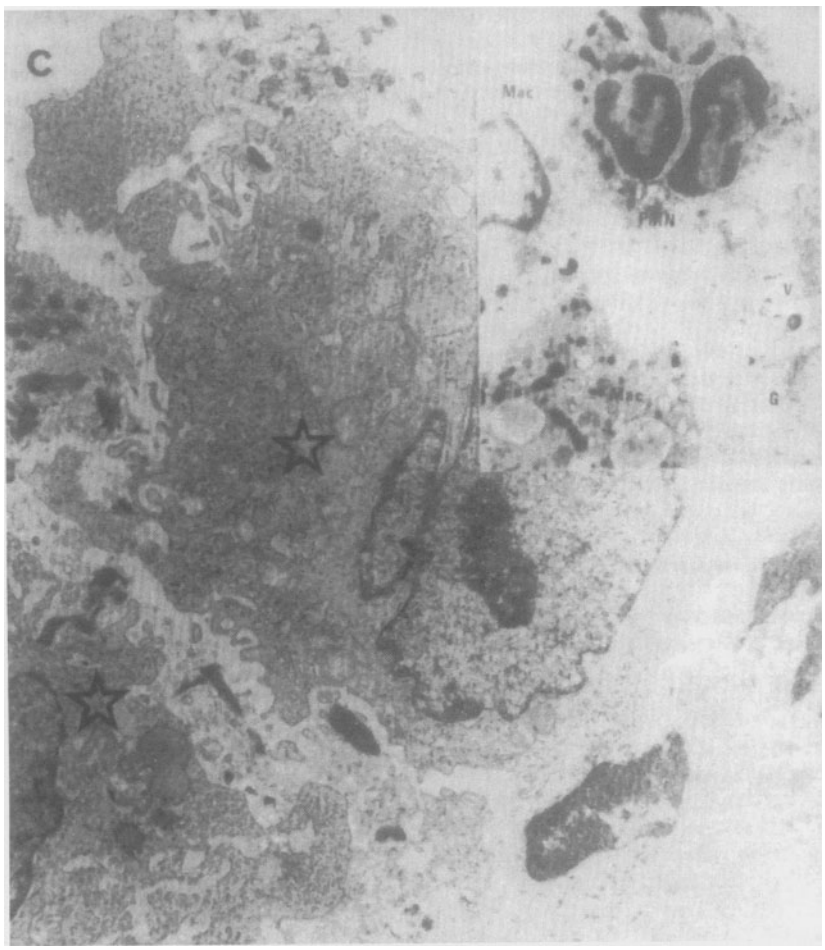

Figure 72. Biopsy of parietal peritoneum, taken during an episode of peritonitis, from a chronic uraemic patient on peritoneal dialysis. Recently implanted (1–2 days) mesothelial cells (stars), apparently coming from the abdominal cavity (C), are repopulating the denuded peritoneal surface (original magnification ×8400).

Upper right inset. A different area of the same biopsy showing a recently implanted mesothelial cell with caveolae (V), rough endoplasmic reticulum (R) and hypertrophic Golgi complex (G). Notice the presence of macrophages (Mac) and polymorphonuclears (PMN) (original magnification ×12 600).

intact unexposed mice that showed a prevalence of mitosis around 0.33% [28] (Fig. 7) and a substantial increase after a 2 h exposure to a high glucose concentration fluid (Fig. 64). Additional still-unpublished histochemical studies (Shostak, Wajsbrot and Gotloib) have detected in the unexposed mouse, passage of mesothelial cells through the G1 checking point, demonstrated by immunohistochemical assessment of PCNA (proliferative cell nuclear antigen) (Fig. 73). Furthermore, unexposed mesothelial cells enter S phase as indicated by their capability to incorporate tritriated thymidine, as shown by observations made using autoradiography (Figs 74 and 75). As observed with mitosis, this activity is substantially stimulated by a 2 h *in-vivo* and *in-situ* exposure to a high glucose concentration solution (Fig. 76). In addition, mitotic cells can be observed surrounding areas devoid of mesothelium (Fig. 67), indicating the relevance of the local regenerative capabilities of the injured mesothelial monolayer [476].

4. Free-floating cells of the serosal cavity settle on the injured areas and gradually differentiate into new mesothelial cells [391, 392, 428, 469] (Figs 47 and 50). It should be noted that desquamated, mature mesothelial cells show degenerative changes which, as previously stated, are absent in the young, free-floating mesothelial cells. The relevance of this mechanism is attested by experiments showing the feasibility of autologous

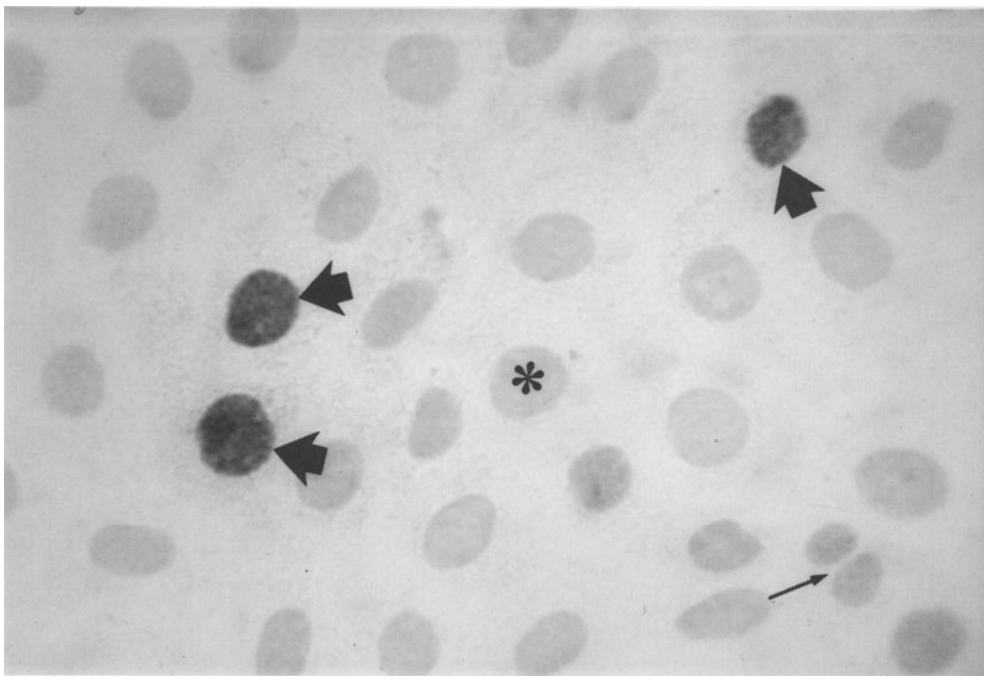

Figure 73. Imprint taken from an intact, unexposed control mouse. Arrows point at mesothelial cells passing through the G1 checkpoint (thick arrows) (*: cells before the G1 checkpoint; thin arrow: binucleated mesothelial cell) (PCNA staining; streptavidin–biotin system; ×400).

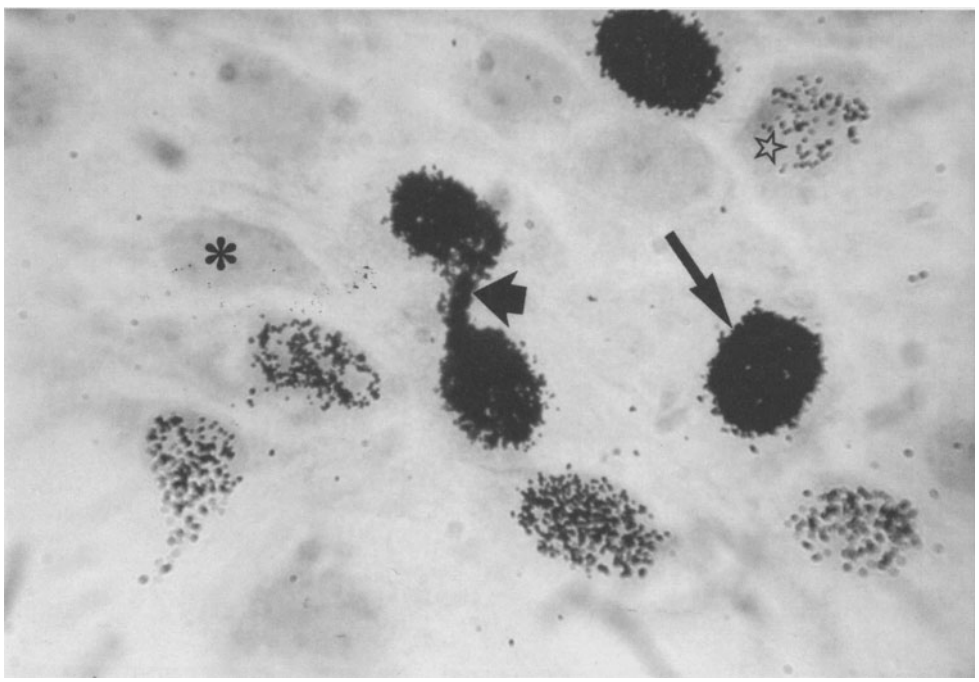

Figure 74. This photograph of a mesothelial cell imprint was taken from the anterior liver surface of a mouse. It shows, using the technique of autoradiography, the incorporation of tritiated thymidine within mesothelial cells, as well as different moments of the cell cycle. Asterisk indicates a cell in G1. Open star directs attention to a cell at the beginning of S phase. Long arrow indicates another cell at the end of S phase, or probably in G2. Short black arrow points at one cell processed at the time of cariokinesis (haematoxylin–eosin; ×1000).

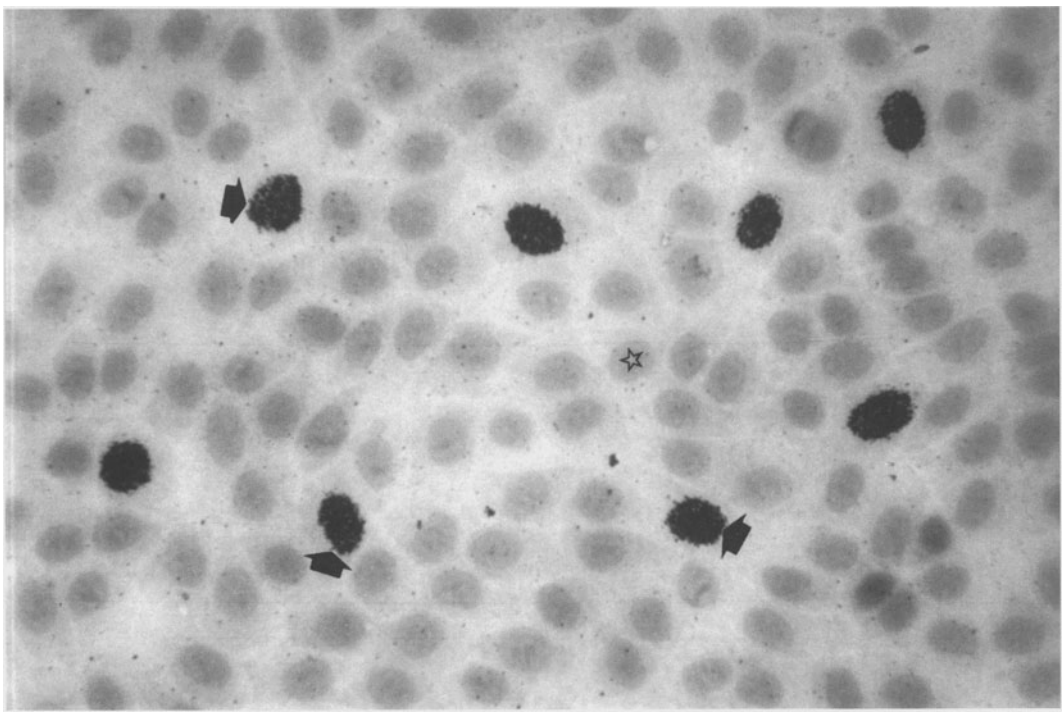

Figure 75. Thymidine incorporation seen in an imprint obtained from an intact, unexposed control animal (arrows: cells incorporating thymidine; open star: cells in G1) (autoradiography and haematoxylin–eosin; ×400).

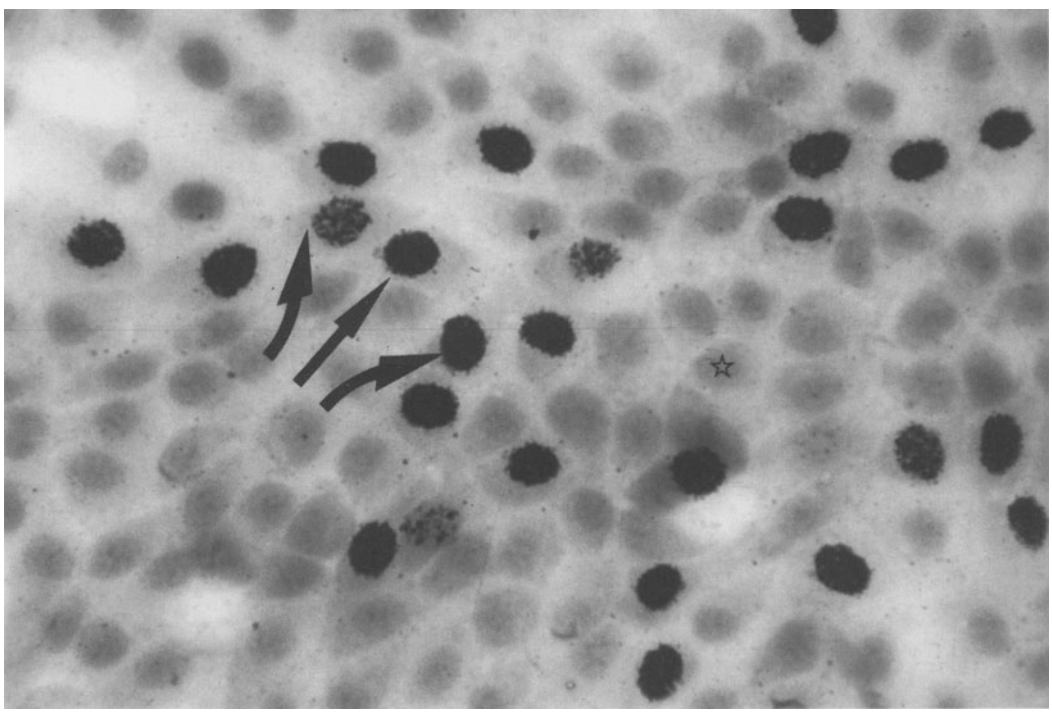

Figure 76. Mesothelial cell imprint obtained from a mice 2 h after intraperitoneal injection of a 4.25% glucose-enriched fluid for peritoneal dialysis. Note the substantial increase of cells incorporating thymidine (arrows); compare with previous figure (open arrow: cell in G1) (autoradiography and haematoxylin–eosin; ×400).

mesothelial cell implants in both experimental animals and human patients' [407].

All this evidence suggests that, most likely, mesothelial cell regeneration takes place through three different processes occurring simultaneously: implantation of young wandering mesothelial cells, migration of mesothelial cell precursors coming from the underlying connective tissue, and mitosis of young cells bordering the injured area.

Structural changes during septic peritonitis

This condition results in acute inflammatory changes affecting all the peritoneal structures. The density distribution of mesothelial cells is substantially reduced, and the presence of microorganisms can be detected in the denuded peritoneal surface as well as within mesothelial cells (Fig. 77). Mesothelial cells, necrotic or showing severe degenerative changes, exfoliate. The submesothelial basement membrane disappears (Fig. 21), together with the normally present anionic fixed charges (Figs 21 and 78).

Experimental studies have shown that the anionic fixed charges of mesothelial glycocalyx and microvilli, which were still present 24 h after induction of peritonitis, were not observed 5 days later, and partially reappeared 13 days after the onset of the experiment [177].

The interstitium becomes grossly oedematous (Fig. 21), as well as infiltrated by acute inflammatory cells. The microvessels occasionally show wide-open intercellular junctions (Fig. 25, inset), as well as a sharp decrease in the subendothelial density distribution of anionic fixed charges (Fig. 25, left; Fig. 28) [177]. Endothelial mitochondria show signs of severe injury [Fig. 79).

Almost simultaneously, macrophages and young mesothelial cells start to repopulate the denuded luminal peritoneal surface (Fig. 70). Polymorphonuclears (Fig. 70, inset; Fig. 79) and monocytes are usually present at the luminal surface, as well as in

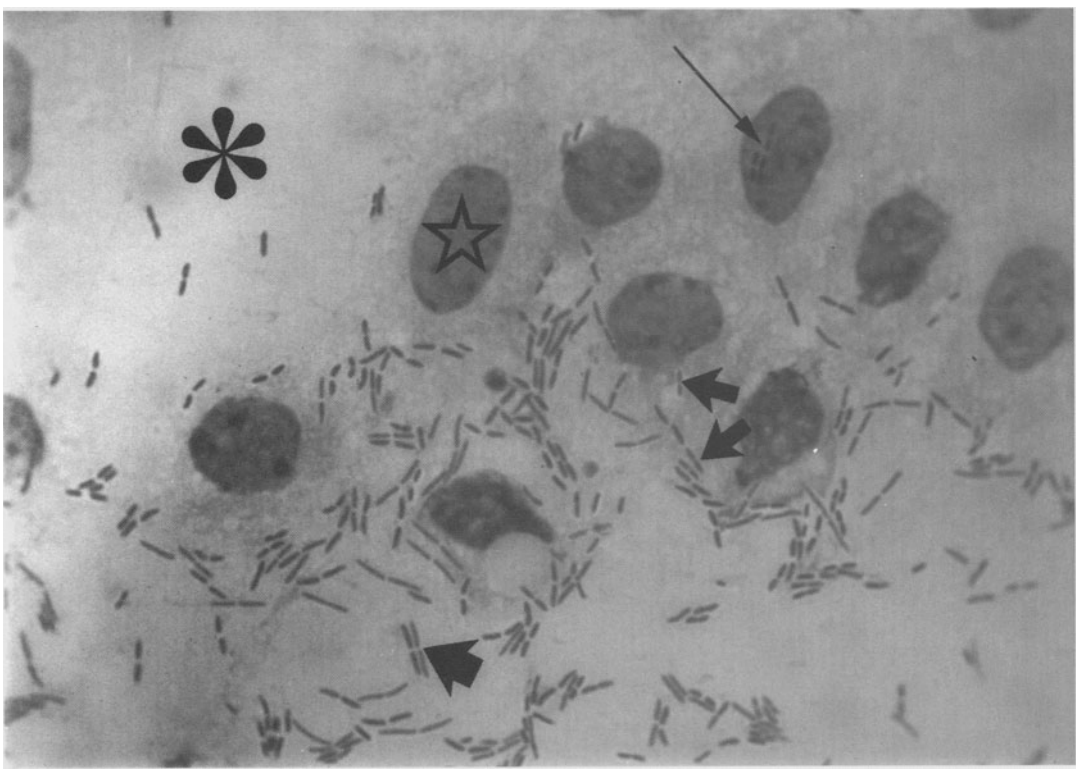

Figure 77. This imprint was taken from the peritoneum covering the anterior liver surface of a mouse with *E. coli* peritonitis. Bacterial rods (thick arrow) can be seen in areas devoid of mesothelial dressing, as well as within the cell cytoplasmic compartment (small arrows), and even into the nuclei (long thin arrow). Note the low-density distribution of mesothelial cells. (Open star: nucleus of mesothelial cell) and the presence of large peritoneal areas deprived of the monolayer (*) (haematoxylin–eosin; blue filter; ×1000).

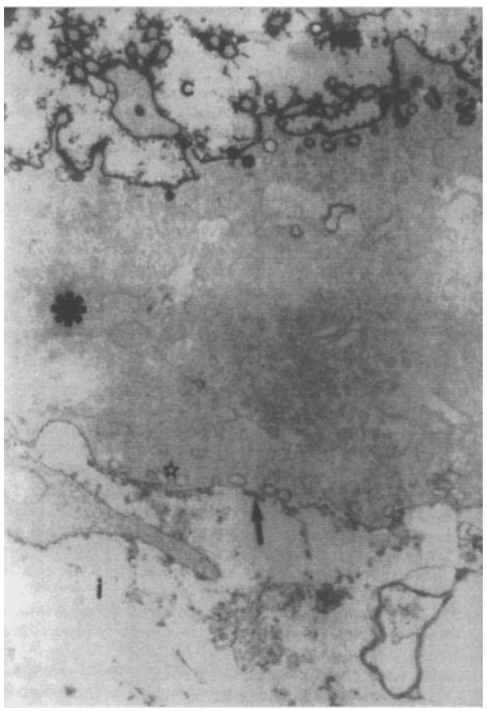

Figure 78. Section of rat mesentery taken 24 h after induction of *E. coli* peritonitis. The glycocalyx of mesothelial cell plasmalemma (short black arrow), as well as that of microvilli (open arrow) are still present. The mesothelial cell (*) is lying on an interrupted and disorganized basement membrane (long black arrow). Note the absence of submesothelial anionic sites as well as the intensity of the interstitial oedema (i) (star: uncoated pinocytotic vesicles; C: abdominal cavity) (original magnification ×24 600).

the submesothelial connective tissue. Light and electron microscopic studies have demonstrated that omental milky spots are the major route through which leukocytes migrate into the peritoneal cavity [477–479], as well as the main providers of peritoneal macrophages in situations where their increased presence is required [480].

Complete morphological and functional return to normality may be expected to occur approximately 2 weeks after recovery from the infectious episode.

Final remarks

It was not the purpose of the authors merely to deliver a cold and tedious description of anatomical structures. On the contrary, our goal has been to offer the reader a comprehensive and balanced analytical approach of structure and function covering, at least in part, their interactions. It is evident that the function of the peritoneum as a dialysis membrane cannot be evaluated only within the frame of passive diffusion through water-filled, cylindrical pores [202] and/or mathematical models [481], based on assumptions that, at times, lose sight of the formidable barrier of the living cell membrane as well as the structural organization of the tissues.

Research during the past 15 years provided enough evidence to characterize the peritoneum not as an inert dialysing sheet, but as a living and reusable membrane for dialysis [269], as predicted 20 years ago [482].

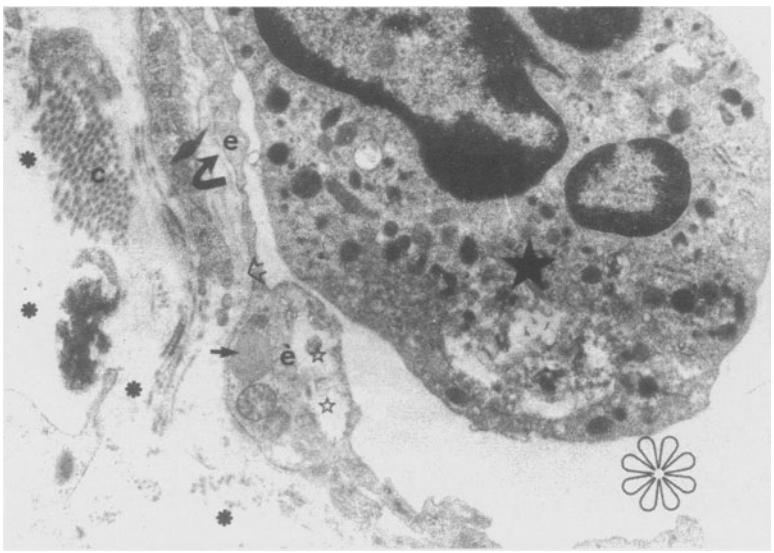

Figure 79. Mesenteric capillary of a mouse with *E. coli*-induced peritonitis. One endothelial cell (è) shows signs of severe injury, mitochondrion with inner compartment swelling (short arrow) and vascuolization of the cytoplasm (open stars). The subendothelial basement membrane (curved arrow) is, at times, absent (open arrow). The interstitial tissue is oedematous (black asterisks) (black star: polymorphonuclear cell; open asterisk: capillary lumen) (×12 600).

In addition, it becomes evident that the mesothelial monolayer continuously exposed to dialysis solutions *in vivo* is structurally and functionally different, at least from the histochemical point of view, from that observed in unexposed–intact cells, or in those growing in the *in-vitro* set-up of culture and later exposed to experimental incubation [420]. Therefore, we have the feeling that a good deal of creative thinking is required to integrate data obtained during 40 years of physiological studies and mathematical models, with the realities of tissue structure and cell biology.

We do hope that this chapter offers the message we promised to ourselves during the preparation of the manuscript, and serves as a catalytic element for further research.

References

1. Robinson B. The Peritoneum. Chicago, IL: WT Keener, 1897, p. 13.
2. Ganter G. Uber die Beseitigung giftiger Stoffe aus dem Blute durch dialyse. Munchen Med Wochenschr 1923; 70: 1478–80.
3. Boen ST. Peritoneal dialysis in clinical medicine. Springfield, IL: Charles C. Thomas, 1964.
4. Tenckhoff H. Schechter H. A bacteriologically safe peritoneal access device for repeated dialysis. Trans Am Soc Artif Intern Organs 1968; 14: 181–7.
5. Popovich RP, Moncrief JW, Decherd JF, Bomar JB, Pyle WK. Preliminary verification of the low dialysis clearance hypothesis via a novel equilibrium peritoneal dialysis technique. Abst Am Soc Artif Intern Organs 1976; 5: 64.
6. Nolph KD, Sorkin M, Rubin J, Arfania D, Prowant B, Fruto L, Kennedy D. Continuous ambulatory peritoneal dialysis: three-year experience at one center. Ann Intern Med 1980; 92: 609–13.
7. Luschka H. Die Structure der serosen haute des menschen. Tubingen, 1851.
8. Putiloff PV. Materials for the study of the laws of growth of the human body in relation to the surface areas of different systems: the trial on Russian subjects of planigraphic anatomy as a mean of exact anthropometry. Presented at the Siberian branch of the Russian Geographic Society, Omsk, 1886.
9. Wegner G. Chirurgische bemerkingen uber die peritoneal Hole, mit Besonderer Berucksichtigung der ovariotomie. Arch Klin Chir 1877; 20: 51–9.
10. Esperanca MJ, Collins DL. Peritoneal dialysis efficiency in relation to body weight. J Pediatr Surg 1966; 1: 162–9.
11. Gotloib L, Digenis GE, Rabinovich S, Medline A, Oreopolous DG. Ultrastructure of normal rabbit mesentery. Nephron 1983; 34: 248–55.
12. Gosselin RE, Berndt WO. Diffusional transport of solutes through mesentery and peritoneum. J Theor Biol 1962; 3: 487.
13. Haar JL, Ackerman GA. A phase and electron microscopic study of vasculogenesis and erythropoiesis in the yolk sac of the mouse. Anat Rec 1971; 170: 199–224.
14. Ukeshima A, Hayashi Y, Fujimore T. Surface morphology of the human yolk sac: endoderm and mesothelium 1986; 49: 483–94.
15. Puulmala RM. Morphologic comparison of parietal and visceral peritoneal epithelium in fetus and adult. Anat Rec 1937; 68: 327–30.
16. Robertson JD. Molecular structure of biological membranes. In: Lima de Faria, A., ed. Handbook of Molecular Cytology. Amsterdam: North Holland, 1969, p. 1404.
17. Kolossow A. Weber die struktur des endothels der pleuroperitoneal hole der blut und lymphgefasse. Biol Centralbl Bd 1892; 12: S87–94.
18. Odor L. Observations of the rat mesothelium with the electron and phase microscopes. Am J Anat 1954; 95: 433–65.
19. Felix DM, Dalton AJ. A comparison of mesothelial cells and macrophages in mice after the intraperitoneal inoculation of melanine granules. J Biophys Biochem Cytol 1956; 2 (suppl. part 2): 109–17.
20. Baradi AF, Hope J. Observations on ultrastructure of rabbit mesothelium. Exp Cell Res 1964; 34: 33–4.
21. Baradi AF, Crae SN. A scanning electron microscope study of mouse peritoneal mesothelium. Tissue Cell 1976; 8: 159.
22. Whitaker D, Papadimitriou JM, Walters MNI. The mesothelium and its reactions: a review. CRC Crit Rev Toxicol 1982; 10: 81–144.
23. Di Paolo N, Sacchi G, De-Mia M *et al.* Morphology of the peritoneal membrane during continuous ambulatory peritoneal dialysis. Nephron 1986; 44: 204–11.
24. Kondo T, Takeuchi K, Doi Y, Yonemura S, Nagata S, Tsukita S. ERM (ezrin–radixin/moesin)-based molecular mechanism of microvillar breakdown at an early stage of apoptosis. J Cell Biol 1997; 139: 749–58.
25. Bonelli G, Sacchi MC, Barbiero G *et al.* Apoptosis of L929 cells by etoposide: a quantitative and kinetic approach. Exp Cell Res 1996; 228: 292–305.
26. Boe R, Gjertsen BT, Doskeland SO, Vintermyr OK. 8-Chloro-cAMP induces apoptotic cell death in a human mammary carcinoma cell (MCF–7) line. Br J Cancer 1995; 72: 1151–9.
27. Efskind L. Experimentelle Untersuchungen uber die Biologie des Peritoneums. 1. Die morphologische reaktion des peritoneums auf riexze. Oslo: Det Norske Videnk aps Academii, 1940.
28. Gotloib L, Wajsbrut V, Shostak A, Kushnier R. Acute and long-term changes observed in imprints of mouse mesothelium exposed to glucose-enriched, lactated, buffered dialysis solutions. Nephron 1995; 70: 466–77.
29. Fukata H. Electron microscopic study on normal rat peritoneal mesothelium and its changes in adsorption of particulate iron dextran complex. Acta Pathol Jpn 1963; 13: 309–25.
30. Lieberman-Meffet D, White H. The greater omentum: anatomy, physiology, pathology, surgery with an historical survey. Berlin: Springer-Verlag, 1983, p. 6.
31. Madison LD, Bergstrom MU, Porter B, Torres R, Shelton E. Regulation of surface topography of mouse peritoneal cells. J Cell Biol 1979; 82: 783.
32. Gotloib L, Shostak A. Ultrastructural morphology of the peritoneum: new findings and speculations on transfer of solutes and water during peritoneal dialysis. Perit Dial Bull 1987; 7: 119–29.
33. Gotloib L. Anatomical basis for peritoneal permeability. In: La Greca G, Chiaramonte S, Fabris A, Feriani M, Ronco G, eds. Peritoneal Dialysis. Milan: Wichtig Ed, 1986, pp. 3–10.
34. Gotloib L, Shostak A, Jaichenko J. Ruthenium red stained anionic charges of rat and mice mesothelial cells and basal lamina: the peritoneum is a negatively charged dialyzing membrane. Nephron 1988; 48, 65–70.
35. Luft JH. Fine structure of capillary and endocapillary layer as revealed by ruthenium red. Fed Proc 1966; 25: 1173–83.
36. Gotloib L, Bar-Sella P, Jaichenko J, Shostak A. Ruthenium red stained polyanionic fixed charges in peritoneal microvessels. Nephron 1987; 47: 22–8.
37. Curry FE, Michel CC. A fiber matrix model of capillary permeability. Microvasc Res 1980; 20: 96–9.
38. Morris RG, Hargreaves AD, Duvall E, Wyllie AH. Hormone-induced cell death. 2. Surface changes in thymocytes undergoing apoptosis. Am J Pathol 1984; 115: 426–36.
39. Moog F. The lining of the small intestine. Sci Am 1981; 2455: 116–25.

40. Gotloib L. Anatomy of the peritoneal membrane. In: La Greca G, Biasoli G, Ronco G, eds. Milan: Wichtig Ed., 1982, pp. 17–30.
41. Leak LV. Distribution of cell surface charges on mesothelium and lymphatic endothelium. Microvasc Res 1986; 31: 18–30.
42. Lewis WH. Pinocytosis. Bull Johns Hopkins Hosp 1931; 49: 17–23.
43. Casley-Smith JR. The dimensions and numbers of small vesicles in cells, endothelial and mesothelial and the significance of these for endothelial permeability. J Microsc 1969; 90: 251–69.
44. Casley-Smith JR, Chin JC. The passage of cytoplasmic vesicles across endothelial and mesothelial cells. J Microsc 1971; 93: 167–89.
45. Fedorko ME, Hirsch JG, Fried B. Studies on transport of macromolecules and small particles across mesothelial cells of the mouse omentum. Exp Cell Res 1971; 63: 313–23.
46. Simionescu N, Simionescu M, Palade GE. Structural basis of permeability in sequential segments of the microvasculature. II. Pathways followed by microperoxidase across the endothelium. Microvasc Res 1978; 15: 17–36.
47. Palade GE, Simionescu M, Simionescu N. Structural aspects of the permeability of the microvascular endothelium. Acta Physiol Scand Suppl 1979; 463: 11–32.
48. Palade GE. Fine structure of blood capillaries. J Appl Phys 1953; 24: 1424.
49. Florey HW. The transport of materials across the capillary wall. Q J Exp Physiol 1964; 49: 117–28.
50. Pappenheimer JR, Renkin EM, Borrero LM. Filtration, diffusion and molecular sieving through peripheral capillary membranes. A contribution to the pore theory of capillary permeability. Am J Physiol 1951; 167: 13–46.
51. Frokjaer-Jensen J. The plasmalemmal vesicular system in capillary endothelium. Prog Appl Microcirc 1983; 1: 17–34.
52. Wagner RC, Robinson CS. High voltage electron microscopy of capillary endothelial vesicles. Microvasc Res 1984; 28: 197–205.
53. Smart EJ, Foster DC, Ying YS, Kamen BA, Anderson RGW. Protein kinase G activators inhibit receptor-mediated potocytosis by preventing internalization of caveolae. J Cell Biol 1994; 124: 307–13.
54. Lisanti MP, Scherer PE, Vidugiriene J *et al.* Characterization of caveolin-rich membrane domains isolated from an endothelial-rich source: implications for human disease. J Cell Biol 1994; 126: 111–26.
55. Moldovan NI, Heltianu G, Simionescu N, Simionescu M. Ultrastructural evidence of differential solubility in Triton X–100 of endothelial vesicles and plasma membrane. Exp Cell Res 1995; 219: 309–13.
56. Shasby DM, Roberts RL. Transendothelial transfer of macromolecules *in vivo*. Fed Proc 1987; 46: 2506–10.
57. Shasby DM, Shasby SS. Active transendothelial transport of albumin. Interstitium to lumen. Circ Res.1985; 57: 903–8.
58. Milici AJ, Watrous NE, Stukenbrok M, Palade GE. Transcytosis of albumin in capillary endothelium. J Cell Biol 1987; 105: 2603–12.
59. Ghitescu L, Bendayan M. Transendothelial transport of serum albumin: a quantitative immunocytochemical study. J Cell Biol 1992; 17: 747–55.
60. Schnitzer JE, Oh P. Albondin-mediated capillary permeability to albumin. Differential role of receptors in endothelial transcytosis and endocytosis of native and modified albumins. J Biol Chem 1994; 269: 6072–82.
61. Ghitescu L, Galis Z, Simionescu M, Simionescu N. Differentiated uptake and transcytosis of albumin in successive vascular segments. J Submicrosc Cytol Pathol 1988; 20: 657–69.
62. Williams SK, Devenny JJ, Bitensky MW. Micropinocytic ingestion of glycosylated albumin by isolated microvessels: possible role in pathogenesis of diabetic microangiopathy. Proc Natl Acad Sci USA 1981; 78: 2393–7.
63. Ghitescu L, Fixman A, Simionescu M, Simionescu N. Specific binding sites for albumin restricted to plasmalemmal vesicles of continuous capillary endothelium: receptor-mediated transcytosis. J Cell Biol 1986; 102: 1304–11.
64. Predescu D, Simionescu M, Simionescu N, Palade GE. Binding and transcytosis of glycoalbumin by the microvascular endothelium of the murine myocardium: evidence that glycoalbumin behaves as a bifunctional ligand. J Cell Biol 1988; 107: 1729–38.
65. Dehouck B, Fenart L, Dehouck MP, Pierce A, Torpier G, Cecchelli R. A new function for the LDL receptor: transcytosis of LDL across the blood–brain barrier. J Cell Biol 1997; 138: 877–89.
66. Simionescu N, Simionescu M. Interactions of endogenous lipoproteins with capillary endothelium in spontaneously hyperlipoproteinemic rats. Microvasc Res. 1985; 30: 314–32.
67. Snelting-Havinga I, Mommaas M, Van-Hinsbergh VW, Daha MR, Daems WT, Vermeer BJ. Immunoelectron microscopic visualization of the transcytosis of low density lipoproteins in perfused rat arteries. Eur J Cell Biol 1989; 48: 27–36.
68. Vasile E, Simionescu M, Simionescu N. Visualization of the binding, endocytosis, and transcytosis of low-density lipoprotein in the arterial endothelium *in situ*. J Cell Biol 1983; 96: 1677–89.
69. Ghinea N, Hai MTV, Groyer-Picard MT, Milgrom E. How protein hormones reach their target cells. Receptor mediated transcytosis of hCG through endothelial cells. J Cell Biol 1994; 125: 87–97.
70. Bendayan M, Rasio EA. Transport of insulin and albumin by the microvascular endothelium of the rete mirabile. J Cell Sci 1996; 109: 1857–64.
71. Schmidt AM, Vianna M, Gerlach M *et al.* Isolation and characterization of two binding proteins for advanced glycosylation end products from bovine lung which are present on the endothelial cell surface. J Biol Chem 1992; 267: 14987–97.
72. Predescu D, Predescu S, McQuistan T, Palade GE. Transcytosis of alpha 1-acidic glycoprotein in the continuous microvascular endothelium. Proc Natl Acad Sci USA 1998; 95: 6175–80.
73. Pappenheimer JR. Passage of molecules through capillary walls. Physiol Rev 1953; 33: 387–423.
74. Grotte G. Passage of dextran molecules across the blood–lymph barrier. Acta Chir Scand 1956; Suppl. 211: 1–84.
75. Nolph KD. The peritoneal dialysis system. Contrib Nephrol 1979; 17: 44–9.
76. Gotloib L, Shostak A. Endocytosis and transcytosis of albumin–gold through mice peritoneal mesothelium. Kidney Int 1995; 47: 1274–84.
77. Schnitzer JE, Allard J, Oh P. NEM inhibits transcytosis, endocytosis and capillary permeability: implication of caveolae fusion in endothelia. Am J Physiol 1995; 168: H48–55.
78. Schnitzer JE, Oh P, Pinney E, Allard J. Filipin-sensitive caveolae-mediated transport in endothelium: reduced transcytosis, scavenger endocytosis, and capillary permeability of select macromolecules. J Cell Biol 1994; 127: 1217–32.
79. Tiruppathi G, Song W, Bergenfeldt M, Sass P, Malik AB. Gp60 activation mediates albumin transcytosis in endothelial cells by tyrosine kinase-dependent pathway. J Biol Chem 1997; 272: 25968–75.
80. Schnitzer JE, Oh P, Jacobson BS, Dvorak AM. Caveolae from luminal plasmalemma of rat lung endothelium: microdomains enriched in caveolin, Ca (2+)-ATPase, and inositol triphosphate receptor. Proc Natl Acad Sci USA 1995; 92: 1759–63.
81. Glenney JR, Soppet D. Sequence and expression of caveolin, a protein component of caveolae plasma membrane domains phosphorylated on tyrosine in Rous sarcoma virus-transformed fibroblasts. Proc Natl Acad Sci USA 1992; 89: 10517–21.
82. Bush KT, Stuart RO, Li SH *et al.* Epithelial inositol 1,4,5-triphosphate receptors. Multiplicity of localization, solubility, and isoforms. J Biol Chem 1994; 269: 23694–9.

83. Brown D, Lydon J, McLaughlin M, Stuart-Tilley A, Tyszkowski R, Alper S. Antigen retrieval in cryostat tissue sections and cultured cells by treatment with sodium dodecyl sulfate (SDS). Histochem Cell Biol 1996; 105: 261–7.
84. Breton S, Lisante MP, Tyszkowski R, McLaughlin M, Brown D. Basolateral distribution of caveolin-1 in the kidney. Absence from ATPase-coated endocytic vesicles in intercalated cells. J Histochem Cytochem 1998; 46: 205–14.
85. Schmid SL. Clathrin-coated vesicle formation and protein sorting: an integrated process. Annu Rev Biochem 1997; 66: 511–48.
86. Pfeffer SR, Drubin DG, Kelly RB. Identification of three coated vesicle components as alpha- and beta-tubulin linked to a phosphorylated 50,000-dalton polypeptide. J Cell Biol 1983; 97: 40–7.
87. Pearse BMF. Clathrin: a unique protein associated with intracellular transfer of membrane by coated vesicles. Proc Natl Acad Sci USA 1976; 73: 1255–9.
88. Lin HC, Duncan JA, Kozasa T, Gilman AG. Sequestration of the G protein beta gamma subunit complex inhibits receptor-mediated endocytosis. Proc Natl Acad Sci USA 1998; 95: 5057–60.
89. Damke H. Dynamin and receptor-mediated endocytosis. FEBS Lett 1996; 389: 48–51.
90. Sweitzer SM, Hinsshaw JE. Dynamin undergoes a GTP dependent conformational change causing vesiculation. Cell 1998; 93: 1021–9.
91. Henley JR, Krueger EW, Oswald BJ, McNiven MA. Dynamin-mediated internalization of caveolae. J Cell Biol 1998; 141: 85–99.
92. Oh P, McIntosh DP, Schnitzer JE. Dynamin at the neck of caveolae mediates their budding to form transport vesicles by GTP-driven fission from the plasma membrane of endothelium. J Cell Biol 1998; 141: 101–14.
93. Chambers R, Zweifach BW. Capillary cement in relation to permeability. J Cell Comp Physiol 1940; 15: 255–72.
94. Rippe B. A three-pore model of peritoneal transport. Perit Dial Int 1993; 13 (suppl. 2): S35–8.
95. Simionescu N, Simionescu M, Palade GE. Differentiated microdomains on the luminal surface of capillary endothelium. I. Preferential distribution of anionic sites. J Cell Biol 1981; 90: 605–13.
96. Steinman RM, Mellman IS, Muller WA, Cohn ZA. Endocytosis and the recycling of plasma membrane. J Cell Biol 1983; 96: 1–27.
97. Shea SM, Karnovsky MJ. Brownian motion: a theoretical explanation for the movement of vesicles across the endothelium. Nature, Lond 1966; 212: 353–4.
98. Simionescu M, Simionescu N, Palade GE. Morphometric data on the endothelium of blood capillaries. J Cell Biol 1974; 60: 128–52.
99. Wagner JC, Johnson NF, Brown DG, Wagner MMF. Histology and ultrastructure of serially transplanted rat mesotheliomas. Br J Cancer 1982; 46: 294–9.
100. Petersen OW, Van Deurs B. Serial section analysis of coated pits and vesicles involved in adsorptive pinocytosis in cultured fibroblasts. J Cell Biol 1983; 96: 277–81.
101. Peters KR, Carley WW, Palade GE. Endothelial plasmalemmal vesicles have a characteristic stripped bipolar surface structure. J Cell Biol 1985; 101: 2233–8.
102. Takahashi H, Hasegawa H, Kamijo T *et al.* Regulation and localization of peritoneal water channels in rats. Perit Dial Int 1998; 18 (suppl. 2): S70.
103. Henle FGH. Splacnologie. Vol. II, p. 175, 1875.
104. Simionescu M, Simionescu N, Silbert J, Palade GE. Differentiated microdomains on the luminal surface of the capillary endothelium. II. Partial characterization of their anionic sites. J Cell Biol 1981; 90: 614–21.
105. Simionescu M, Simionescu N. Organization of cell junctions in the peritoneal mesothelium. J Cell Biol 1977; 74: 98.
106. Von Recklinghausen FD. Zur Fettresorption. Arch Pathol Anat Physiol 1863; Bd 26: S172–208.
107. Bizzozero G, Salvioli G. Sulla suttura della membrana serosa e particolarmente del peritoneo diaphragmatico. Giorn R Acad Med Torino 1876; 19: 466–70.
108. Allen L. The peritoneal stomata. Anat Rec 1937; 67: 89–103.
109. French JE, Florey HW, Morris B. The adsorption of particles by the lymphatics of the diaphragm. Q J Exp Physiol 1959; 45: 88–102.
110. Tourneux F, Herman G. Recherches sur quelques epitheliums plats dans la serie animale (Deuxieme partie). J Anat Physiol 1876; 12: 386–424.
111. Kolossow A. Uber die struktur des pleuroperitoneal und gefassepithels (endothels). Arch Mikr Anat 1893; 42: 318–83.
112. Simer PM. The passage of particulate matter from the peritoneal cavity into the lymph vessels of the diaphragm. Anat Rec 1948; 101: 333–51.
113. Leak LW, Just EE. Permeability of peritoneal mesothelium. J Cell Biol 1976; 70: 423a.
114. Tsilibarry EC, Wissig SL. Absorption from the peritoneal surface of the muscular portion of the diaphragm. Am J Anat 1977; 149: 127–33.
115. French JE, Florey HW, Morris B. The absorption of particles by the lymphatics of the diaphragm. Q J Exp Physiol 1959; 45: 88–102.
116. Abu-Hijleh MF, Scothorne RJ. Studies on haemolymph nodes. IV. Comparison of the route of entry of carbon particles into parathymic nodes after intravenous and intraperitoneal injection. J Anat 1996; 188: 565–73.
117. Allen L. The peritoneal stomata. Anat Rec 1937; 67: 89–103.
118. Hashimoto B, Filly RA, Callen PW, Parer JT. Absorption of fetal intraperitoneal blood after intrauterine transfusion. J Ultrasound Med 1987; 6: 421–3.
119. Smedsrood B, Aminoff D. Studies on the sequestration of chemically and enzymatically modified erythrocytes. Am J Hematol 1983; 15: 123–33.
120. Fowler JM, Knight R, Patel KM. Intraperitoneal blood transfusion in African adults with hookworm anaemia. Br Med J 1968; 3: 200–1.
121. Chandler K, Fitzpatrik J, Mellor D, Milne M, Fishwick G. Intraperitoneal administration of whole blood as a treatment for anaemia in lambs. Vet Rec 1998; 142: 175–6.
122. Aba MA, Pissani AA, Alzola RH, Videla-Dorna I, Ghezzi MS, Marcilese NA. Evaluation of intraperitoneal route for the transfusion of erythrocytes using rats and dogs. Acta Physiol Pharmacol Ther Latinoam 1991; 41: 387–95.
123. Remmele W, Richter IE, Wildenhof H. Experimental investigations on cell resorption from the peritoneal cavity by use of the scanning electron microscope. Klin Wochenschr 1975; 53: 913–22.
124. Dumont AE, Maas WK, Iliescu H, Shin RD. Increased survival from peritonitis after blockade of transdiaphragmatic absorption of bacteria. Surg Gynecol Obstet 1986; 162: 248–52.
125. Leak LV. Permeability of peritoneal mesothelium: a TEM and SEM study. J Cell Biol 1976; 70: 423–33.
126. Leak LV. Polycationic ferritin binding to diaphragmatic mesothelial and lymphatic endothelial cells. J Cell Biol 1982; 95: 103–11.
127. Ettarh RR, Carr KE. Ultrastructural observations on the peritoneum in the mouse. J Anat 1996; 188: 211–5.
128. Wassilev M, Wedel T, Michailova K, Kuhnel W. A scanning electron microscopy study of peritoneal stomata in different peritoneal regions. Anat Anz 1998; 180: 137–43.
129. Li J, Zhou J, Gao Y. The ultrastructure and computer imaging of the lymphatic stomata in the human pelvic peritoneum. Anat Anz 1997; 179: 215–20.
130. Yoffey JM, Courtice FC. Lymphatics, Lymph and Lymphoid Tissue. London: Edward Arnold, 1956, p. 176.
131. Andrews PM, Porter KR. The ultrastructural morphology and possible functional significance of mesothelial microvilli. Anat Rec 1973; 177: 409–14.
132. Ghadially FN. Ultrastructural Pathology of the Cell. London: Butterworths, 1978, p. 403.

133. Todd RB, Bowman W. The Physiological Anatomy and Physiology of Man, Vols I and II. London, 1845 and 1846.
134. Muscatello G. Uber den Bau und das Aufsaugunsvermogen des Peritanaums. Virchows Archiv Path Anat 1895; Bd 142: 327–59.
135. Baron MA. Structure of the intestinal peritoneum in man. Am J Anat 1941; 69: 439–96.
136. Maximow A. Bindgewebe und blutbildende gewebe. Handbuch der mikroskopischen Anatomie des menschen. von Mollendorf, 1927; Bd 2 T 1: S232–583.
137. Kanwar YS, Farquhar MG. Anionic sites in the glomerular basement membrane. *In vivo* and *in vitro* localization to the laminae rarae by cationic probes. J Cell Biol 1979; 81: 137–53.
138. Rohrbach R. Reduced content and abnormal distribution of anionic sites (acid proteoglycans) in the diabetic glomerular basement membrane. Virchows Arch B Cell Pathol Incl Mol Pathol 1986; 51: 127–35.
139. Ghinea N, Simionescu N. Anionized and cationized hemeundecapeptides as probes for cell surface charge and permeability studies: differentiated labeling of endothelial plasmalemmal vesicles. J Cell Biol 1985; 100: 606–12.
140. Gotloib L, Shostak A, Jaichenko J. Loss of mesothelial electronegative fixed charges during murine septic peritonitis. Nephron 1989; 51: 77–83.
141. Shostak A, Gotloib L. Increased peritoneal permeability to albumin in streptozotocin diabetic rats. Kidney Int 1996; 49: 705–14.
142. Gotloib L, Shostak A, Bar-Sella P, Eiali V. Reduplicated skin and peritoneal blood capillaries and mesothelial basement membrane in aged non-diabetic chronic uremic patients. Perit Dial Bull 1984; 4: S28.
143. Di Paolo N, Sacchi G. Peritoneal vascular changes in continuous ambulatory peritoneal dialysis (CAPD): an *in-vivo* model for the study of diabetic microangiopathy. Perit Dial Int 1989; 9: 41–5.
144. Gersh I, Catchpole HR. The organization of ground substances and basement membrane and its significance in tissue injury, disease and growth. Am J Anat 199; 85: 457–522.
145. Williamson JT, Vogler NJ, Kilo CH. Regional variations in the width of the basement membrane of muscle capillaries in man and giraffe. Am J Pathol 1971; 63: 359–67.
146. Vracko R. Skeletal muscle capillaries in non-diabetics. A quantitative analysis. Circulation 1970; 16: 285–97.
147. Parthasarathy N, Spiro RG. Effect of diabetes on the glycosaminoglycan component of the human glomerular basement membrane. Diabetes 1982; 31: 738–41.
148. Vracko R. Basal lamina scaffold – anatomy and significance for maintenance of orderly tissue structure. A review. Am J Pathol 1974; 77: 313–46.
149. Vracko R, Pecoraro RE, Carter WB. Basal lamina of epidermis, muscle fibers, muscle capillaries, and renal tubules: changes with aging and diabetes mellitus. Ultrastruct Pathol 1980; 1, 559–74.
150. Hruza Z. Connective tissue. In: Kaley G, Altura BM, eds. Microcirculation. Baltimore, MD: University Park Press, 1977, Vol. I, pp. 167–183.
151. Comper WD, Laurent TC. Physiological function of connective tissue polysaccharides. Physiol Rev 1978; 58: 255–315.
152. Flessner MF. The importance of the interstitium in peritoneal transport. Perit Dial Int 1996; 16 (suppl. 1): S76–9.
153. Parker JC, Gilchrist S, Cartledge JT. Plasma–lymph exchange and interstitial distribution volumes of charged macromolecules in the lung. J Appl Physiol 1985; 59: 1128–36.
154. Lai-Fook SJ, Brown LV. Effects of electric charge on hydraulic conductivity of pulmonary interstitium. J Appl Physiol 1991; 70: 1928–32.
155. Gilchrist SA, Parker JC. Exclusion of charged macromolecules in the pulmonary interstitium. Microvasc Res 1985; 30: 88–98.
156. Haljamae H. Anatomy of the interstitial tissue. Lymphology 1978; 11: 128–32.
157. Guyton AC. A concept of negative interstitial pressure based on pressures in implanted perforated capsules. Circ Res 963; 12: 399–414.
158. Scholander PF, Hargens AR, Miller SL. Negative pressure in the interstitial fluid of animals. Fluid tensions are spectacular in plants; in animals they are elusively small, but just as vital. Science 1968; 161: 321–8.
159. Aukland K, Reed PK. Interstitial–lymphatic mechanisms in the control of extracellular fluid volume. Physiol Rev 1993; 73: 1–78.
160. Rutili G, Arfors KE. Protein concentration in interstitial and lymphatic fluids from the subcutaneous tissue. Acta Physiol Scand 1977; 99: 1–8.
161. Rutili G, Kvietys P, Martin D, Parker JC, Taylor AE. Increased pulmonary microvascular permeability induced by alpha-naphthylthiourea. J Appl Physiol 1982; 52: 1316–23.
162. Flessner MF. Peritoneal transport physiology: insights from basic research. J Am Soc Nephrol 1991; 2: 122–35.
163. Gotloib L, Mines M, Garmizo AL, Varka I. Hemodynamic effects of increasing intra-abdominal pressure in peritoneal dialysis. Perit Dial Bull 1981; 1: 41–2.
164. Flessner MF, Schwab A. Pressure threshold for fluid loss from the peritoneal cavity. Am J Physiol 1996; 270: F377–90.
165. Simionescu N. Cellular aspects of transcapillary exchange. Physiol Rev 983; 63: 1536–79.
166. Wolff JR. Ultrastructure of the terminal vascular bed as related to function. In: Kaley G, Altura BM, eds. Microcirculation. Baltimore, MD: University Park Press, 1977, Vol. I, pp. 95–130.
167. Majno G. Ultrastructure of the vascular membrane. Handbook of Physiology. Section II – Circulation, vol. III. Washington, DC: Am Physiol Soc, 1965, pp. 2293–375.
168. Gotloib L, Shostak A, Jaichenko J. Fenestrated capillaries in mice submesothelial mesenteric microvasculature. Int J Artif Organs 1989; 12: 20–4.
169. Gotloib L, Shostak A. In search of a role for submesothelial fenestrated capillaries. Perit Dial Int 1993; 13: 98–102.
170. Gotloib L, Shostak A, Bar-Sella P, Eiali V. Fenestrated capillaries in human parietal and rabbit diaphragmatic peritoneum. Nephron 1985; 41: 200–2.
171. Friederici HHR. The tridimensional ultrastructure of fenestrated capillaries. J Ultrastruct Res 1968; 23: 444–56.
172. Clough G, Smaje LH. Exchange area and surface properties of the microvasculature of the rabbit submandibular gland following duct ligation. J Physiol 1984; 354: 445–56.
173. Gotloib L, Shostak A, Jaichenko J, Galdi P, Fudin R. Anionic fixed charges in the fenestrated capillaries of the mouse mesentery. Nephron 1990; 55: 419–22.
174. Rhodin JAG. The diaphragm of capillary endothelial fenestrations. J Ultrastruc Res 1962; 6: 171–85.
175. Gotloib L, Shostak A, Bar-Sella P, Eiali V. Heterogeneous density and ultrastructure of rabbit's peritoneal microvasculature. Int J Artif Organs 1984; 7: 123–5.
176. Rhodin YAG. Ultrastructure of mammalian venous capillaries, venules and small collecting veins. J Ultrastruct Res 1968; 25: 452–500.
177. Gotloib L, Shostak A, Jaichenko J. Loss of mesothelial and microvascular fixed anionic charges during murine experimentally induced septic peritonitis. In: Avram M and Giordano G, eds. Ambulatory Peritoneal Dialysis. New York: Plenum, 1990, pp. 63–6.
178. Simionescu M, Simionescu N, Palade GE. Differentiated microdomains on the luminal surface of capillary endothelium: distribution of lectin receptors. J Cell Biol 1982 94, 406–13.
179. Schneeberger EE, Hamelin M. Interactions of serum proteins with lung endothelial glycocalyx: its effect on endothelial permeability. Am J Physiol 1984; 247: H206–17.
180. Bundgaard M, Frokjaer-Jensen J. Functional aspects of the ultrastructure of terminal blood vessels: a quantitative study

on consecutive segments of the frog mesenteric microvasculature. Microvasc Res 1982; 23: 1–30.
181. Palade GE. Transport in quanta across the endothelium of blood capillaries. Anat Rec 1960; 116: 254.
182. Milici AJ, L'Hernault N, Palade GE. Surface densities of diaphragmed fenestrae and transendothelial channels in different murine capillary beds. Circ Res 1985; 56, 709–17.
183. Lombardi T, Montesano R, Furie MB, Silverstein SC, Orci L. *In-vitro* modulation of endothelial fenestrae: opposing effects of retinoic acid and transforming growth factor beta. J Cell Sci 1988; 91: 313–8.
184. Kitchens CS, Weiss L. Ultrastructural changes of endothelium associated with thrombocytopenia. Blood 1975; 46: 567–78.
185. Horiuchi T, Weller PF. Expression of vascular endothelial growth factor by human eosinophils: upregulation by granulocyte macrophage colony-stimulating factor and interleukin-5. Am J Respir Cell Mol Biol 1997; 17: 70–7.
186. Collins PD, Connolly DT, Williams TJ. Characterization of the increase in vascular permeability induced by vascular permeability factor *in vivo*. Br J Pharmacol 1993; 109: 195–9.
187. Yeo KT, Wang HH, Nagy JA, Sioussat TM *et al.* Vascular permeability factor (vascular endothelial growth factor) in guinea pig and human tumor inflammatory effusions. Cancer Res 1993; 53: 2912–18.
188. Taichman NS, Young S, Cruchley AT, Taylor P, Paleolog E. Human neutrophils secrete vascular endothelial growth factor. J Leukoc Biol 1997; 62: 397–400.
189. Roberts WG, Palade GE. Increased microvascular permeability and endothelial fenestration induced by vascular endothelial growth factor: J Cell Sci 1995; 108: 2369–70.
190. Roberts WG, Palade GE. Neovasculature induced by vascular endothelial growth factor is fenestrated. Cancer Res 1997; 57: 765–72.
191. Simionescu M, Simionescu N, Palade GE. Sulfated glycosaminoglycans are major components of the anionic sites of fenestral diaphragms in capillary endothelium. J Cell Biol 1979; 83: 78a.
192. Milici AJ, L'Hernault N. Variation in the number of fenestrations and channels between fenestrated capillary beds. J Cell Biol 1983; 97: 336.
193. Peters KR, Milici AJ. High resolution scanning electron microscopy of the luminal surface of a fenestrated capillary endothelium. J Cell Biol 1983; 97: 336a.
194. Bankston PW, Milici AJ. A survey of the binding of polycationic ferritin in several fenestrated capillary beds: indication of heterogeneity in the luminal glycocalyx of fenestral diaphragms. Microvasc Res 1983; 26: 36–49.
195. Levick JR, Smaje LH. An analysis of the permeability of a fenestra. Microvasc Res 1987; 33: 233–56.
196. Wayland H, Silberberg A. Blood to lymph transport. Microvasc Res 1978; 15: 367–74.
197. Bearer EL, Orci L. Endothelial fenestral diaphragms: a quick freeze, deep-etch study. J Cell Biol 1985; 100: 418–28.
198. Simionescu M, Simionescu N, Palade GE. Preferential distribution of anionic sites on the basement membrane and the abluminal aspect of the endothelium in fenestrated capillaries. J Cell Biol 1982; 95: 425–34.
199. Deen WN, Satvat B. Determinants of the glomerular filtration of proteins. Am J Physiol 1981; 241: F162–70.
200. Deen WM, Bohrer MP, Robertson CR, Brenner BM. Determinants of the transglomerular passage of macromolecules. Fed Proc 1977; 36: 2614–8.
201. Kanwar YS, Linker A, Farquhar MG. Characterization of anionic sites in the glomerular basement membrane: *in vitro* and *in vivo* localization to the lamina rarae by cationic probes. J Cell Biol 1980; 86: 688–93.
202. Renkin EM. Multiple pathways of capillary permeability. Circ Res 1977; 41: 735–43.
203. Charonis AS, Wissig SL. Anionic sites in basement membranes. Differences in their electrostatic properties in continuous and fenestrated capillaries. Microvasc Res 1983; 25: 265–85.
204. Renkin EM. Cellular and intercellular transport pathways in exchange vessels. Am Rev Respir Dis 1992; 146: S28–31.
205. Farquhar MG, Palade GE. Junctional complexes in various epithelia. J Cell Biol 1963; 17: 375–442.
206. Simionescu M, Simionescu N, Palade GE.: Segmental differentiations of cell junctions in the vascular endothelium. J Cell Biol 1975; 67: 863–85.
207. Thorgeirsson G, Robertson AL Jr. The vascular endothelium. Pathobiologic significance. Am J Pathol 198; 95: 801–48.
208. Gumbiner B. Breaking through the tight junction barrier. J Cell Biol 1993; 123: 1631–3.
209. Gumbiner B. Structure, biochemistry, and assembly of epithelial tight junctions. Am J Physiol 1987; 253: C749–58.
210. Furuse M, Hirase T, Itoh M *et al.* Occludin: a novel integral membrane protein localized at tight junctions. J Cell Biol 1993; 123: 1777–88.
211. Furuse M, Itoh M, Hirase T *et al.* Direct association of occludin with ZO-1 and its possible involvement in the localization of occludin at tight junctions. J Cell Biol 1994; 127: 1617–26.
212. Hirase T, Staddon JM, Saitou M *et al.* Occludin as a possible determinant of tight junction permeability in endothelial cells. J Cell Sci 1997; 110: 1603–13.
213. Balda MS, Anderson JM. Two classes of tight junctions are revealed by ZO-1 isoforms. Am J Physiol 1993; 264: C918–24.
214. Mitic LL, Anderson JM. Molecular architecture of tight junctions. Annu Rev Physiol 1998; 60: 121–42.
215. Navarro P, Caveda L, Breviario F, Mandoteanu I, Lampugnani MG, Dejana E. Catenin-dependent and independent functions of vascular endothelial cadherin. J Biol Chem 1995; 270: 30965–72.
216. Leach L, Firth JA. Structure and permeability of human placental microvasculature. Microsci Res Tech 1997; 38: 137–44.
217. Alexander JS, Blaschuk OW, Haselton FR. An N-cadherin-like protein contributes to solute barrier maintenance in cultured endothelium. J Cell Physiol 1993; 156: 610–8.
218. Bundgaard M. The three dimensional organization of tight junctions in capillary endothelium revealed by serial-section electron microscopy. J Ultrastruct Res 1984; 88: 1–17.
219. Zand T, Underwood JM, Nunnari JJ, Majno G, Joris I. Endothelium and 'silver lines'. An electron microscopic study. Virchows Arch Pathol Anat 1982; 395: 133–44.
220. Anderson JM, Van-Itallie CM. Tight junctions and the molecular basis for regulation of paracellular permeability. Am J Physiol 1995; 269: G467–75.
221. Robinson PJ, Rapoport SI. Size selectivity of blood–brain barrier permeability at various times after osmotic opening. Am J Physiol 1987; 253: R459–66.
222. Blum MS, Toninelli E, Anderson JM *et al.* Cytoskeletal rearrangement mediates human microvascular endothelial tight junction modulation by cytokines. Am J Physiol 1997; 273: H286–94.
223. Schneeberger EE, Lynch RD. Structure, function and regulation of cellular tight junctions. Am J Physiol 1992; 262: L647–61.
224. Burns AR, Walker DC, Brown ES *et al.* Neutrophil transendothelial migration is independent of tight junctions and occurs preferentially at tricellular corners. J Immunol 1997; 159: 2893–903.
225. Rohrbach DH, Hassell JR, Klechman HK, Martin GR. Alterations in basement membrane (heparan sulfate) proteoglycan in diabetic mice. Diabetes 1982; 31: 185–8.
226. Chakrabarti S, Ma N, Sima AAF. Anionic sites in diabetic basement membranes and their possible role in diffusion barrier abnormalities in the BB-rat. Diabetologia 1991; 34: 301–6.

227. Shimomura H, Spiro RG. Studies on macromolecular components of human glomerular basement membrane and alterations in diabetes. Decreased levels of heparan sulfate, proteoglycan and laminin. Diabetes 1987; 36: 374–81.
228. Abrahamson DR. Recent studies on the structure and pathology of basement membranes. J Pathol 1986; 149: 257–78.
229. Hasslacher G, Reichenbacher R, Getcher F, Timpl R. Glomerular basement membrane synthesis and serum concentration of type IV collagen in streptozotocin-diabetic rats. Diabetologia 984; 26: 150–4.
230. Li W, Shen S, Khatami M, Rockey JH. Stimulation of retinal capillary pericyte protein and collagen synthesis in culture by high glucose concentration. Diabetes 1984; 33: 785–9.
231. Cagliero E, Maiello M, Boeri D, Roy S, Lorenzi M. Increased expression of basement membrane components in human endothelial cells cultured in high glucose. J Clin Invest 1988; 82: 735–8.
232. Ashworth CT, Erdmann RR, Arnold NJ. Age changes in the renal basement membrane of rats. Am J Pathol 1960; 36: 165–79.
233. Pino RM, Essner E, Pino LC. Location and chemical composition of anionic sites in Bruch's membrane of the rat. J Histochem Cytochem 1982; 30: 245–52.
234. Kanwar YS, Rosenzweig LJ, Kerjaschki DI. Glycosaminoglycans of the glomerular basement membrane in normal and nephrotic states. Ren Physiol 1981; 4: 121–30.
235. Kitano Y, Yoshikawa N, Nakamura H. Glomerular anionic sites in minimal change nephrotic syndrome and focal segmental glomerulosclerosis. Clin Nephrol 1993; 40: 199–204.
236. Torihara K, Suganuma T, Ide S, Morimitsu T. Anionic sites in blood capillaries of the mouse cochlear duct. Hear Res 1994; 77: 69–74.
237. Lawrenson JG, Reid AR, Allt G. Molecular characterization of anionic sites on the luminal front of endoneural capillaries in sciatic nerve. J Neurocytol 1994; 23: 29–37.
238. Lawrenson JG, Reid AR, Allt G. Molecular characteristics of pial microvessels of the rat optic nerve. Can pial microvessels be used as a model for the blood–brain barrier? Cell Tissue Res 1997; 288: 259–65.
239. Vorbrodt AW. Ultracytochemical characterization of anionic sites in the wall of brain capillaries. J Neurocytol 1989; 18: 359–68.
240. Dos-Santos WL, Rahman J, Klein N, Male DK. Distribution and analysis of surface charge on brain endothelium *in vitro* and *in situ*. Acta Neuropathol Berl 1995; 90: 305–11.
241. Ohtsuka A, Yamana S, Murakami T. Localization of membrane associated sialomucin on the free surface of mesothelial cells of the pleura, pericardium, and peritoneum. Histochem Cell Biol 1997; 107: 441–7.
242. Meirelles MN, Souto-Padron T, De-Souza W. Participation of cell surface anionic sites in the interaction between *Trypanosoma cruzi* and macrophages. J Submicrosc Cytol 1984; 16: 533–45.
243. Danon D, Marikovsky Y. The aging of the red blood cell. A multifactor process. Blood Cells 1988; 14: 7–18.
244. Lupu G, Calb M. Changes in the platelet surface charge in rabbits with experimental hypercholesterolemia. Artherosclerosis 1988; 72: 77–82.
245. Curry FE. Determinants of capillary permeability: a review of mechanisms based on single capillary studies in the frog. Circ Res 1986; 59: 367–80.
246. Haraldsson B. Physiological studies of macromolecular transport across capillary walls. Acta Physiol Scand 1986; 128 (suppl. 553): 1–40.
247. Hardebo JE, Kahrstrom J. Endothelial negative surface charge areas and blood–brain barrier function. Acta Physiol Scand 1985; 125: 495–9.
248. Brenner BM, Hostetter TH, Humes HD. Glomerular permeability: barrier function based on discrimination of molecular size and charge. Am J Physiol 1978; 234: F455–60.
249. Bray J, Robinson GB. Influence of charge on filtration across renal basement membrane films *in vitro*. Kidney Int 1984; 25: 527–33.
250. Skutelsky E, Danon D. Redistribution of surface anionic sites on the luminal front of blood vessel endothelium after interaction with polycationic ligand. J Cell Biol 1976; 71: 232–41.
251. Reeves WH, Kanwar YS, Farquhar MG. Assembly of the glomerular filtration surface. Differentiation of anionic sites in glomerular capillaries of newborn rat kidney. J Cell Biol 1980 85: 735–53.
252. Adamson RH, Huxley VH, Curry FE. Single capillary permeability to proteins having similar size but different charge. Am J Physiol 1988; 254: H304–12.
253. Nakao T, Ogura M, Takahashi H, Okada T. Charge-affected transperitoneal movement of amino acids in CAPD. Perit Dial Int 1996; 16 (suppl. 1): S88–90.
254. Leypoldt JK, Henderson LW. Molecular charge influences transperitoneal macromolecule transport. Kidney Int 1933; 43: 837–44.
255. Myers BD, Guasch A. Selectivity of the glomerular filtration barrier in healthy and nephrotic humans. Am J Nephrol 1993; 13: 311–7.
256. Krediet RT, Koomen GC, Koopman MG *et al.* The peritoneal transport of serum proteins and neutral dextran in CAPD patients. Kidney Int 1989; 35: 1064–72.
257. Vernier RL, Steffes MW, Sisson-Ross S, Mauer SM. Heparan sulfate proteoglycan in the glomerular basement membrane in type 1 diabetes mellitus. Kidney Int 1992; 41: 1070–80.
258. Vernier RL, Klein DJ, Sisson SP, Mahan JD, Oegema TR, Brown DM. Heparan sulfate-rich anionic sites in the human glomerular basement membrane. N Engl J Med 1983; 309: 1001–9.
259. Van-den-Heuvel LP, Van-den-Born J, Jalanko H *et al.* The glycosaminoglycan content of renal basement membranes in the congenital nephrotic syndrome of the Finnish type. Pediatr Nephrol 1992; 6: 10–15.
260. Washizawa K, Kasai S, Mori T, Komiyama A, Shigematsu H. Ultrastructural alteration of glomerular anionic sites in nephrotic patients. Pediatr Nephrol 1993; 7: 1–5.
261. Ramjee G, Coovadia HM, Adhikari M. Direct and indirect tests of pore size and charge selectivity in nephrotic syndrome. J Lab Clin Med 1996; 127: 195–9.
262. Rosenzweig LJ, Kanwar YS. Removal of sulfated (heparan sulfate) or nonsulfated (hyaluronic acid) glycosaminoglycans results in increased permeability of the glomerular basement membrane to ^{125}I–bovine serum albumin. Lab Invest 1982; 47: 177–84.
263. Wu VY, Wilson B, Cohen MP. Disturbances in glomerular basement membrane glycosaminoglycans in experimental diabetes. Diabetes 1987; 36: 679–83.
264. Van-den-Born J, Van-Kraats AA, Bakker MA *et al.* Reduction of heparan sulphate-associated anionic sites in the glomerular basement membrane of rats with streptozotocin-induced diabetic nephropathy. Diabetologia 1995; 38: 1169–75.
265. Galdi P, Shostak A, Jaichenko J, Fudin R, Gotloib L. Protamine sulfate induces enhanced peritoneal permeability to proteins. Nephron 1991; 57: 45–51.
266. Arfors KE, Rutili G, Svensjo E. Microvascular transport of macromolecules in normal and inflammatory conditions. Acta Physiol Scand Suppl 1979; 463: 93–103.
267. Gotloib L, Shostak A, Jaichenko J, Galdi P. Decreased density distribution of mesenteric and diaphragmatic microvascular anionic charges during murine abdominal sepsis. Resuscitation 1988; 16: 179–92.
268. Gotloib L, Shostak A, Galdi P, Jaichenko J, Fudin R. Loss of microvascular negative charges accompanied by interstitial edema in septic rats' heart. Circ Shock 1992; 36: 45–6.

269. Gotloib L, Shostak A. Lessons from peritoneal ultrastructure: from an inert dialyzing sheet to a living membrane. Contrib Nephrol 1992; 100: 207–35.
270. Shostak A, Gotloib L. Increased mesenteric, diaphragmatic, and pancreatic interstitial albumin content in rats with acute abdominal sepsis. Shock 1998; 9: 135–7.
271. Gotloib L, Barzilay E, Shostak A, Lev A. Sequential hemofiltration in monoliguric high capillary permeability pulmonary edema of severe sepsis: preliminary report. Crit Care Med 1984; 12: 997–1000.
272. Gotloib L, Barzilay E, Shostak A, Wais Z, Jaichenko J, Lev A. Hemofiltration in septic ARDS. The artificial kidney as an artificial endocrine lung. Resuscitation 1986; 13: 123–32.
273. Klein NJ, Shennan GI, Heyderman RS, Levin M. Alteration in glycosaminoglycan metabolism and surface charge on human umbilical vein endothelial cells induced by cytokines, endotoxin and neutrophils. J Cell Sci 1992; 102: 821–32.
274. Bone RC. The pathogenesis of sepsis. Ann Intern Med 1991; 115: 457–69.
275. Bone RS. Immunologic dissonance: a continuing evolution in our understanding of the systemic inflammatory response syndrome (SIRS) and the multiple organ dysfunction syndrome (MODS). Ann Intern Med 1996; 125: 680–87.
276. Gotloib L, Wajsbrot V, Shostak A, Kushnier R. Population analysis of mesothelium *in situ* and *in vivo* exposed to bicarbonate-buffered peritoneal dialysis fluid. Nephron 1996; 73: 219–27.
277. Sirois MG, Edelman ER. VEGF effect on vascular permeability is mediated by synthesis of platelet-activating factor. Am J Physiol 1997; 272: H2746–56.
278. Ryan GB, Grobety J, Majno G. Mesothelial injury and recovery. Am J Pathol 1973; 71: 93–112.
279. Gabbiani G, Badonnel MC, Majno G. Intra-arterial injections of histamine, serotonin, or bradykinin: a topographic study of vascular leakage. Proc Soc Exp Biol Med 1970; 135: 447–52.
280. Ryan GB, Majno G. Acute inflammation. A review. Am J Pathol 1977; 86: 183–276.
281. Joris I, Majno G, Corey EJ, Lewis RA. The mechanism of vascular leakage induced by leukotriene E4. Endothelial contraction. Am J Pathol 1987; 126: 19–24.
282. Gardner TW, Lesher T, Khin S, Vu G, Barber AJ, Brennan WA Jr. Histamine reduces ZO-1 tight-junction protein expression in cultured retinal microvascular endothelial cells. Biochem J 1996; 320: 717–21.
283. Kevil CG, Payne DK, Mire E, Alexander JS. Vascular permeability factor/vascular endothelial cell growth factor-mediated permeability occurs through disorganization of endothelial junctional proteins. J Biol Chem 1998; 273: 15099–103.
284. Predescu D, Palade GE. Plasmalemmal vesicles represent the large pore system of continuous microvascular endothelium. Am J Physiol 1993; 265: H725–33.
285. Esser S, Wolburg K, Wolburg H, Breier G, Kurzchalia T, Risau W. Vascular endothelial growth factor induces endothelial fenestrations *in vitro*. J Cell Biol 1998; 140: 947–59.
286. Feng D, Nagy JA, Hipp J, Pyne K, Dvorak AM. Reinterpretation of endothelial cell gaps induced by vasoactive mediators in guinea-pig, mouse and rat: many are transcellular pores. J Physiol Lond 1997; 504: 747–61.
287. Carlsson O, Nielsen S, Zakaria-el R, Rippe B. *In vivo* inhibition of transcellular water channels (aquaporin-1) during acute peritoneal dialysis in rats. Am J Physiol 1996; 271: H2254–62.
288. Panekeet MM, Mulder JB, Weening JJ, Struijk DG, Zweers MM, Krediet RT. Demonstration of aquaporin-CHIP in peritoneal tissue of uremic and CAPD patients. Perit Dial Int 1996; 16 (suppl. 1): S54–7.
289. Schnitzer JE, Oh P. Aquaporin-1 in plasma membrane and caveolae provides mercury-sensitive water channels across lung endothelium. Am J Physiol 1996; 270: H416–22.
290. Nielsen S, Smith BL, Christensen EI, Agre P. Distribution of the aquaporin CHIP in secretory and resorptive epithelia and capillary endothelia. Proc Natl Acad Sci USA 1993; 90: 7275–79.
291. Wintour EM. Water channels and urea transporters. Clin Exp Pharmacol Physiol 1997; 24: 1–9.
292. Ikomi F, Hunt J, Hanna G, Schmid-Schonbein GW. Interstitial fluid, plasma protein, colloid, and leukocyte uptake into initial lymphatics. J Appl Physiol 1996; 81: 2060–7.
293. Rutili G, Parker JC, Taylor AE. Fluid balance in ANTU-injured lungs during crystalloid and colloid infusions. J Appl Physiol 1984; 56: 993–8.
294. Drake RE, Gabel JC. Abdominal lymph flow response to intraperitoneal fluid in awake sheep. Lymphology 1991; 24: 77–81.
295. Ottaviani G, Azzali G. Ultrastructure of lymphatic vessels in some functional conditions. In: Comel M, Laszt L, eds. Morphology and Histochemistry of the Vascular Wall. Basel: Karger, 1966, pp. 325.
296. Foldi M, Csanda E, Simon M *et al.* Lymphogenic haemangiopathy. 'Prelymphatic' pathways in the wall of cerebral and cervical blood vessels. Angiologica 1968; 5: 250–62.
297. Hauck G. The connective tissue space in view of the lymphology. Experientia 1982; 38: 1121–2.
298. Crone G. Exchange of molecules between plasma, interstitial tissue and lymph. Pflugers Arch Suppl 1972: 65–79.
299. Casley-Smith JR. Lymph and lymphatics. In: Kaley G, Altura BM, eds. Microcirculation, vol. 4. Baltimore, MD: University Park Press, 1981, pp. 423.
300. Schmid-Schonbein GW. Mechanisms causing initial lymphatics to expand and compress to promote lymph flow. Arch Histol Cytol 1990; 53 (suppl. 1): 107–14.
301. Rhodin JA, Sue SL. Combined intravital microscopy and electron microscopy of the blind beginnings of the mesenteric lymphatic capillaries of the rat mesentery. A preliminary report. Acta Physiol Scand Suppl 1979; 463: 51–8.
302. Jones WR, O'Morchoe CC, Jarosz HM, O'Morchoe PJ. Distribution of charged sites on lymphatic endothelium. Lymphology 1986; 19: 5–14.
303. Schmid-Schonbein GW. Microlymphatics and lymph flow. Physiological Rev 1990; 70: 987–1028.
304. Leak LV, Burke JF. Fine structure of the lymphatic capillary and the adjoining connective tissue area. Am J Anat 1966; 118: 785–809.
305. Leak LV, Burke JF. Electron microscopic study of lymphatic capillaries in the removal of connective tissue fluids and particulate substances. Lymphology 1968; 1: 39–52.
306. Gerli R, Ibba L, Fruschelli G. Ultrastructural cytochemistry of anchoring filaments of human lymphatic capillaries and their relation to elastic fibers. Lymphology 1991; 24: 105–12.
307. Taylor AE. The lymphatic edema safety factor: the role of edema dependent lymphatic factors (EDLF). Lymphology 190; 23: 111–23.
308. Hogan RD, Unthank JL. The initial lymphatics as sensors of interstitial fluid volume. Microvasc Res 1986 31: 317–24.
309. Leak LV. Distribution of cell surface charges on mesothelium and lymphatic endothelium. Microvasc Res 986; 31: 18–30.
310. Leak V. Electron microscopic observations on lymphatic capillaries and the structural components of the connective tissue–lymph interface. Microvasc Res 1970; 2: 361–91.
311. Leak LV. The structure of lymphatic capillaries in lymph formation. Fed Proc 1976 35: 1863–71.
312. Shinohara H, Nakatani T, Matsuda T. Postnatal development of the ovarian bursa of the golden hamster *(Mesocricetus auratus):* its complete closure and morphogenesis of lymphatic stomata. Am J Anat 1987; 179: 385–402.
313. Hauck G. Capillary permeability and micro-lymph drainage. Vasa 1994; 23: 93–7.
314. McCallum WG. On the mechanisms of absorption of granular material from the peritoneum. Bull Johns Hopkins Hosp 1903; 14, 105–15.

315. Tsilibary EC, Wissig SL. Absorption from the peritoneal cavity. SEM study of the mesothelium covering the peritoneal surface of the muscular portion of the diaphragm. Am J Anat 1977; 149: 127–33.
316. Leak LV, Rahil K. Permeability of the diaphragmatic mesothelium. The ultrastructural basis for stomata. Am J Anat 1978; 151: 557–92.
317. Leak LV. Lymphatic endothelial–interstitial interface. Lymphology 187; 20: 196–204.
318. Simer PM. Omental lymphatics in man. Anat Rec 1935; 63: 253–62.
319. Vajda J. Innervation of lymph vessels. Acta Morphol Acad Sci Hung 1966; 14: 197–208.
320. Hargens AR, Zweifach BW. Contractile stimuli in collecting lymph vessels. Am J Physiol 1977; 233: H57–65.
321. Gnepp DR, Green FH. Scanning electron microscopic study of canine lymphatic vessels and their valves. Lymphology 1980; 13: 91–9.
322. Ohtani O. Structure of lymphatics in rat cecum with special reference to submucosal collecting lymphatics endowed with smooth muscle cells and valves. I. A scanning electron microscopic study. Arch Hist Cytol 1992; 55: 429–36.
323. Moller R. Arrangement and fine structure of lymphatic vessels in the human spermatic cord. Andrologia 1980; 12: 564–76.
324. Zweifach BW, Prather JW. Micromanipulation of pressure in terminal lymphatics in the mesentery. Am J Physiol 1975; 228: 1326–35.
325. Horstmann E. Anatomie und Physiologie des lymphgefa B systems im bauchraum. In: Bartelheimer H, Heising N, eds. Actuelle Gastroenterologie. Stuttgart: Verh, Thieme, 1968, p. 1.
326. Ohhashi T, Azuma T, Sakaguchi M. Active and passive mechanical characteristics of bovine mesenteric lymphatics. Am J Physiol 1980; 239: H88–95.
327. Watanabe N, Kawai Y, Ohhashi T. Demonstration of both B1 and B2 adrenoreceptors mediating negative chronotropic effects on spontaneous activity in isolated bovine mesenteric lymphatics. Microvasc Res 1990; 39: 50–9.
328. Ohhashi T, Azuma T. Sympathetic effects on spontaneous activity in bovine mesenteric lymphatics (retracted by Ohhashi T, Azuma T. In: Am J Physiol 1986; 251: H226). Am J Physiol 1984; 247: H610–15.
329. Ohhashi T, Azuma T Pre and postjunctional alpha-adrenoceptors at the sympathetic neuroeffector junction in bovine mesenteric lymphatics. Microvac Res 1986; 31: 31–40.
330. Watanabe N, Kawai Y, Ohhashi T. Dual effects of histamine on spontaneous activity in isolated bovine mesenteric lymphatics. Microvasc Res 1988; 36: 239–49.
331. Ferguson MK, Shahinian HK, Michelassi F. Lymphatic smooth muscle responses to leukotrienes, histamine and platelet activating factor. J Surg Res 1988; 44: 172–7.
332. Ohhashi T, Kawai Y, Azuma T. The response of lymphatic smooth muscles to vasoactive substances. Pflugers Arch 1978; 375: 183–8.
333. Azuma T, Ohhashi T, Roddie IC. Bradykinin-induced contractions of bovine mesenteric lymphatics. J Physiol Lond 1983; 342: 217–27.
334. Ohhashi T, Olschowka JA, Jacobowitz DM. Vasoactive intestinal peptide inhibitory innervation in bovine mesenteric lymphatics. A histochemical and pharmacological study. Circ Res 1983; 53: 535–8.
335. Abu-Hiljeh MF, Habbai OA, Moqattash ST. The role of the diaphragm in lymphatic absorption from the peritoneal cavity. J Anat 1995; 186: 453–67.
336. Fruschelli G, Gerli R, Alessandrini G, Sacchi G. Il controllo neurohumorale dalla contratilita dei vasi linfatici. In: Atti dalla Societa Italiana di Anatomia. 39th Convegno Nazaionale, 19/21 September. Firenze: I Sedicesimo, 1983, p. 2.
337. Starling EH, Tubby A. On absorption from and secretion into the serous cavities. J Physiol (Lond) 1894; 16: 140–55.
338. Starling EH. On the absorption of fluid from the connective tissue spaces. J Physiol (Lond) 1896; 19: 312–21.
339. Drinker CF, Field ME. The protein of mammalian lymph and the relation of lymph to tissue fluid. Am J Physiol 1931; 97: 32–45.
340. Allen L, Vogt E. Mechanisms of lymphatic absorption from serous cavities. Am J Physiol 1937; 119: 776–82.
341. Brace RA, Guyton AC. Interstitial fluid pressure: capsule, free fluid, gel fluid and gel absorption pressure in subcutaneous tissue. Microvasc Res 1979; 18: 217–28.
342. Guyton AC, Granger HJ, Taylor AE. Interstitial fluid pressure. Physiol Rev 1971; 51: 527–63.
343. Guyton AC, Taylor AE, Granger HJ, Gibson WH. Regulation of interstitial fluid volume and pressure. Adv Exp Med Biol 1972; 33: 111–8.
344. Guyton AC, Taylor AE, Brace RA. A synthesis of interstitial fluid regulation and lymph formation. Fed Proc 976; 35: 1881–5.
345. Zink J, Greenway CV. Intraperitoneal pressure in formation and reabsorption of ascites in cats. Am J Physiol 1977; 233: H185–90.
346. Zink J, Greenway CV. Control of ascites absorption in anesthetized cats: effects of intraperitoneal pressure, protein, and furosemide diuresis. Gastroenterology 1977; 73: 119–24.
347. Imholz AL, Koomen GC, Struijk DG, Arisz L, Krediet RT. Effect of an increased intraperitoneal pressure on fluid and solute transport during CAPD. Kidney Int 1993; 44: 1078–85.
348. Durand PY, Chanliau J, Gamberoni J, Hestin D, Kessler M. Intraperitoneal pressure, peritoneal permeability and volume of ultrafiltration in CAPD. Adv Perit Dial 1992; 8: 22–5.
349. Gotloib L, Garmizo AL, Varka I, Mines M. Reduction of vital capacity due to increased intra-abdominal pressure during peritoneal dialysis. Perit Dial Bull 1981; 1: 63–4.
350. Flessner MF. Net ultrafiltration in peritoneal dialysis: role of direct fluid absorption into peritoneal tissue. Blood Purif 1992; 10: 136–47.
351. Flessner MF, Parker RJ, Sieber SM. Peritoneal lymphatic uptake of fibrinogen and erythrocytes in the rat. Am J Physiol 1983; 244: H89–96.
352. Silk YN, Goumas WM, Douglass HO Jr, Huben RP. Chylous ascites and lymphocyst management by peritoneovenous shunt. Surgery 1991; 110: 561–5.
353. Casley Smith JR. A fine structural study of variations in protein concentration in lacteals during compression and relaxation. Lymphology 1979; 12: 59–65.
354. O'Morchoe CC, Jones WR 3d, Jarosz HM, O'Morchoe PJ, Fox LM. Temperature dependence of protein transport across lymphatic endothelium *in vitro*. J Cell Biol 1984; 98: 629–40.
355. Dobbins WO, Rollins EL Intestinal mucosal lymphatic permeability: an electron microscopic study of endothelial vesicles and cell junctions. J Ultrastruct Res 1970; 33: 29–59.
356. Shasby DM, Peterson MW. Effects of albumin concentration on endothelial albumin transport *in vitro*. Am J Physiol 1987; 253: H654–61.
357. Albertini KH, O'Morchoe CC. Renal lymphatic ultrastructure and translymphatic transport. Microvasc Res 1980; 19: 338–51.
358. Haller A. Primae linae physiologiae in usum Praelectionum Academicarum avetae et emendato. Gottingae, Capit 25, 1751, p. 41.
359. Furness JB. Arrangement of blood vessels and their relation with adrenergic nerves in the rat mesentery. J Anat 1973; 115: 347–64.
360. Beattie JM. The cells of inflammatory exudations: an experimental research as to their function and density, and also as to the origin of the mononucleated cells. J Pathol Bacteriol 1903; 8: 130–77.
361. Durham HE. The mechanism of reaction to peritoneal infection. J Pathol Bacteriol 1897; 4: 338–82.

362. Josey AL. Studies in the physiology of the eosinophil. V. The role of the eosinophil in inflammation. Folia Haematol 1934; 51: 80–95.
363. Webb RL. Changes in the number of cells within the peritoneal fluid of the white rat, between birth and sexual maturity. Folia Haematol 1934; 51: 445–51.
364. Padawer J, Gordon AS. Cellular elements in the peritoneal fluid of some mammals. Anat Rec 1956; 124: 209–22.
365. Fruhman GJ. Neutrophil mobilization into peritoneal fluid. Blood 1960; 16: 1753–61.
366. Seeley SF, Higgins GM, Mann FC. The cytologic response of the peritoneal fluid to certain substances. Surgery 1937; 2: 862–76.
367. Bercovici B, Gallily R. The cytology of the human peritoneal fluid. Cytology 1978; 22: 124.
368. Becker S, Halme J, Haskill S. Heterogeneity of human peritoneal macrophages: cytochemical and flow cytometric studies. J Reticuloendothel Soc 1983; (ES) 33: 127–38.
369. De Brux JA, Dupre-Froment J, Mintz M.: Cytology of the peritoneal fluids sampled by coelioscopy or by cul de sac puncture. Its value in gynecology. Acta Cytol 1968; 12: 395–403.
370. Mahoney CA, Sherwood N, Yap EH, Singleton TP, Whitney DJ, Cornbleet PJ. Ciliated cell remnants in peritoneal dialysis fluid. Arch Pathol Lab Med 1993; 117: 211–3.
371. Fruhmann GJ. Adrenal steroids and neutrophil mobilization. Blood 1962; 20: 335–63.
372. Spriggs AI, Boddington MM. The Cytology of Effusions, 2nd edn. New York: Grune & Straton, 1968, pp. 5–17.
373. Domagala W, Woyke S. Transmission and scanning electron microscopic studies of cells in effusions. Acta Cytol 1975; 19: 214–24.
374. Efrati P, Nir E. Morphological and cytochemical investigation of human mesothelial cells from pleural and peritoneal effusions. A light and electron microscopy study. Israel J Med Sci 976; 12: 662–73.
375. Bewtra Ch, Greer KP. Ultrastructural studies of cells in body cavity effusions. Acta Cytol 1985 29: 226–38.
376. Chapman JS, Reynolds RC. Eosinophilic response to intraperitoneal blood. J Lab Clin Med 1958; 51: 516–20.
377. Northover BJ. The effect of various anti-inflammatory drugs on the accumulation of leucocytes in the peritoneal cavity of mice. J Pathol Bacteriol 1964; 88: 332–5.
378. Hurley JV, Ryan GB, Friedman A. The mononuclear response to intrapleural injection in the rat. J Pathol Bact 1966; 91: 575–87.
379. Rubin J, Rogers WA, Taylor HM. *et al.* Peritonitis during continuous ambulatory peritoneal dialysis. Ann Intern Med 1980; 92: 7–13.
380. Cichoki T, Hanicki Z, Sulowicz W, Smolenski O, Kopec J, Zembala M. Output of peritoneal cells into peritoneal dialysate. Cytochemical and functional studies. Nephron 1983; 35: 175–82.
381. Strippoli P, Coviello F, Orbello G *et al.* First exchange neutrophilia is not always an index of peritonitis during CAPD. Adv Perit Dial 1989; 4: 121–3.
382. Kubicka U, Olszewski WL, Maldyk J, Wierzbicki Z, Orkiszewska A. Normal human immune peritoneal cells: phenotypic characteristics. Immunobiology 1989; 180: 80–92.
383. Gotloib L, Mines M, Garmizo AL, Rodoy Y. Peritoneal dialysis using the subcutaneous intraperitoneal prosthesis. Dial Transplant 1979; 8: 217–20.
384. Hoeltermann W, Schlotmann-Hoelledr E, Winkelmann M, Pfitzer P. Lavage fluid from continuous ambulatory peritoneal dialysis. A model for mesothelial cell changes. Acta Cytol 1989; 33: 591–4.
385. Chan MK, Chow L, Lam SS, Jones B. Peritoneal eosinophilia in patients on continuous ambulatory peritoneal dialysis: a prospective study. Am J Kidney Dis 1988; 11: 180–3..
386. Gokal R, Ramos JM, Ward MK, Kerr DN. 'Eosinophilic' peritonitis in continuous ambulatory peritoneal dialysis (CAPD). Clin Nephrol 1981; 15: 328–30.
387. Leak LV. Interaction of mesothelium to intraperitoneal stimulation. Lab Invest 1983; 48: 479–90.
388. Raftery AT. Regeneration of parietal and visceral peritoneum: an electron microscopical study. J Anat 1973; 115: 375–92.
389. Raftery AT. Mesothelial cells in peritoneal fluid. J Anat 1973; 115: 237–53.
390. Koss LG. Diagnostic Cytology and its Histopathologic Bases, 3rd edn. Philadelphia, PA: Lippincot, 1979, chs 16–25.
391. Ryan GB, Grobety J, Majno G. Postoperative peritoneal adhesions: a study of the mechanisms. Am J Pathol 1971; 65: 117–48.
392. Ryan GB, Grobety J, Majno G. Mesothelial injury and recovery. Am J Pathol 1973; 71: 93–112.
393. Di Paolo N, Sacchi G, De Mia M *et al.* Does dialysis modify the peritoneal structure? In: La Greca G, Chiaramonte S, Fabris A, Feriani M, Ronco G, eds. Peritoneal Dialysis, Milan: Wichtig Ed., 1956, pp. 11–24.
394. Dobbie JW, Zaki M, Wilson L. Ultrastructural studies on the peritoneum with special reference to chronic ambulatory peritoneal dialysis. Scot Med J 1981; 26: 213–23.
395. Verger G, Brunschvicg O, Le Charpentier Y, Lavergne A, Vantelon J. Structural and ultrastructural peritoneal membrane changes and permeability alterations during continuous ambulatory peritoneal dialysis. Proc EDTA 1981; 18: 199–205.
396. Susuki S, Enosawa S, Kakefuda T *et al.* A novel immunosuppressant, FTY720, with a unique mechanism of action, induces long-term graft acceptance in rat and dog allotransplantation. Transplantation 1996; 61: 200–5.
397. Nagata S. Fas-mediated apoptosis. Adv Exp Med Biol 1996; 406: 119–24.
398. Laster SM, Mackenzie JM Jr. Bleb formation and F-actin distribution during mitosis and tumor necrosis factor-induced apoptosis. Microsci Res Tech 1996; 34: 272–80.
399. Yang AH, Chen JY, Lin YP, Huang TP, Wu CW. Peritoneal dialysis solution induces apoptosis of mesothelial cells. Kidney Int 1997; 51: 1280–8.
400. Laiho KU, Trump BF. Mitochondria of Ehrlich ascites tumor cells. Lab Invest 1975; 32: 163–82.
401. Pentilla A, Trump BF. Studies on the modification of the cellular response to injury. III. Electron microscopic studies on the protective effect of acidosis on p-chloromercuribenzene sulfonic acid (PCMBS) induced injury of Ehrlich ascites tumor cells. Virchows Arch B Cell Pathol 1975; 18: 17–34.
402. Trump BF, Berezesky IK, Chang SH, Phelps PC. The pathways of cell death: oncosis, apoptosis, and necrosis. Toxicol Pathol 1997; 25: 82–8.
403. Dobbie JW, Anderson JD. Ultrastructure, distribution, and density of lamellar bodies in human peritoneum. Perit Dial Int 1996; 16: 488–96.
404. Slater ND, Cope GH, Raftery AT. Mesothelial hyperplasia in response to peritoneal dialysis fluid: a morphometric study in the rat. Nephron 1991; 58: 466–71.
405. Witowski J, Jorres A, Coles GA, Williams JD, Topley N. Superinduction of IL-6 synthesis in human peritoneal mesothelial cells is related to the induction and stabilization of IL-6 mRNA. Kidney Int 1996; 50: 1212–23.
406. Topley N, Williams JD. Effect of peritoneal dialysis on cytokine production by peritoneal cells. Blood Purif 1996; 14: 188–97.
407. Di Paolo N, Garosi G, Traversari L, Di Paolo M. Mesothelial biocompatibility of peritoneal dialysis solutions. Perit Dial Int 1993; 13 (suppl. 2): S109–12.
408. Breborowicz A, Rodela H, Oreopoulos DG. Toxicity of osmotic solutes on human mesothelial cells *in vitro*. Kidney Int 1992; 41: 1280–5.

409. Jorres A, Gahl GM, Topley N *et al. In vitro* biocompatibility of alternative CAPD fluids: comparison of bicarbonate-buffered and glucose-polymer-based solutions. Nephrol Dial Transplant 1994; 9: 785–90.
410. Shostak A, Pivnik K, Gotloib L. Daily short exposure of cultured mesothelial cells to lactated, high-glucose, low pH peritoneal dialysis fluid induces a low-profile regenerative steady state. Nephrol Dial Transplant 1996; 11: 608–13.
411. Topley N, Kaur D, Petersen MM *et al. In vitro* effects of bicarbonate and bicarbonate-lactate buffered peritoneal dialysis solutions on mesothelial and neutrophil function. J Am Soc Nephrol 1996; 7: 128–224.
412. Breborowicz A, Rodela H, Karon J, Martis L, Oreopoulos DG. *In vitro* stimulation of the effect of peritoneal dialysis solution on mesothelial cells. Am J Kidney Dis 1997; 29: 404–9.
413. Topley N. *In vitro* biocompatibility of bicarbonate-based peritoneal dialysis solutions. Perit Dial Int 1997; 17: 42–7.
414. Jorres A, Williams JD, Topley N. Peritoneal dialysis solution biocompatibility: inhibitory mechanisms and recent studies with bicarbonate-buffered solutions. Perit Dial Int 1997; 17 (suppl. 2): S42–6.
415. Di Paolo N, Garosi G, Monaci G, Brardi S. Biocompatibility of peritoneal dialysis treatment. Nephrol Dial Transplant 1997; 12 (suppl. 1): 78–83.
416. Holmes CJ. Peritoneal host defense mechanisms. Perit Dial Int 1996; 16 (suppl. 1): S124–5.
417. Zemel D, Krediet RT. Cytokine patterns in the effluent of continuous ambulatory peritoneal dialysis. Relationship to peritoneal permeability. Blood Purif 1996; 14: 198–216.
418. Topley N, Petersen MM, Mackenzie R *et al.* Human peritoneal mesothelial cell prostaglandin synthesis: induction of cyclooxygenase mRNA by peritoneal macrophage-derived cytokines. Kidney Int 1994; 46: 900–9.
419. Shostak A, Pivnik E, Gotloib L. Cultured rat mesothelial cells generate hydrogen peroxide: a new player in peritoneal defense? J Am Soc Nephrol 1996; 7: 2371–78.
420. Gotloib L. Large mesothelial cells in peritoneal dialysis: a sign of degeneration or adaptation? Perit Dial Int 1996; 16: 118–20.
421. Raftery AT. An enzyme histochemical study of mesothelial cells in rodents. J Anat 1973; 115: 365–73.
422. Whitaker D, Papadimitriou JM, Walters MN. The mesothelium; techniques for investigating the origin, nature and behaviour of mesothelial cells. J Pathol 1980; 132, 263–71.
423. Gotloib L, Shostak A, Wajsbrot V, Kushnier R. The cytochemical profile of visceral mesothelium under the influence of lactated-hyperosmolar peritoneal dialysis solutions. Nephron 1995; 69: 466–71.
424. Gotloib L, Wajsbrot V, Shostak A, Kushnier R. Morphology of the peritoneum: effect of peritoneal dialysis. Perit Dial Int 1995; 15 (suppl.): S9–11.
425. Di Paolo N, Garosi G, Petrini G, Monaci G. Morphological and morphometric changes in mesothelial cells during peritoneal dialysis in the rabbit. Nephron 1996; 74: 594–9.
426. Gotloib L, Wajsbrot V, Shostak A, Kushnier R. Effect of hyperosmolality upon the mesothelial monolayer exposed *in-vivo* and *in-situ* to a mannitol enriched dialysis solution. Nephron 1999; 81: 301–9.
427. Wajsbrot V, Shostak A, Gotloib L, Kushnier R. Biocompatibility of a glucose-free, acidic lactated solution for peritoneal dialysis evaluated by population analysis of mesothelium. Nephron 1998; 79, 322–32.
428. Walters WB, Buck RC. Mitotic activity of peritoneum in contact with a regenerative area of peritoneum. Virchows Arch B Zellpathol 1973; 13, 48–52.
429. Gotloib L, Shostak A, Wajsbrot V, Kushnier R. High glucose induces an hypertrophic, senescent mesothelial cell phenotype after long, *in vivo* exposure. Nephron 1999; 82: 164–7.
430. Vincent F, Brun H, Clain E, Ronot X, Adolphe M. Effects of oxygen free radicals on proliferation kinetics of cultured rabbit articular chondrocytes. J Cell Physiol 1989; 141: 262–6.
431. De Bono DP, Yang WD. Exposure to low concentrations of hydrogen peroxide causes delayed endothelial cell death and inhibits proliferation of surviving cells. Atherosclerosis 1995; 114: 235–45.
432. Bladier G, Wolvetang EJ, Hutchinson P, De Haan JB, Kola I. Response of a primary human fibroblast cell line to H_2O_2: senescence-like growth arrest or apoptosis? Cell Growth Difer 1997; 8: 589–98.
433. Nicotera P, Dypbukt JM, Rossi AD, Manzo L, Orrenius S. Thiol modification and cell signalling in chemical toxicity. Toxicol Lett 1992; 64–5 (Spec No.): 563–7.
434. Dypbukt JM, Ankarcrona M, Burkitt M *et al.* Different prooxidant levels stimulate growth, trigger apoptosis, or produce necrosis of insulin-secreting RINm5F cells. The role of intracellular polyamines. J Biol Chem 1994; 269: 30553–60.
435. Orrenius S, Burkitt MJ, Kass GE, Dypbukt JM, Nicotera P. Calcium ions and oxidative cell injury. Ann Neurol 1992; 32 (suppl.): S33–42.
436. Curcio F, Ceriello A. Decreased cultured endothelial cell proliferation in high glucose medium is reversed by antioxidants: new insights on the pathophysiological mechanisms of diabetic vascular complications *in Vitro*. Cell Dev Biol 1992; 28A: 787–90.
437. Kashiwagi A, Asahina T, Ikebuchi M *et al.* Abnormal glutathione metabolism and increased cytotoxicity caused by H_2O_2 in human umbilical vein endothelial cells cultured in high glucose medium. Diabetologia 1994; 37: 264–9.
438. Breborowicz A, Witowski J, Wieczorowska K, Martis L, Serkes KD, Oreopoulos DG. Toxicity of free radicals to mesothelial cells and peritoneal membrane. Nephron 1993; 65: 62–6.
439. Donnini D, Zambito AM, Perrella G, Ambesi-Impiombato FS, Curcio F. Glucose may induce cell death through a free radical-mediated mechanism. Biochem Biophys Res Commun 1996; 219: 412–7.
440. Kashwem A, Nomoto Y, Tanabe R *et al.* The effect of dialysate glucose on phagocyte superoxide generation in CAPD patients. Perit Dial Int 1998; 18: 52–9.
441. Elgawish A, Glomb M, Friedlander M, Monnier VM. Involvement of hydrogen peroxide in collagen cross-linking by high glucose *in vitro* and *in vivo*. J Biol Chem 1996; 272: 12964–71.
442. Friedlander MA, Wu YC, Elgawish A, Monnier VM. Early and advanced glycosylation end products. Kinetics of formation and clearance in peritoneal dialysis. J Clin Invest 1996; 97: 728–35.
443. Dobbie JW, Anderson JD, Hind G. Long-term effects on peritoneal dialysis on peritoneal morphology. Perit Dial Int 1994; 14 (suppl. 3): S14–20.
444. Dobbie JW: Pathogenesis of peritoneal fibrosing syndromes (sclerosing peritonitis) in peritoneal dialysis. Perit Dial Int 1992; 12: 14–27.
445. Verger G, Celicout B, Larpent L, Goupil A. Encapsulating peritonitis during continuous ambulatory peritoneal dialysis. A physiopathologic hypothesis. Presse Med 1986; 15: 1311–4.
446. Gandhi VC, Humayun HM, Ing TS *et al.* Sclerotic thickening of the peritoneal membrane in maintenance peritoneal dialysis patients. Arch Intern Med 1980; 140: 1201–3.
447. Slingeneyer A, Mion G, Mourad G, Canaud B, Faller B, Beraud JJ. Progressive sclerosing peritonitis: a late and severe complication of maintenance peritoneal dialysis. Trans Am Soc Artif Intern Organs 1983; 29: 633–40.
448. Foo KT, Ng-Kc, Rauff A, Foong WC, Sinniah R. Unusual small intestinal obstruction in adolescent girls: the abdominal cocoon. Br J Surg 1978; 65: 427–30.
449. Lee RE, Baddeley H, Marshall AJ, Read AE. Practolol peritonitis. Clin Radiol 1977; 28: 119–28.
450. Harty RF. Sclerosing peritonitis and propranolol. Arch Intern Med. 1978; 138: 1424–6.

451. Baxter-Smith DC, Monypenny IJ, Dorricott NJ. Sclerosing peritonitis in patient on timolol. Lancet 1978; 2: 149.
452. Clarck CV, Terris R. Sclerosing peritonitis associated with metoprolol. Lancet 1983; 1: 937.
453. Phillips RK, Dudley HA. The effect of tetracycline lavage and trauma on visceral and parietal peritoneal ultrastructure and adhesion formation. Br J Surg 1984; 71: 537–9.
454. Di Paolo N, Di Paolo M, Tanganelli P, Brardi S, Bruci A. Technique nefrologiche e dialitici. Perugia: Bios Editore, 1988, p. 5.
455. Myhre-Jensen O, Bergmann Larsen S, Astrup T. Fibrinolytic activity in serosal and synovial membranes. Rats, guinea pigs and rabbits. Arch Pathol 1969; 88: 623–30.
456. Gervin AS, Puckett ChL, Silver D. Serosal hypofibrinolysis. A cause of postoperative adhesions. Am J Surg 1973; 1225: 80–8.
457. Buckman RF, Woods M, Sargent L, Gervin AS. A unifying pathogenetic mechanism in the etiology of intraperitoneal adhesions. J Surg Res 1976; 20: 1–5.
458. Gotloib L, Shostak A, Bar-Sella P, Cohen R. Continuous mesothelial injury and regeneration during long term peritoneal dialysis. Perit Dial Bull 1987; 7: 148–55.
459. Gotloib L, Wajsbrot V, Shostak A, Kushnier R. Experimental approach to peritoneal morphology. Perit Dial Int 1994; 14 (suppl. 3): S6–11.
460. Honda K, Nitta K, Horita S, Yumura W, Nihei H. Morphological changes in the peritoneal vasculature of patients on CAPD with ultrafiltration failure. Nephron 1996; 72: 171–6.
461. Eskeland G, Kjaerheim A. Regeneration of parietal peritoneum in rats. 2. An electron microscopical study. Acta Pathol Microbiol Scand 1966; 68, 379–95.
462. Watters WB, Buck RC. Scanning electron microscopy of mesothelial regeneration in the rat. Lab Invest 1972; 26: 604–9.
463. Whitaker D, Papadimitriou J. Mesothelial healing: morphological and kinetic investigations. J Pathol Bac 1957; 73: 1–10.
464. Renvall SY. Peritoneal metabolism and intrabdominal adhesion formation during experimental peritonitis. Acta Chirurg Scand Suppl 1980; 503: 1–48.
465. Ellis H, Harrison W, Hugh TB. The healing of peritoneum under normal and pathological conditions. Br J Surg 1965; 52: 471–6.
466. Ellis H. The cause and prevention of postoperative intraperitoneal adhesions. Surg Gynecol Obstet 1971; 133: 497–511.
467. Whitaker D, Papadimitriou J. Mesothelial healing: morphological and kinetic investigations. J Pathol 1985; 145: 159–75.
468. Cameron GR, Hassan SM, De SN. Repair of Glisson's capsule after tangential wounds on the liver. J Pathol Bacteriol 1957; 73: 1–10.
469. Johnson FR, Whitting HW. Repair of parietal peritoneum. Br J Surg 1962; 49, 653–60.
470. Eskeland G. Regeneration of parietal peritoneum in rats. A light microscopical study. Acta Pathol Microbiol Scand 1966; 68: 355–78.
471. Williams DC. The peritoneum. A plea for a change in attitude towards this membrane. Br J Surg 42: 1955; 401–5.
472. Shaldon S. Peritoneal macrophage: the first line of defense. In: La Greca G, Chiaramonte S, Fabris A, Feriani M, Ronco G, eds. Peritoneal Dialysis. Milan: Wichtig. Ed., 1986, p. 201.
473. Raftery AT. Regeneration of parietal and visceral peritoneum. A light microscopical study. Brit J Surgery 1973; 60: 293–9.
474. Maximow AA, Bloom W. A Textbook of Histology. Philadelphia, PA: Saunders, 1942, pp. 63–66.
475. Gonzales S, Friemann J, Muller KM, Pott F. Ultrastructure of mesothelial regeneration after intraperitoneal injection of asbestos fibres on rat omentum. Pathol Res Pract 1991; 187: 931–5.
476. Watters WB, Buck RC. Mitotic activity of peritoneum in contact with a regenerating area of peritoneum. Virchows Arch B Cell Pathol 1973; 13: 48–54.
477. Mironov VA, Gusev SA, Baradi AF. Mesothelial stomata overlying omental milky spots: scanning electron microscopic study. Cell Tissue Res 1979; 201, 327–30.
478. Doherty NS, Griffiths RJ, Hakkinen JP, Scampoli DN, Milici AJ. Post-capillary venules in the 'milky spots' of the greater omentum are the major site of plasma protein and leukocyte extravasation in rodent models of peritonitis. Inflamm Res 1995; 44: 169–77.
479. Fukatsu K, Saito H, Han I. *et al.* The greater omentum is the primary site of neutrophil exudation in peritonitis. J Am Coll Surg 1996; 183: 450–6.
480. Krist LF, Eestermans IL, Steenbergen JJ. Cellular composition of milky spots in the human greater omentum: an immunochemical and ultrastructural study. Anat Rec 1995; 241: 163–74.
481. Leypoldt JK. Evaluation of peritoneal membrane pore models. Blood Purif 1992; 10: 227–38.
482. Gotloib L, Oreopoulos DG. Transfer across the peritoneum: passive or active? Nephron 1981; 29: 201–2.